THE UNIVERSITY OF CHICAGO

ACETYLATION OF THE ZIKA VIRUS NS3 PROTEIN BY A SINGLE ISOFORM OF HOST ENZYME KAT5 (KAT5γ) PROMOTES VIRAL REPLICATION

A DISSERTATION SUBMITTED TO

THE FACULTY OF THE DIVISION OF THE BIOLOGICAL SCIENCES

AND THE PRITZKER SCHOOL OF MEDICINE

IN CANDIDACY FOR THE DEGREE OF

DOCTOR OF PHILOSOPHY

COMMITTEE ON MICROBIOLOGY

BY

TARYN MAE SERMAN

CHICAGO, ILLINOIS

DECEMBER 2022

TABLE OF CONTENTS

LIST OF FIGURES

ACKNOWLEDGEMENTS

I firstly want to thank my P.I, Dr. Michaela Gack, for giving me the fully-funded opportunity to work in her laboratory, even across a move from Chicago to Florida. Further, I want to thank my additional scientific mentors and colleagues, Dr. Michiel van Gent and Dr. Cindy Chiang, for teaching me how to be a scientist, both at the bench and outside of the lab.

I want to deeply thank my friends who supported me throughout this arduous experience. Andrea Watson, thank you for your unwavering kindness and optimism. Paula Lockwood, thank you for sitting next to me in 8th grade science class and keeping me young ever since. Victoria Riedinger, Kelly Cerri, Marla Shipton, Kelsey Peterson, and Sylke Lopez: thank you for providing me with so many laughs and wonderful experiences.

I also want to thank those scientists who I looked up to along the way: Dr. Claire Reynolds, Dr. Joyce Lee, Dr. Anne Marie Skalka, Dr. Kate Buettner, Dr. Lisa Rohan, Dr. Galit Regev, Dr. Sheila Grab, Dr. Lucia Rothman-Denes, and Dr. Yasmine Baktash. Thanks for making science look so damn cool.

Finally, I want to thank my parents for their constant support and gentle reminders. You believed in me when I didn't. I love you both.

CHAPTER 1

INTRODUCTION

Some elements of this chapter are adapted or directly from: Serman, T and Gack, M.U. Evasion of Innate and Intrinsic Antiviral Pathways by the Zika Virus. Viruses 2019, 11(10): 970.

1.1 Flaviviruses

The *Flaviviridae* family of viruses is comprised of several genera, of which, the Flavivirus genus will be highlighted. The Flavivirus genus can be further subdivided into four clades based on the arthropod vector (or lack of vector) required for transmission of the virus. Mosquito-transmitted flaviviruses represent a major clade of human pathogens, of which Zika virus (ZIKV), dengue virus (DENV), yellow fever virus (YFV), Japanese encephalitis virus (JEV), and West Nile virus (WNV) are members. Of note, the major human pathogen Hepatitis C virus (HCV) is a member of the *Flaviviridae* family, but resides in a separate genus (hepacivirus). The name “flavivirus” originates from the Latin word for yellow, “flavus”, and was derived from the jaundice symptoms caused by infection with YFV, the “prototypical” flavivirus [1]. The disease symptoms of flaviviruses are quite variable within a human host, but the two major types of disease progression are (1) neurological symptoms such as encephalitis, meningitis, and acute paralysis and (2) hemorrhagic symptoms, such as severe headache, seizures, and lethargy [2]. These divergent symptoms depend on the tropism of the specific flavivirus infection; however, both disease progressions have the potential to be lethal. Despite different pathological presentations, all flaviviruses have a highly conserved molecular structure. In general, flaviviruses are 40-65 nm in size and harbor an ~11 kb single-stranded, positive-sense RNA genome. Upon entry into host cells, these genomes are directly translated into a single polyprotein that is subsequently cleaved into ~10 multi-functional proteins [3]. These proteins and their functions are largely conserved across flaviviruses, with some distinct molecular differences.

1.1.1 The Flavivirus lifecycle

Flaviviruses enter specific target cells via attachment and receptor-mediated endocytosis, coordinated largely by the viral envelope (E) and pre-membrane (prM) proteins displayed on the surface of flavivirus virions [3]. Some attachment factors and receptors have been identified for flaviviruses, though they tend to be cell-type and virus-specific. For example, the C-type lectin DC-SIGN enables attachment of both DENV and WNV to dendritic cells and ZIKV into HEK293T cells [4], while the mannose-receptor allows for entry of DENV into macrophages [5]. Moreover, the TAM subfamily of receptor tyrosine kinases, consisting of Tyro3, Axl, and MerTK, have been implicated in the attachment of a broad range of flaviviruses. For example, Axl and its cognate ligand, Gas6, allow for DENV and ZIKV entry into specific host cells [6, 7].

Upon receptor binding, virions are endocytosed in a clathrin-dependent manner. In the low pH environment of the endosome, the viral E protein undergoes a conformational change that allows for fusion between the endosomal membrane and the viral envelope. This fusion process permits the viral RNA to enter into the host cell cytoplasm [8]. Upon entry into the cytoplasm, the flavivirus ~11 kb single-stranded, positive-sense RNA genome is directly translated into one large polyprotein that encodes three structural proteins – capside (C), pre-membrane/Membrane (prM/M), and envelope (E) – and seven nonstructural proteins (NS1, NS2a, NS2b, NS3, NS4a, NS4b, and NS5), which contribute to both viral replication and modulation of host processes (**Fig 1.1**).

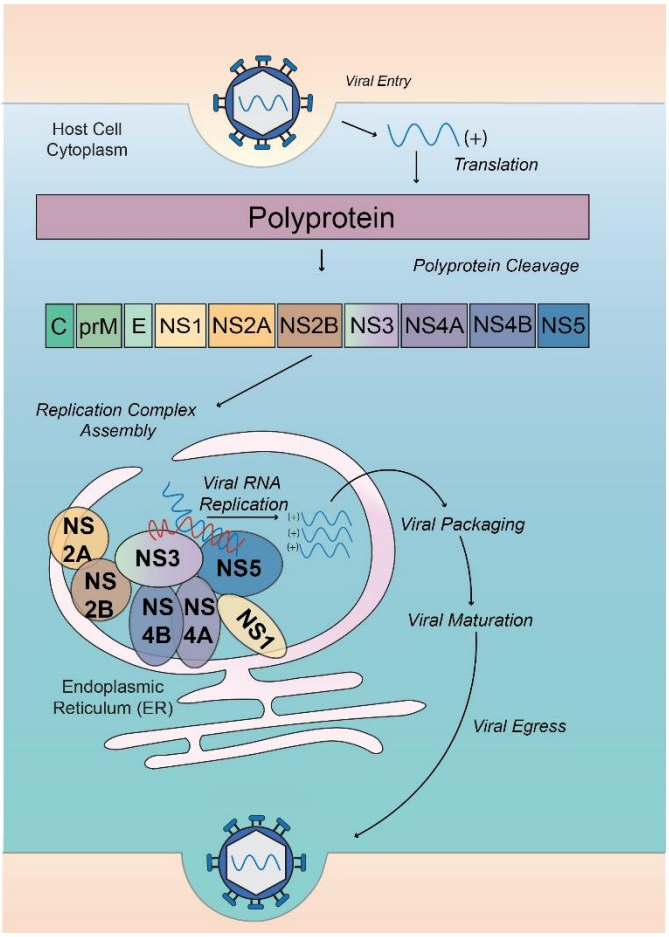

Fig 1.1. Flavivirus polyprotein processing and assembly of the replication complex at ER membrane-derived replication organelles. After viral entry, the host machinery translates the viral genome into a single polyprotein. This polyprotein is subsequently cleaved (by host and viral proteases) into 3 structural proteins and 7 nonstructural (NS) proteins. The NS proteins assemble at the ER membrane, forming replication organelles on which the enzymatically-active replication complex forms. NS2a, 2b, 4b, 4a, and NS1 have transmembrane helices for anchoring into the ER membrane, while the enzymes NS3 and NS5 remain in the replication complex through binding to other NS proteins. The NS5 polymerase synthesizes new genomic positive-sense RNA from the negative-sense anti-genome, while the NS3 helicase domain unwinds dsRNA intermediates that form during replication. After replication of the RNA genome, the RNA is packaged into virions that are secreted from the infected cell through the secretory pathway.

The polyprotein is cleaved by host proteases and the viral protease, NS3, in complex with its essential cofactor NS2b, and this proteolytically-active complex is referred to as “NS2b3”. Cleaved nonstructural (NS) proteins assemble at the ER

membrane, forming a replication organelle (RO) that houses the enzymatically-active replication complex (RC) within remodeled ER-membrane vesicles in the host cytoplasm [2]. These RO's can be further subdivided into vesicle packets (VPs), in which viral RNA replication occurs, and convoluted membranes (CMs), which are less well-defined and are likely the site of polyprotein processing [9]. The key function of these RO's is to concentrate the viral RNA and enzymes of the RC, as well as to shield the viral RNA from host proteases/nucleases and from detection by the host innate immune system [10]. Flavivirus NS4a and NS4b have been shown to play a crucial role in remodeling host membranes to set up the RO [9]. Within the RC, NS3 and NS5 are central to replication of the RNA genome, providing both helicase and RNA-dependent RNA polymerase activities, respectively. These two catalytically-active enzymes interact with each other during viral RNA replication and function to generate a complementary negative strand of RNA ("anti-genome") from which many new positive-strand RNA genomes are produced [2]. In addition to its role as a helicase that unwinds dsRNA intermediates formed by NS5 during replication, NS3 also contains an RNA triphosphatase domain that cleaves nascent RNA, allowing for capping activity by the NS5 methyltransferase domain. Additionally, NS4b acts as an integral membrane protein that binds NS3, forming the RC core. NS2b, in addition to its central hydrophilic domain that functions within the NS2b3 protease, also has two transmembrane domains that anchor it within the RC membrane during replication. NS2a also likely integrates into the RC membrane. Flavivirus NS1, which takes on diverse forms during viral replication, also localizes to the replication complex, acting as a cofactor for viral replication [11].

Outside of their roles in replication, NS proteins have been shown to play many other roles during infection. In particular, NS1 can act as a secreted hexameric protein, playing both an immune evasion role by targeting the complement system, as well as an immunogenic role by activating TLR4 [12]. Recently, a new role for NS1-induced hyperpermeability of endothelial cells suggests a mechanism for fluid extravasation from tissue, a severe pathology of flavivirus infection [13]. Additionally, NS3, NS4a, and NS4b have been shown to play roles in lipid metabolism, potentially to provide membranes for replication complex assembly [14, 15]. Further, both NS2a and the transmembrane domain of NS2b have been linked to viral assembly and the formation of new viral particles [2].

The flavivirus RNA contains a type 1 cap at its 5'-end but lacks a 3'-poly-adenylated end. The RNA genome contains only one open reading frame encoding the single polyprotein, with a long 5' and 3' untranslated region (UTR) that contain elaborate secondary structures. The 5'-UTR has two conserved stem-loop (SL) structures, SLA and SLB, while the 3'-UTR has three distinct regions of stem loops. The first 3'-UTR region contains highly variable stem loops that are resistant to degradation by host exonuclease Xrn-1, and are therefore referred to as “xrRNA-1” and “xrRNA-2” [16]. Interestingly, when the host Xrn-1 stalls at these two RNA structures, subspecies of RNA can be generated, called subgenomic flaviviral RNA (sfRNA), which have been shown to promote viral replication and pathogenicity [17-19]. The second 3'-UTR region contains two tandem dumbbell (DB) structures, called DB1 and DB2, which are further stabilized by two RNA pseudoknots. These pseudoknots have been shown to play a functional role during viral RNA replication, translation, and generation of sfRNA.

The third domain of the 3'-UTR contains a large and highly conserved stem loop, called “3′SL”, which has been shown to interact with host and viral proteins to modulate RNA synthesis and translation. Interestingly, the entire RNA genome has been proposed to exist as either a linear or cyclized form, in which base pairing occurs at inverted complementary sequences of the 5' and 3' UTR. Genome cyclisation likely acts as a switch from viral RNA replication (on cyclized forms) to polyprotein translation (on linearized forms) [16].

Concomitantly with viral RNA replication, a single copy of the genomic RNA is packaged into the mature virion at ER membranes of the RO. The virion is comprised of the three viral structural proteins: C, prM/M, and E. The newly-synthesized single copy of genomic RNA is bound by 60 capsid dimers in a process called “encapsidation”. During encapsidation, the transmembrane α5 helix of the C protein is proteolytically processed by flavivirus NS2b3 and host signalase, allowing for capsid dimerization. At the same time, prM-E glycoprotein heterodimers start to trimerize and assemble on the nucleocapsid, with the transmembrane domains of the prM-E forming “trimeric spikes” that bind to the dimerized C proteins [20]. These immature virions, containing 60 heterotrimeric spikes of prM and E subsequently acquire host ER-derived membranes by budding into the ER lumen. Assembled virions exit the host cell via the secretory pathway, which involves passing through the highly acidic trans-Golgi network (TGN). Within the low pH environment of the TGN, the E protein undergoes conformational changes and the prM protein exposes a cleavage site that is recognized by the host protease furin. Cleavage of prM to M by furin is required for mature virion production, causing the virus to obtain a smooth fusogenic, infectious

surface for subsequent host cell infection [1, 21]. Upon egress through the secretory pathway, viral particles are exocytosed to begin a new infection cycle.

1.1.2 The Flavivirus NS3 protein and its functions

The flavivirus NS3 protein is a 68-75 kDa multi-functional protein composed of two major domains, the N-terminal chymotrypsin-like serine protease domain and the C-terminal DEAH-like SF2-family member helicase domain. NS3 is well-conserved, with approximately 67% sequence identity across mosquito-transmitted flaviviruses. The N-terminal protease domain (residues 1-169) contains a chymotrypsin-like fold and a catalytic triad composed of a histidine, aspartic acid, and serine residue. Importantly, the NS3 protease domain is not catalytically active unless it interacts with its NS2b cofactor, which facilitates the folding of the NS3 protease and stabilizes its catalytic triad [2].

The C-terminal helicase domain (residues 179-618) possesses three essential catalytic activities: (1) dsRNA helicase unwinding activity, to provide single-stranded templates for replication by the NS5 polymerase domain, (2) NTPase activity, to cleave ATP and power helicase unwinding, and (3) RTPase activity, to prime nascent RNA strands to allow for capping by the NS5 methyl-transferase domain. The NS3 helicase domain contains three subdomains: subdomain 1 and 2, which possess RecA-like folds (a hallmark of SF2 helicases) and eight conserved motifs (I, Ia, II, III, IV, Iva, V, VI), and subdomain 3, which is unique to viral/DEAH-like helicases. Subdomain 1 and 2 form an ATP binding site between them, while the third subdomain functions to form the RNA binding tunnel between itself and subdomains 1 and 2. During viral RNA replication, the NS3 helicase first interacts with double-stranded RNA at a region between subdomain 2 and 3, known as the helical gate, which contains a structural feature known as the “β-

wedge/hairpin" or the "RNA binding loop" (res 244-255) [22]. Currently, it is not clear exactly how NS3 recognizes its RNA substrate, and whether a dsRNA substrate can be unwound directly or if it must first be processed to provide a single-strand for helicase loading. *In vitro* studies have revealed a preference for the NS3 to load onto a 3′ overhang at the end of dsRNA [23]. Nevertheless, after NS3 loading onto viral RNA, the third subdomain shifts to allow for accommodation of a single RNA strand, while the β-wedge/hairpin separates the dsRNA as NS3 traffics along the strand, allowing the negative-sense RNA to pass out of the complex through the RNA binding tunnel. Unwinding occurs in a 3'→5' direction, with an 11 bp step size, and is powered by the catalytic ATPase activity [24]. The coupling of RNA unwinding and ATPase hydrolysis by the NS3 helicase is still not entirely understood. A variety of crystallographic studies have predicted that the NS3 enzyme unwinds one base-pair of RNA per ATP hydrolysis event, though the mechanism of translocation (ie, Brownian or backbone stepping motor) of NS3 unwinding is still contested in the field [25]. However, molecular dynamic stimulations suggest that binding to the RNA substrate alters the water molecule positioning and dynamics within the ATPase site, potentially stimulating the ATPase cycle [25]. More specifically, upon RNA binding, the E285 residue, positioned in the rear of the ATPase active site, shifts to act as a nucleophilic base for ATP cleavage [22, 25]. The two catalytic domains (protease/helicase) of NS3 are combined by a flexible linker region (res 169-179), allowing for both activities to be maintained either separately and concomitantly [26]. Some studies have shown that activity of the NS3 protease domain can enhance the activity of the NS3 helicase dsRNA unwinding function, while other studies have shown no influence of the protease domain on helicase function [26-28].

In terms of the residues of NS3 that play a role in RNA binding, crystal structures of various flavivirus NS3 proteins have identified residues in subdomain 1 motif 1a and subdomain 2 motifs IV, IVa, and V as important for providing contact with the phosphodiester backbone of the nucleic oligomer [22]. Tian et al. published the first ZIKV NS3 helicase structure that was bound to ssRNA, in this case, a 12-mer synthetic RNA substrate. Compared with its apo-form, the ZIKV helicase underwent robust conformational changes to accommodate the RNA, in a “double-leaf swing gate” mechanism, with subdomain 2 and 3 moving in the reverse direction of each other. This rotation in the ZIKV helicase was quite distinct from DENV helicase’s rotation from the apo to the RNA-bound state. Interestingly, while the residues near the RNA binding region are well conserved at the sequence level between ZIKV and DENV, the RNA recognition mode highlighted by the two RNA-bound NS3 structures differed from each other. For example, the side chain of K431 in the ZIKV helicase points inwards and forms a salt bridge with side chain D410, while the DENV NS3 corresponding residue (K430) projects its side chain into the solvent [29]. Based on this structure, Xu et al. tested the function of these two residues, K431 and D410A, in terms of RNA binding and unwinding. As the structure predicted, a bacterially-purified NS3 K431A or D410A mutant both had reduced RNA binding capacities compared with NS3 WT, as determined by fluorescent polarization. Likewise, the dsRNA unwinding ability of both mutants was also reduced, suggesting these residues play a bonafide role in RNA binding of the bacterially-purified NS3 helicase domain [23].

In addition to RNA binding residues predicted by the ZIKV helicase crystal structure, RNA binding residues in other flavivirus NS3 have been previously identified. For

example, mutation of a conserved R/K residue in motif IVa of multiple flavivirus helicase domains (DENV4 R387M, WNV R388M, HCV R393A) has proven important for RNA binding [25, 28, 30, 31]. The first study found that mutation of a neighboring residue of this conserved dipeptide in *E. coli*-purified HCV NS3 (Y392A) reduced duplex unwinding activity (ssDNA), single-stranded polynucleotide binding capacity, and polynucleotide-stimulated ATPase activity [31]. More recently, Davidson et al. used molecular dynamics simulations of the DENV NS3 protein bound to a 7-bp long RNA and found DENV NS3 R387 stabilized RNA through interaction with the RNA phosphate backbone. This interaction led to a hypothesized step of NS3 translocation along RNA, linked with NTPase activity. The authors hypothesized that upon DENV NS3 binding to ssRNA, the R387 residue shifts from the “up” conformation to a “down” conformation. When transitioning to the “down” conformation, R387 goes from binding the RNA phosphate background residues P1 and P2 to binding P3 and P4, while the neighboring K388 motif fills in for the R387 “up” position by binding P1 and P2. These two residues are highly conserved in the NS3 SF2 helicase subfamily, with K388 more solvent exposed than R387, allowing for its fluctuation around the phosphate groups of the RNA. Further, these molecular dynamic simulations suggested that the NS3-mediated NTP binding and hydrolysis power the R387 shift from “up” to “down” position, and thereby power translocation along viral RNA [25]. Supporting this hypothesis, Lam et al. found that the cognate residue in HCV NS3 (R393), when mutated, resulted in abrogation of nucleic binding, translocation, and unwinding functions [30]. For ZIKV, the ssRNA-bound NS3 structure also shows R387 in the “down” conformation [29]. Additionally, mutation of WNV NS3 R387 to methionine resulted in completely abrogated replication of a WNV replicon.

A mechanistic look into this defect found that RNA binding and RNA unwinding were reduced by the R387M mutation [28]. Therefore, this “arginine fork” likely plays an important role in the helicase function of the NS3 protein.

In addition to RNA binding, several studies have shown that NS3 directly binds to the viral RNA-dependent RNA polymerase NS5, and that this interaction modulates the enzymatic activities of both proteins. As early as 1995, Kapoor et al. reported the interaction of DENV NS3 and NS5 by co-immunoprecipitation (co-IP) and immunofluorescence (IF) studies in DENV-infected cells. Moreover, DENV NS3 only bound to NS5 purified from cytoplasmic extracts, as NS3 does not localize to the nucleus, although NS5 does [32]. Further, in 2008, Chen et al. found that after UV-crosslinking, both JEV NS3 and NS5, likely within a protein complex, immunoprecipitated with the plus-strand 3′ noncoding region of the JEV ssRNA genome [33].

Moreover, studies have shown that the interaction between NS3 and NS5 stimulates the enzymatic activity of NS3. Zou et al. found that mutation of DENV NS5 K330 to an alanine residue resulted in completely abrogated DENV replication by plaque assay and IF of a GFP virus, but only mildly reduced RNA-dependent RNA polymerase activity (by 20%) and ZIKV RNA production. Interestingly, revertant virus analysis over passaging revealed that an NS5 G840R compensatory mutation rescued the replication defect of the K330A virus. This phenotype was subsequently linked the restored ability of NS5 to bind to both the full-length NS3 protein and the NS3 helicase domain alone [34]. This data suggested that the K330A virus was defective in NS3-NS5 binding, supporting previous results that predicted that the NS5 residues 320-368 are responsible for mediating the DENV NS5 interaction with the NS3 helicase domain [35].

As far as the region of NS3 required for NS5 binding, Tay et al. showed by competitive NS3-NS5 ELISA that the C-terminal region of NS3, specifically residues 566-585, is important for NS5 binding, since a peptide encoding this region disrupted the DENV NS3:NS5 interaction. Moreover, a peptide encoding the region 566-585 containing a N570A mutation could no longer disrupt this interaction, suggesting that the N570 site of DENV NS3 facilitates its interaction with NS5 [36]. The interaction between NS3 and NS5 can also facilitate NS3 enzymatic activity, as the unwinding activity of ZIKV NS3 was enhanced by two-fold in the presence of ZIKV NS5 *in vitro*. Additionally, mutation of NS3 N569 and E573 to alanines reduced *in vitro* binding of bacterially-purified NS3 and NS5 binding by western blot [23]. In summary, these results suggest that the C-terminal region of NS3 (566-585) – especially residues N569/N570 (ZIKV/DENV) and residue E573 (ZIKV) – facilitates the interaction with NS5, dependent on NS5 residue K330, and that this interaction may enhance the enzymatic activity of both of these proteins [23].

Outside of its role in RNA replication, flavivirus NS3 also plays a role in RNA genome encapsidation and virion assembly. During encapsidation, the capsid protein is cleaved by NS2b3 on the cytosolic side of the RO, followed by an additional cleavage by host signalase in the ER lumen. This coordinated cleavage has been shown to be essential for proper virion assembly [37]. Additionally, flavivirus NS3 alone has been implicated in virion assembly, as mutations in the NS3 protein result in poor production of functional viral particles. For example, Patkar et al. (2008) showed that a single mutation in the YFV NS3 helicase domain reduced virus production [38]. Moreover, Gebhard et al. identified a novel proline-rich N-terminal unstructured region of DENV NS3 that contains several amino acid residues involved in infectious particle formation [39]. It has also been

hypothesized that the NS3 helicase domain interacts with the bonafide packaging protein NS2A, since an assembly-defective YFV virus, harboring a mutation in NS2A, was rescued by a compensatory mutation in NS3 [40].

While NS3 plays myriad roles in the replication cycle of flaviviruses, it also has several functions that alter host pathways during infection. For example, DENV NS3 has been shown to stimulate fatty acid biosynthesis at sites of viral replication. As part of an RNAi screen for DENV host factors, Heaton et al. discovered that fatty acid synthase (FASN) is required for DENV replication. Further, DENV NS3 was found to bind to FASN and stimulate fatty acid biosynthesis, likely to increase the surface area of remodeled membranous structures that form the RO at the ER [14].

Additionally, flavivirus NS3 has been shown to manipulate the host innate immune response to viral infection. Early defense against viral pathogens is exerted by the innate immune system, which is comprised of pattern-recognition receptors (PRRs) that serve to detect conserved features of invading pathogens, universally called pathogen-associated molecular patterns (PAMPs). While many different PRRs exist in mammalian species, they all serve to activate transcription of type I IFNs (*e.g.,* IFN-α subtypes and IFN-β) and other antiviral genes, whose transcription is mediated by IFN-regulatory factors (IRFs). IFN-α/β secreted from the infected cell binds to the IFNα/β receptor (IFNAR) on either the same cell or neighboring uninfected cells, thereby mediating autocrine and paracrine antiviral effects [41]. Activation of IFNAR induces a second transcriptional cascade that is mediated by signal transducer and activator of transcription factor 1 and 2 (STAT1 and STAT2) and results in the upregulation of many antiviral factors, generally known as IFN-stimulated genes (ISGs). In terms of RNA virus detection,

the RIG-I-like (RLR) sensors, with the primary members being RIG-I and MDA5, play a major role in detecting viral RNA in the cytoplasm [42]. Upon activation by viral RNA, RIG-I and MDA5 translocate from the cytosol to mitochondria and mitochondria-associated membranes where they interact with mitochondrial antiviral signaling (MAVS) protein, causing it to form large protein 'filaments', which then signal further downstream to ultimately trigger transcription of IFNs and other cytokines as well as ISGs [43]. This cytosol to mitochondria translocation of RIG-I and MDA5 is mediated by host chaperone proteins 14-3-3ε and 14-3-3η, respectively [44, 45]. Recent work showed that ZIKV is able to counteract RIG-I- and MDA5-mediated innate immunity by disrupting the interactions of both RLRs with their respective scaffold proteins, 14-3-3ε and 14-3-3η [44-47]. Knockdown of 14-3-3ε and 14-3-3η in SVGA cells strongly diminished ZIKV-induced antiviral gene expression to levels consistent with RIG-I or MDA5 silencing. Conversely, ectopic expression of 14-3-3ε or 14-3-3η reduced ZIKV replication, suggesting that these two scaffolding proteins restrict ZIKV infection by participating in the RLR-mediated IFN induction pathway. ZIKV NS3 was shown to competitively bind to 14-3-3ε via a phosphomimetic motif, in which the conserved cellular 14-3-3 binding domain Rxx(pS/pT)xP (where 'x' indicates any residue and 'pS/pT' indicates a phosphorylated serine or threonine residue) is mimicked by the presence of a phosphomimetic 64-RLDP-67 motif in NS3, resulting in inhibition of 14-3-3ε-mediated cytosol-to-mitochondria translocation of RIG-I [46]. ZIKV NS3 was also shown to bind 14-3-3η via its phosphomimetic motif and to inhibit the relocalization of MDA5 from the cytosol to mitochondria, and subsequent antiviral signaling. Infection with a recombinant ZIKV harboring a mutated 14-3-3-binding motif (64-RLDP-67 → 64-KIKP-67) enhanced

cytokine and ISG induction and reduced viral replication compared to its WT counterpart, supporting the importance of RLR/14-3-3 inhibition for IFN antagonism during ZIKV infection [46]. The evasion of RIG-I sensing by competitive binding of NS3 to 14-3-3ε is also conserved in DENV and WNV [47].

1.1.3 Zika Virus (ZIKV) Epidemiology and Tropism

ZIKV is primarily spread through the *Aedes* species of mosquito, which thrives in tropical climates. Since its discovery in 1947, ZIKV infection in humans has been historically linked to sporadic cases of self-limiting symptoms such as fever, rash, and conjunctivitis [48]. After a 2013 outbreak in French Polynesia, ZIKV infection was associated with neurological complications in adults, including acute paralysis and the Guillain–Barré syndrome [49]. Following the onset of a widespread 2015 epidemic in South America, ZIKV was identified as a causative agent of severe birth defects, such as microcephaly and cerebral calcifications, following *in utero* exposure to the virus [50-52]. While the increase in herd immunity over the past several years has reduced the number of human ZIKV infections worldwide, ZIKV remains a public health threat, given its potential for re-emergence [1].

ZIKV has a broad cell tropism *in vitro*, infecting human skin cells, such as dermal fibroblasts and epidermal keratinocytes; human myeloid cells, such as dendritic cells (DCs) and macrophages; and human progenitor cells of neuronal, placental, and testicular origin [53]. In order to gain access into specific target cells, including human microglia, astrocytes, and fetal endothelial cells, ZIKV is bound by Gas6, a ligand that recognizes phosphatidylserine on the viral membrane, which subsequently binds to its receptor Axl [6]. This bridging activity provided by Gas6 allows ZIKV to indirectly interact

with Axl, facilitating entry into the cell [6, 7]. In *in vivo* settings, ZIKV has been detected in the brain and spinal cord as well as in several cell types of both male and female reproductive tissue [6, 7, 53, 54].

1.1.4 West Nile Virus (WNV) Epidemiology and Tropism

West Nile Virus (WNV) was first discovered in the West Nile district of Uganda in 1937, though it has since spread to many regions across the African continent, several regions of Asia and Europe, and sporadically to the United States, Central America, and Canada. In 1999, WNV was detected in New York City, resulting in the largest epidemic of neuroinvasive WNV disease ever reported worldwide. The original detection of WNV in the Western hemisphere was based on epidemiological evidence of several patients presenting with meningoencephalitis and muscle weakness in the city. At the same time, an enhanced number of deaths in birds were also observed [55].

WNV typically spreads to humans by the bite of an infected mosquito (largely of the *Culex* family) after feeding on infected birds such as crows and jays. The *Culex* species of mosquito thrives in cooler climates than do *Aedes* mosquitos, allowing for the Northern spread of the virus to areas such as the USA and Canada. Humans, horses, and other mammals are considered “dead-end” hosts, as the levels of WNV in the blood do not reach high enough levels for transmission amongst mammalian hosts (by a mosquito vector). Between humans, WNV is primarily spread by blood transfusion and organ transplantation [56]. However, there have been some reports of spread through breast feeding and transplacental transmission [55].

Most cases of WNV are associated with asymptomatic progression; however, around 20% of infected human patients present with neurological complications, such as

fever, headache, demyelination of peripheral nerves (Guillain-Barre syndrome), and seizures. In 1-2% of these cases, severe neurological symptoms such as meningitis and encephalitis can develop. Of the WNV cases with CNS involvement, about 10% are lethal infections. In fatal WNV cases, autopsies confirm the diffuse inflammation of the brain and spinal cord, resulting in extensive neuronal degeneration [55].

Tissue tropism of WNV in *in vivo* mouse models has found broad tropism for WNV infection, in nearly all tested tissues, including heart, lung, kidney, pancreas, and more. Moreover, the clinical presentation of lethal encephalitis caused by neuroinvasive WNV in humans is mirrored in the WNV mouse model. However, spread to the liver, a hallmark of flaviviruses such as DENV and YFV, has not been detected during WNV *in vivo* [57]. *In vitro* cell lines used to study WNV replication dynamics typically focus on neuronal cell types [56].

1.1.5 Antiviral drugs and vaccines

In general, there are no specific, marketed antiviral drugs targeting mosquito-transmitted flaviviruses for post-exposure patients, though several vaccination strategies have been developed for the prevention of a few of these viruses.

The design and development of small molecule anti-flaviviral therapeutics have focused largely on direct targeting of crucial enzymes of the flavivirus life cycle. While inhibitors targeting several flavivirus proteins, such as the E protein and the C protein have been developed, the two most attractive and widely targeted viral enzymes are NS3 (protease/helicase) and NS5 (polymerase) [58].

NS3 is a major target for anti-flaviviral drug design due to its essential function within the viral lifecycle. In general, the conserved active site of the NS3 protease domain

has been the main focus of drug design. However, there has been limited success in these developments due to the shape of the active site and the permeability of the required charged cleavage substrates. However, some progress has been made for a few inhibitors that compete with substrates of the NS3 protease active site. The most promising candidate is novobiocin, a previously-approved FDA drug that shows significant inhibition of the ZIKV NS3 protease activity. On the other hand, non-competitive inhibitors that allosterically inhibit the NS2b3 protease have also been developed, and these have better permeability and inhibitory activities due to bypassing the need for direct active site targeting. Despite these promising steps towards a flavivirus NS3 inhibitor, effective compounds have only been tested in cell-based assays and must be further investigated for their therapeutic potential in a human host, which relies on factors such as cytotoxicity, cell permeability, and stability. Likewise, these inhibitors harbor a high risk for adverse effects in humans due to the high structural similarity between host and viral serine proteases [59].

In addition to targeting the NS3 protease, many drug development strategies have focused on targeting the essential helicase role of NS3. Drugs that target the unwinding activity of helicases typically act to (1) inhibit ATPase activity by blocking ATP binding and/or hydrolysis, (2) prevent nucleic acid binding, or (3) block translocation of the helicase along nucleic acid. However, the ATPase site of the NS3 helicase is highly similar to those of host helicases, and compounds targeting this region would likely be cytotoxic to the host [60]. Likewise, the lack of a clear mechanism and conserved sequence for viral NS3-mediated RNA binding and unwinding has impeded drug development efforts towards this end [59].

In terms of the NS5 RNA-dependent RNA polymerase, the largest and most highly conserved flavivirus enzyme, several RNA replication inhibitors have been characterized using viral replicon systems in cell-based assays [60]. Most of these studies have focused on the NS5 polymerase active site for drug targeting; however, like the NS3 protease active site, this site has high similarity to host polymerases. Nevertheless, NS5 polymerase inhibitors have been shown to be therapeutic in human HCV infections [61] as well as ZIKV infections in mice [62]. Moreover, virtual and *in silico* screening has identified potential inhibitors of the ZIKV NS5 MTase domain [63] and allosteric inhibitors of the DENV NS5 active site [58, 64].

Despite the long journey towards development of targeted antivirals, prevention of flavivirus infection by vaccination has yielded a promising field of therapeutics. The most successful of these are the YFV and JEV vaccines. The 17D vaccine is a live-attenuated vaccine that has been marketed for the prevention of YFV since the 1930's. The 17D vaccine strain was obtained by serial passaging of the wild-type YFV Asibi strain in chicken tissues, and this resultant vaccine strain stimulates a robust immune response in humans without causing adverse effects. Currently, a single immunization can provide a lifelong immune response. Likewise, the SA14-14-2 vaccine, marketed for prevention of JEV infection, was also obtained by serial passages of the virulent JEV SA14 strain in hamster kidney and chick embryo cells [65].

Additionally, DENV, which causes the majority of human pathogenesis out of all mosquito-transmitted viruses, has one licensed, FDA-approved vaccine called Dengvaxia, which is available in 11 countries where DENV infection is endemic. Dengvaxia is a tetravalent, live-attenuated dengue vaccine that replaces several

sequences of the YFV 17D vaccine strain with homologous sequences from the four dengue virus serotypes. However, Dengvaxia is available only for patients aged 9-16 who have laboratory-confirmed previous DENV infection and live in an area where DENV is endemic. Some live-attenuated vaccines are currently in development for the prevention of DENV infection, though these pose risks due to the potential of antibody-dependent enhancement and virulence-restoring mutagenesis. Currently, TV003, a tetravalent DENV vaccine shows significant antibody responses after a single dose in phase II human clinical trials [66, 67]. Moreover, DENVax, a weakened DENV-2-based vaccine that harbors recombinant prM and E proteins with features of the other three serotypes, has also shown promise in clinical trials. A few additional inactivated, recombinant protein, and DNA plasmid-based DENV vaccines are also currently in clinical trials [68].

Currently, there are no available WNV vaccines for human use, although several WNV vaccines have been licensed for veterinary use and a few WNV vaccine candidates have shown promise in human clinical trials. For example, the ChimeriVax-WN02 vaccine, a live-attenuated vaccine developed by Sanofi, encodes the WNV prM and attenuated E protein in the backbone of the 17D YFV vaccine strain. This vaccine was highly immunogenic in phase II clinical trials. Another live-attenuated vaccine developed by the National Institute of Allergy and Infectious Diseases (NIAID) is based on recombinant insertion of the WNV prM and E genes into the attenuated DENV vaccine strain (DENV4Δ30) backbone. This vaccine candidate is currently in phase I clinical trials. Finally, an inactivated WNV vaccine, a DNA plasmid-based vaccine, and a purified recombinant WNV subunit vaccine are all in Phase I clinical trials [69].

Akin to WNV, there are no ZIKV vaccines yet marketed for human use. However, one inactivated ZIKV vaccine has been tested in preclinical studies and has completed multiple phase I clinical trials. This vaccine was well-tolerated and elicited a robust neutralizing antibody response in healthy adults. However, the lack of an ongoing epidemic has slowed this vaccine's progress to market. Additionally, two DNA-based vaccines and an mRNA vaccine candidate are in preclinical trials [69].

1.2 Post-translational Modifications (PTMs)

Post-translational modifications (PTMs) refer to the addition of a chemical, small molecule, or even small protein, to an amino acid side chain of a translated protein. Currently, more than 400 different types of PTMs have been identified, modulating a multitude of downstream protein functions [70]. Due to recent advances in high resolution mass spectrometry (MS) approaches, the molecular understanding of PTMs is continually growing. Common chemical group modifications include phosphorylation (the most highly-studied PTM), methylation, oxidation, and acetylation. On the other hand, small molecule modifications can take the form of sugars, in the case of N-linked and O-linked glycosylation, or lipids in the case of S-palmitoylation, myristoylation, and prenylation. Finally, ISGylation, SUMOylation, and ubiquitination are some representative PTMs involving the addition of a small protein- ISG15, SUMO, and ubiquitin, respectively - to the recipient amino acid side chain [70]. Generally, addition and reversible removal of these side chain modifications are carried out by special classes of modifying enzymes – or "PTMases"—that are specific to the type of modification. Each of these diverse PTMs act to functionally modify a myriad of protein functions, thereby diversifying the functional repertoire of the proteome. Some exemplary protein functions controlled by PTMs are

signal transduction, gene expression, cell-cycle control, subcellular localization, and protein-protein/protein-nucleic acid interactions, among many more [71].

1.2.1 PTMs of flavivirus proteins

Many viruses in the family *Flaviviridae* have been found to be post-translationally modified by host enzymes, resulting in modulation of various viral protein activities. The most highly studied flavivirus, HCV, has been extensively characterized as a PTMase target. While some PTMs mediate antiviral restriction of HCV, such as host E6AP-mediated ubiquitination of the HCV core protein, which results in its proteasomal degradation and downstream restriction of viral replication [72], others function to promote viral replication. For example, the host E3 ligase MARCH8 was found to mediate K63-linked ubiquitination of the HCV NS2 protein, mediating its binding to host budding factor ESCRT, and thus successful envelopment of the HCV virion. Interestingly, silencing of MARCH8 also resulted in impaired DENV and ZIKV replication, though the mechanism was not further investigated in the context of these viruses [73]. In addition to ubiquitination of the HCV core protein, Abe et al. found that the host ISGylase HERC5 mediates the ISGylation of HCV NS5a, a membrane-associated RNA binding protein, promoting virus replication by downstream recruitment of the critical proviral host factor cyclophilin A [74]. Moreover, the HCV NS2 protein, in addition to regulation by MARCH8-mediated ubiquitination, has also been found to be palmitoylated during overexpression and also authentic HCV infection. Blocking this PTM reduced NS2-NS3 auto-processing and downstream HCV infection [75].

In addition to HCV, members of the mosquito-transmitted flaviviruses have also been found to be regulated by host PTMases and their associated modifications. For

example, ubiquitination of DENV NS1 was shown to prevent its interaction with NS4b, preventing the formation of the replication complex [76]. Additionally, Hishiki et al. found that depletion of ISG15 during DENV replication reduced viral particle release, suggesting a role for this PTM in controlling the viral replication cycle. Interestingly, during overexpression of ISG15 and candidate proteins NS3 and NS5, ISGylation of both proteins was detected, although the endogenous ISGylation of these enzymes has not yet been reported [77]. In addition to small protein modifications, DENV NS1 has also been found to be post-translationally glycosylated. In fact, DENV NS1 glycosylation enhanced the stability of its hexameric, secreted form and helped aid in immune evasion by binding to complement proteins and mannose-binding lectin (MBL), preventing neutralization by the lectin pathway of complement activation [78]. Interestingly, glycosylation has also been shown to regulate WNV infection, although in a distinct manner from DENV. Glycosylation of the WNV (Sarafend strain) E protein at site S154 was found to be required for successful viral replication, as mutating this site reduced viral replication by plaque assay in multiple cell types [79].

Glycosylation has also been shown to regulate ZIKV replication. Lazear et al. found that modern Asian strains of ZIKV, which are glycosylated at residues N154 and T156 of the E protein, were more pathogenic in IFNAR$^{-/-}$ mice than the historical African lineage strain. Further, mutating these Asian-strain specific glycosylation sites strikingly reduced ZIKV pathogenicity in mice, and diminished the interaction of virions with cells expressing DC-SIGN lectins [80]. In addition to glycosylation of the ZIKV E protein, K63-linked polyubiquitination of the ZIKV E protein at K38 and K281 by the host E3 ligase TRIM7 has also been characterized as a proviral mechanism for enhancing viral attachment and

entry. Interestingly, a portion of viral particles released from infected cells contained poly-ubiquitinated E protein, which enhanced virus entry by mediating TIM1-receptor binding. Moreover, recombinant ZIKV encoding E mutants that lacked the ubiquitinated site(s) were attenuated in human cells and mice, and monoclonal antibodies targeting K63-linked polyubiquitin reduced viremia in mice [81].

Nonstructural proteins of ZIKV have also been suggested as targets for post-translational regulation. In a screen of ISGs, PARP12 was identified as a ZIKV restriction factor, and subsequently, overexpression of PARP12 was found to reduce the protein abundance of ectopic ZIKV NS1 and NS3 by proteasomal degradation, mediated specifically by its PARP domain. Since the PARP domain is known to be able to catalyze poly-ADP-ribosylation (PAR) and ubiquitination, it was tested whether NS proteins of ZIKV were subjected to these modifications when overexpressed along with PARP12. As a result, ZIKV NS1 and NS3 were shown to be post-translationally PARylated when cotransfected with PARP12. Additional overexpression of a K48-only ubiquitin mutant showed enhanced ubiquitination of both NS1 and NS3 during PARP12 overexpression, suggesting that PARP12-mediated PARylation enhances K48-linked ubiquitination and subsequent degradation of NS1 and NS3 through the proteasome [82]. However, the PARylation of these ZIKV proteins during authentic infection has not been tested.

1.2.2 Modulation of protein function by acetylation

Generally, lysine acetylation refers to the co- or post-translational transfer of an acetyl group from the donor metabolite acetyl-CoA onto the positively-charged epsilon amino group of a lysine residue. Addition of this acetyl group functionally neutralizes the positive charge of a lysine residue, which can have many downstream functional

consequences for the acetylated protein. Lysine acetylation is a tightly regulated and enzymatically-reversible modification carried out by two families of host enzymes: lysine acetyltransferases (KATs), which add the acetyl group onto lysines, and lysine deacetylases (KDACs), which remove them. In the process of deacetylation, KDACs utilize either water or nicotine adenine dinucleotide (NAD+) as a co-substrate for removal of the acetyl group. Another enzyme family, called bromodomain-containing proteins, or acetyl-lysine “readers”, are involved in binding to acetylated lysine residues, and are often involved in the downstream functional consequences of lysine acetylation [83]. For example, during lysine acetylation of histone tails, many transcription factors act as “readers” to bind the acetylated lysines and activate transcription of certain genes (described in more detail below).

In general, a major way for identifying PTMs is through MS analysis, in which proteins are trypsinized and their peptides are qualitatively analyzed in a mass spectrometer. Within the mass spectrometer, tryptic peptides are ionized using either electrospray ionization (ESI) or matrix-assisted laser desorption ionization (MALDI), which work to transform biomolecules into charged ions. The ions then travel through a mass analyzer, which can measure time of flight (TOF) or the rotation of the ions around a central electrode (quadrapole), allowing ions be qualitatively-detected based on their mass/charge (m/z) ratio [84]. In terms of acetylation, the addition of the acetyl group imparts a 42 dalton addition and corresponding m/z shift compared to the nonacetylated peptide, which leads to determination of an acetyl group within the peptide. Due to relatively low levels and site occupancies of lysine acetylation, enrichment of such

peptides with anti-pan-acetyllysine antibodies prior to MS analysis have proven effective in enhancing detection [85].

Once identified, functional consequences of acetylation are typically investigated by mutating the acetyllysine site(s) to either arginine(s) or glutamine(s). This is because an arginine residue is a positively-charged amino acid that cannot be acetylated, therefore mimicking a “non-acetylated” lysine residue. On the other hand, glutamine, a neutrally-charged amino acid with a similar structure to lysine, is used to mimic a “hyper-acetylated” lysine residue [86].

Lysine acetylation is an evolutionarily conserved mechanism of regulation, with this PTM being identified to regulate protein function in *E.coli* and *Saccharomyces cerevisiae.* Moreover, KATs and KDACs are also highly conserved from these species through to humans. Indeed, the number of identified acetylation sites increases with the complexity of the organism. For example, 138 acetylation sites across 91 proteins have been identified in *E.coli*, while an organ-wide analysis of rat tissues identified 15,474 acetylation sites across 4541 proteins [87]. The first analysis of the human acetylome, which trypsin-digested whole cell lysates of MV4-11 human acute myeloid cells, found 3600 acetylation sites on 1750 proteins, although this initial study lacked high resolution MS tools available today [88]. A more recent study has identified 4,994 acetylated peptides across 2206 acetylated proteins in human HeLa cells [89].

To mention, proteins can also be regulated by N-terminal acetylation, which utilizes a separate class of PTMases, whereby an acetyl group is donated to the backbone alpha-amino group on the N terminus of proteins, however, this section will focus on only lysine acetylation [83].

1.2.2.1 Host lysine acetyltransferases and deacetylases

The exact number of lysine acetyltransferases is still disputed in the field; however, 13 KATs are considered “canonical” and fall into three families based on the structure and transfer mechanism of their acetyltransferase domains: the GNAT, p300/CBP, and MYST families. However, a slew of “noncanonical” KATs have been discovered, with diverse and unique acetyltransferase activities. Moreover, a class of “putative” KATs, which contain the structural features of an acetyltransferase domain, but do not yet have identified substrates, have also been postulated [90]. Combined, this makes up a class of 22 total human acetyltransferases, although it is likely that more will be discovered.

Nearly all of the canonical KATs localize to the nucleus where they acetylate both histones and non-histone proteins. Most KATs function in larger, multiprotein complexes with many functional subunits that govern their catalytic activity and substrate specificity. Unlike kinases, KATs do not have preferred consensus sequences that designate substrate specificity, making the determination of the KAT responsible for a specific acetylated substrate more difficult. Moreover, the substrate specificity of KATs for their substrates relies more on substrate localization, interacting partners, and solvent-exposed lysine residues. The apparent lack of sequence specificity of substrates may allow for the reported redundant acetylation of a substrate by multiple acetyltransferases [91].

Currently, 18 human-encoded KDACs have been identified, which can be further divided into two classes: the Zn2+-dependent KDACs and the NAD+-dependent sirtuins. The Zn2+-dependent KDACs are considered “classical KDACs” due to their highly conserved deacetylase domain, and this class is further subdivided based on the

subcellular localization of the representative enzymes. Classical KDACs utilize water as a co-substrate for the removal of the acetyl group from acetylated substrates, producing acetate as a byproduct. On the other hand, sirtuins utilize NAD+ as a co-substrate, producing 2′ or 3′ O-acetyl-ADP-ribose as a by-product [83].

1.2.2.2 Histone Acetylation

Acetylation of lysine residues was first discovered in 1964, as a histone-specific modification and subsequently as a mechanism of regulating gene expression at the chromatin level [92]. In fact, KATs were originally termed histone acetyltransferases (HATs), while KDACs were originally termed histone deacetylases (HDACs). All four different histone proteins (H2A, H2B, H3, and H4) have been identified as acetylation substrates by multiple HATs. Histones bind DNA to form nucleosomes, which assemble into distinct chromatin structures that can be transcriptionally active or inactive. Histone acetylation has been shown to play an important role in the assembly and folding of chromatin, as well as in regulating the switch between inactive and active chromatin. At the molecular level, histone acetylation destabilizes the DNA-histone interaction by neutralizing the lysine side chains present in poly-lysine histone tails. This neutralization weakens the ability of the histone tails to form salt bridges with the negatively-charged phosphate backbone of DNA. Acetylation therefore leads to an open and lightly packed chromatin structure, allowing transcription factors to access and bind DNA, recruit RNAPs, and stimulate transcription. Therefore, in general, increased acetylation is associated with enhanced transcriptional activity [93]. In addition to altering the density of chromatin and therefore transcriptional activation, acetylation of histones is also highly

important for recruiting bromodomain-containing proteins and transcription factors that recognize and bind to acetylated lysine residues [83].

1.2.2.3 Acetylation of Cellular Proteins

Lysine acetylation regulates the function of a wide variety of cellular proteins and enzymes. In general, lysine acetylation plays an important role in regulating metabolic processes, considering its cofactor acetyl-coA (Ac-CoA) is a common metabolite that provides the acetyl group to the citric acid cycle to be oxidized for energy production. Ac-CoA is produced by the breakdown of carbohydrates through glycolysis and fatty acids through β-oxidation. The breakdown of acetyl-CoA within the citric acid cycle is achieved through oxidation of the acetyl group to carbon dioxide and water, producing 11 ATP molecules and one GTP molecule per acetyl group. While non-enzymatic acetylation of proteins can occur, this typically occurs in areas of high acetyl-CoA concentration, such as the mitochondria. Substrates that are regulated by non-enzymatic acetylation tend to be those that are highly controlled and affected by metabolic perturbations [83].

After the discovery of histone acetylation in 1964, the first non-histone cellular substrates to be identified as lysine acetylation substrates were high-mobility group (HMG) proteins and tubulin. In the 1990s, acetylation of the transcription factor and tumor suppressor protein p53 was discovered, followed by the identification of the first mammalian KATs and KDACs [91]. Lysine acetylation of non-histone substrates has now been shown to regulate several major functional networks through manipulation of a variety of protein functions (**Fig 1.2**).

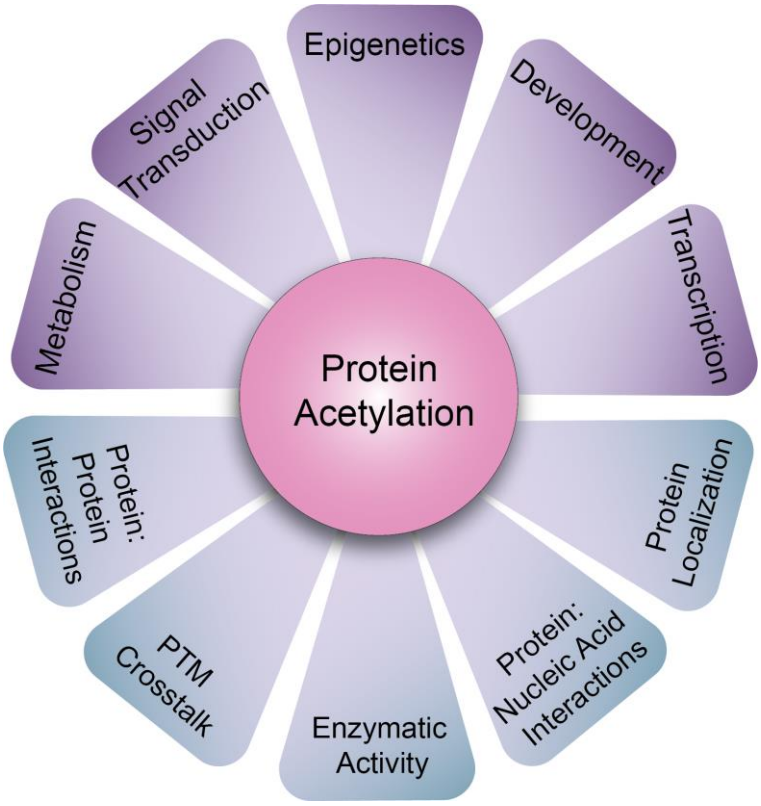

Fig 1.2. Lysine acetylation controls diverse cellular networks by regulating various protein functions. Representative cellular networks that are composed of many protein targets for post-translational lysine acetylation are depicted in purple. Lysine acetylation can manipulate these cellular processes by modulating the representative protein functions depicted in blue.

Moreover, dysregulation of these signaling networks has been shown to play a role in some human diseases. For example, germline mutations in KATs CBP, p300, KAT6A, and KAT6B result in disorders associated with developmental delays and intellectual disabilities. Moreover, somatic mutations in CBP and p300 are frequently linked to leukemia, due to their enzymatic roles in acetylation of tumor suppressor p53. Given their role in human disease, several KAT inhibitors have been developed, including the

CBP/p300-targeting molecule A485, which has anti-proliferative effects in tumor cell lines. Moreover, inhibitors of KAT6A/B reduced tumor growth during lymphoma in mice [83].

While acetylation of protein substrates has a major role in regulation of various protein functions, this section will focus on those related to the thesis work presented herein, namely, regulation of cellular helicases and RNA-binding proteins by acetylation.

1.2.2.3.1 Acetylation of Cellular Helicases

Acetylation has been reported as a regulatory mechanism for controlling several enzymatic activities of cellular DNA and RNA helicases. For example, the p300 acetyltransferase was found to acetylate the host Dna2 helicase, stimulating its 5′-3′ endonuclease and helicase activities by enhancing the affinity for DNA substrates [94]. However, the basis for this enhanced DNA binding affinity was not investigated at the molecular level. Moreover, WRN, a cellular DNA helicase with 3′-5′ helicase and exonuclease activity important for maintaining genomic stability in response to DNA damage, represents another major helicase target for regulatory acetylation. In fact, several studies have shown that acetylation of WRN regulates its translocation from the nucleus to the nucleolus [95], stimulates certain catalytic activities (such as strand displacement) [96], reduces other catalytic activities (such as exonuclease activity) [95], and promotes its stability by inhibiting ubiquitination at acetyl-lysine sites [97]. On the other hand, cellular RNA helicases DDX5 (p68), DDX17 (p72), and DDX3X have also been found to be acetylated. Of these, p68/72 were the first RNA helicases to be reported as acetylation targets. By MS analysis, multiple lysine sites encoded in these enzymes were found to be acetylated during overexpression of p300. Moreover, mutation of some of these acetyl-lysine sites in p68/72 to “non-acetylated” arginines increased their

degradation, suggesting that acetylation may stabilize these proteins by acetylation of lysines that would otherwise be targeted for degradative ubiquitination. However, other acetyl-lysine to arginine mutations reduced the ability of p68/72 to stimulate transcription of target genes by luciferase assay, suggesting that acetylation of certain lysine residues stimulates the co-transactivational activity of these transcription factors [98]. The RNA helicase DDX3X, a protein involved in the formation of stress granules, was also found to be acetylated at multiple residues, blocking the maturation of stress granules (SGs) in cells [99].

Moreover, the RNA sensor RIG-I, which encodes a DExD/H box helicase domain, has been found to be regulated by acetylation [100, 101], described in the below section.

1.2.2.3.2 Acetylation and RNA binding

While the regulation of protein to DNA binding by acetylation is well-characterized given its fundamental alternation of histone-DNA dynamics, functional examples of acetylation regulating protein-RNA binding are less prevalent. However, several studies have reported modulated RNA binding as a functional consequence of lysine acetylation. For example, Gal et al. showed that SG formation could be regulated by acetylation. SGs are ribonucleoprotein aggregates that form in response to oxidative or osmotic stress and upon viral infection. Formation of SGs functions to store non-essential mRNAs, shifting translation towards transcripts required to survive stress. The G3BP1 GTPase is a major protein component of SGs that binds to mRNAs to control SG dynamics. Interestingly, Gal et al. found that G3BP1 was acetylated in its RNA binding domain at K376. Moreover, they found that, during overexpression, HDAC6 could deacetylate G3BP1 at this residue, while CBP (KAT3A) could enhance acetylation. RNA immunoprecipitation (RNA-IP)

followed by qRT-PCR for the known G3BP1 RNA substrates *c-myc* and *tau* revealed that overexpressed WT G3BP1 co-precipitated more *c*-myc and *tau* RNA than a G3BP1 K376Q mutant (mimicking hyper-acetylation), suggesting acetylation may govern the ability of G3BP1 to bind its RNA substrates. Moreover, the RNA-dependent binding of G3BP1 to another stress granule protein PABP1 was reduced in the K376Q mutant, further supporting that acetylation of G3BP1 reduces its RNA binding affinity. Moreover, less SGs were detected by IF during SG induction with sodium arsenate in knock-in G3BP1 K376Q cells compared with WT cells. Likewise, treatment with a CBP (KAT3A)/p300 (KAT3B) inhibitor, A-485, reduced G3BP1 acetylation and delayed the disassembly of G3BP1 SGs. Finally, by proximity ligation assay (PLA), it was shown that acetylated G3BP1 was primarily found outside of the stress granules, further supporting that acetylation of G3BP1 reduces its interaction with RNA, and therefore, prompts the disassembly of SGs [102]. This study provides a precedent for cytoplasmic acetylation regulating the RNA binding dynamics of a cellular non-histone protein.

The same group also investigated the role of RNA binding regulation by acetylation in a different context. In this study, they found that the “fused in sarcoma” (FUS) protein, which is implicated in the development of amyotrophic lateral sclerosis (ALS), was acetylated within its RNA recognition motif at residues K315/316. This acetylation was subsequently shown to reduce the capacity of FUS to bind to RNA and its RNA-dependent protein binding partner PABP1. The functional consequence of mutating K315/316 to a “hyper-acetylated” glutamine in the background of an ALS-associated mutation reduced the number of ALS-associated cytoplasmic inclusions [103]. While this downstream

consequence is not highly understood, this study furthered the principle of acetylation as a mechanism to reduce protein-RNA interactions.

As mentioned earlier, the DExD/H box helicase-containing RIG-I protein is also regulated by acetylation. During virus infection, binding of viral RNAs to the C-terminal domain (CTD) and helicase domain of RIG-I leads to activation of the ATPase activity, triggering a conformational change to expose the N-terminal CARD domains of RIG-I, which function to interact with downstream signaling molecules that perpetuate the IFN response. Choi et al. found that RIG-I is acetylated within its CTD at K858 and K909, located next to the helicase domain, maintaining RIG-I in its inactive conformation. RIG-I harboring hyper-acetylated mutations in these domains showed a complete abolishment of RIG-I binding to tri-phosphate dsRNA, a well-characterized RNA ligand known to activate RIG-I. Interestingly, upon HDAC6-mediated deacetylation of RIG-I at K909, RIG-I was able to bind viral RNA and to activate its downstream signaling cascade that elicits IFN responses. As a result, HDAC6 was shown to be essential for protection of mice against VSV infection, presumably through its ability to activate RIG-I-mediated sensing and the downstream IFN pathway [100]. Moreover, the regulation of RIG-I by acetylation was also found to control its ability to form homo-oligomers, a crucial step in activation of the IFN pathway, as hyper-acetylated RIG-I mimics did not form these oligomers during viral infection [101].

1.2.2.4 Viral protein regulation by acetylation

Many viral proteins have been identified as targets for acetylation, though functional characterization of these sites is lacking for most viruses except the RNA viruses influenza A virus (IAV) and human immunodeficiency virus (HIV). For example,

the IAV nucleoprotein (NP), important for encapsidating the viral RNA genome, was found to be acetylated at multiple sites during infection. Two of these acetylation sites had no effect when mutated to arginine (non-acetylated), while mutation to glutamine (hyper-acetylated) severely diminished or completely abrogated viral replication, suggesting acetylation regulates viral replication in an antiviral manner. However, acetylation of NP at another residue, K229, was shown to modulate viral particle release. Interestingly, mutation of this acetyl site to both a hyper- and a non-acetylation mimic reduced viral replication, suggesting that the regulation of acetylation at K229 is highly important to achieve efficient viral replication [104]. Moreover, the histone acetyltransferases GCN5 (KAT2A) and PCAF (KAT2B) could acetylate IAV NP during overexpression *in vitro* at additional lysine sites (K31 and K90), increasing or reducing polymerase activity during replication, respectively. However, silencing of GCN5 (KAT2A)/PCAF (KAT2B) did not change the acetylation levels of NP during infection [105].

In addition to the NP protein, the IAV PA polymerase subunit was found to be acetylated, promoting its stability. In turn, HDAC6-mediated deacetylation resulted in PA degradation and viral restriction [106]. Moreover, the NS1 protein of IAV (H1N1), known to robustly inhibit the IFN response during viral infection, was also found to be acetylated at site K108. Here, a mutation mimicking ‘non-acetylation’ reduced NS1-mediated IFN antagonism in a panel of overexpression-based assays, corresponding to abrogated replication of a recombinant virus harboring this mutation [107].

The HIV Tat protein, which is essential for expression of the HIV proviral genome, binds to the trans-activating response element (TAR), an RNA stem loop structure in the provirus, and recruits the transcriptional elongation complex pTEFb, to begin expression

of HIV RNA. Acetylation of Tat at K50 by the p300 (KAT3B) acetyltransferase results in decreased binding of Tat to TAR. Simultaneously, acetylated K50 recruits PCAF (KAT2B), which binds to acetylated Tat via its bromodomain. Binding to PCAF (KAT2B) subsequently recruits RNA polymerase II, resulting in HIV gene transcription [108].

In terms of flaviviruses, lysine acetylation has not been identified as a major regulatory mechanism prior to the work presented herein. However, the HCV NS3 protein was identified to be N-terminally acetylated through MS analysis, although the functional relevance of this modification is unknown [109]. Additionally, tubacin, a chemical inhibitor of HDAC6's deacetylase activity, was found to decrease viral RNA synthesis and replication of JEV, although the mechanism for this viral restriction was not investigated [110].

Moreover, viral helicase acetylation has not been extensively identified or studied prior to the work presented herein. Two acetylation sites have been identified by MS in the Middle East respiratory syndrome coronavirus (MERS-CoV) helicase, but the functional relevance of this modification has not been tested [111]. Moreover, the human papillomavirus (HPV) E2 protein, while not a helicase itself, is acetylated during infection, which has downstream effects on HPV E1 helicase activity. The HPV E2 protein binds to DNA in a sequence-specific manner and recruits the E1 DNA helicase for loading onto the origin of replication of the viral DNA genome. Interestingly, K111 of E2 is acetylated by p300 (KAT3B), and mutation of K111 to a non-acetylated arginine reduced E1-mediated DNA replication at the step of duplex DNA unwinding in a replicon system. In contrast, an HPV K11Q replicon was able to achieve replication similar to the wildtype virus [112].

1.2.3 The host lysine acetyltransferase 5 (KAT5)

Lysine acetyltransferase 5 (KAT5) was originally identified as a single 60 kDa protein that co-purified with the HIV-1 Tat transactivator protein, and thereby was originally named TAT interactive protein 60 (TIP60) [113]. However, subsequent identification of four individual isoforms of KAT5 (described in detail in the next section) has complicated the field of KAT5 functional research, as nearly every published study focuses on only the characterization of the TIP60 isoform, also known as "KAT5α". In this thesis, the individual isoform (if known) will be designated, otherwise "KAT5" will be used to designate all four isoforms, especially in the context of KAT5 gene knockdown/knockout, in which all isoforms are targeted. All KAT5 isoforms encode a MYST domain, which imparts HAT activity; an acetyl-CoA binding domain, which transfers the acetyl group; and a chromodomain, which mediates DNA binding to target promoters [114]. Interestingly, despite its initial discovery as an HIV Tat-binding protein, TIP60/KAT5α has not been found to directly acetylate Tat.

1.2.3.1 KAT5 and its cellular functions

Purified TIP60/KAT5α can acetylate free histones H4 and H2B *in vitro* [115]. Homozygous knockout of KAT5 is lethal in embryonic mice, suggesting the importance of its role in development and differentiation [116]. KAT5's cellular roles are two-fold, as it is both a histone acetyltransferase that activates transcription of various genes, as well as a lysine acetyltransferase that directly modifies various cellular proteins [117]. In terms of its transcriptional role, TIP60/KAT5α functions within a larger, multifunctional protein complex, called the Nu4a complex, which is conserved from yeast to humans. This complex acts as a coactivator of transcription of several highly important genes such as

nuclear hormone receptors, β-catenin, NF-κB, MN-dependent superoxide dismutase, and the c-myc oncoprotein [118].

Two major cellular targets of TIP60/KAT5α regulation by acetylation are p53 and ataxia-telangiectasia-mutated kinase (ATM). Both of these protein targets are activated in response to DNA damage. A DNA break is first sensed by host protein MRN, which recruits ATM to phosphorylate H2AX, leading to the recruitment of DNA repair proteins p53 and Chk2. Activation of the ATM kinase has been shown to be dependent on the HAT activity of TIP60/KAT5α, which forms a complex with ATM. Once ATM is activated, it recruits and activates p53, which can then induce cell cycle arrest through the induction of cyclin-dependent kinase inhibitor p21, apoptosis through induction of Bcl2 members like BAX and PUMA, or senescence through induction of p16/Ink4a and the tumor suppressor gene p19/ARF. TIP60/KAT5α directly acetylates p53 at K120 to promote its downstream pro-apoptotic and cell cycle arrest functions [119]. It has also been shown that TIP60/KAT5α prevents proteasome-mediated degradation of p53 by antagonizing the Mdm2 E3 ubiquitin ligase through direct binding. Further, TIP60/KAT5α has been shown to directly acetylate histone 4 at the *puma* promoter, enhancing *puma* gene expression [117].

In addition to direct acetylation of proteins involved in DNA damage repair, TIP60/KAT5α has also been implicated in recruiting ribonucleotide reductase (RNR) and nucleoside disphosphate kinase 3 (NME3) to sites of double stranded breaks (DSBs), both of which function in the role of dNTP synthesis. KAT5 is likely recruited to the DSB site by binding to methylated histone 3, specifically H3K36me3, mediated by its chromodomain [120]. Moreover, TIP60/KAT5α has been shown to maintain genome

integrity by acetylating Aurora B, which allows for successful chromosome alignment and segregation during mitosis [121].

In normal cells, KAT5 is thought to function as a tumor suppressor because it acetylates the major cell cycle regulator p53 to activate its cell cycle arrest/apoptotic function. In turn, defects in KAT5 expression or function have been associated with the progression of some cancers. For example, heterozygous $KAT5^{+/-}$ mice showed increased penetrance for Myc-induced lymphomagenesis [122] and KAT5 knockdown has been shown to promote melanoma and glioblastoma migration and invasion [123, 124]. In human tissues, advanced stage colorectal cancer, gastric cancer, and breast cancer have been associated with low expression of KAT5. However, in prostrate and gastric cancers, KAT5 has been found to act as an oncogene. In prostate cancer, an increase in nuclear KAT5 has been associated with prostate cancer severity [125]. This phenomenon was further found to be associated with enhanced prostate cancer cell proliferation during overexpression of TIP60/KAT5α through TIP60/KAT5α-mediated acetylation of the androgen receptor (AR) [126].

KAT5 mutations have also been linked to Alzheimer's disease (AD) progression, largely through the APP-Fe65-KAT5 axis. Amyloid-β precursor protein (APP) is a widely-expressed cell-surface protein that, when cleaved by β- and γ-secretase, is secreted as the extracellular amyloid-β peptide, known to aggregate and form plaques in the brain of Alzheimer's patients. Interestingly, the cytoplasmic tail left behind after cleavage, called the APP intracellular domain (AICD), binds to the nuclear adaptor protein Fe65 and TIP60/KAT5α, forming a ternary, transcriptionally-active complex called AFT [127].

Aberrant AFT complex formation has been linked to AD pathogenesis due to the downstream dysregulation of KAT5 neuronal target genes [128].

1.2.3.2 KAT5 isoforms: their domain structures, functions, and regulation.

The myriad cellular roles and associated disease states of KAT5 function have been primarily characterized in the context of only one of four isoforms of KAT5, hereafter called KAT5α, the isoform that runs at 60 kDa and that led to the original "TIP60" naming designation. Importantly, human cells encode four distinct isoforms of KAT5- the long (L), α ("TIP60"), β ("PLIP"), and γ isoforms- which can be visualized individually by Western blot of human whole cell lysates. Compared to the prototypical KAT5α, the proteins KAT5β and KAT5γ lack a segment between the chromodomain and the zinc finger domain, due to exclusion of exon 5, and KAT5L and KAT5γ have an additional 33 aa amino-terminal fragment due to inclusion of intron 1. While the genetic basis determining the production of these isoforms has been determined – which involves the splicing or inclusion of either the alternate intron 1 or exon 5 (or both) of the gene – the potentially diverse functions of these isoforms are not well-characterized.

The second isoform of KAT5 that was identified after KAT5α was the β isoform. This isoform was first identified as a cytosolic phospholipase A2 (cPLA2)-interacting protein (PLIP). When compared to the sequence of KAT5α, KAT5β was found to lack the exon 5 [129], resulting in a 53 kDa protein ("TIP53"). KAT5β was found to localize to the nuclear/perinuclear region of cells as determined by IF during overexpression, potentially recruiting cPLA2 from the cytoplasm to the nucleus during calcium influx, resulting in the induction of cPLA2-mediated prostaglandin E2 (PGE2) and downstream apoptosis [129].

The third isoform of KAT5, also called “KAT5 long (KAT5L)”, was identified through examination of expressed KAT5 mRNAs. It was found that many transcripts still contained intron 1, and that the KAT5 translation initiation codon lies within exon 1, suggesting that this intron could be coded into a distinct isoform of KAT5. Indeed, overexpression of a plasmid construct encoding intron 1 resulted in a larger protein form of KAT5, which had similar stability to KAT5α in a pulse-chase assay [130].

The fourth isoform of KAT5, KAT5γ, has been predicted by the deposited genomic sequence of the KAT5 gene and mRNA transcripts. However, experimental validation and functional characterization of this isoform is greatly lacking.

Interestingly, an additional isoform of KAT5, called TIP55, was identified in mice and shown to be essential for organogenesis. This isoform is not a splice isoform, but rather, a truncated version of KAT5α, encoding only a portion of exon 11 due to early termination of the reading frame [131]. However, this isoform has not been identified in humans.

In terms of the subcellular localization of the various KAT5 isoforms, results are still unclear and may be cell-type specific. Furthermore, the reported localization for some of these isoforms is derived from overexpression experiments; therefore, validation of endogenous KAT5 isoform localization is largely lacking. In a study of the nuclear Nu4a complex, of which KAT5 is a member, nuclear extracts ectopically expressing both KAT5α and KAT5β co-immunoprecipitated with other nuclear members of the complex in an indistinguishable manner, suggesting that both isoforms are part of a similar, if not identical, nuclear complex [132]. However, Ran et al. showed that overexpression of KAT5α resulted in only nuclear localization by IF in HeLa cells, while KAT5β had both

nuclear and cytoplasmic distribution. The authors hypothesized this difference in localization to the lack of exon 5 in KAT5β, since this proline-rich region may facilitate nuclear protein-protein interactions and thereby retention in the nucleus [133]. However, this has not been experimentally tested. To further add to the complexity of KAT5 localization, two putative nuclear localization signals (NLS) have been identified in KAT5α: 184-PGRKRKS-191 and 295-RKGTISFFEIDGRKNKS-312 [134]. In a separate study, mutation of the first of these putative NLS regions reduced the nuclear localization of KAT5α during overexpression [135]. However, these sequences are conserved in all four isoforms of KAT5, and would not therefore explain potential isoform-specific subcellular localization [134].

The subcellular localization of KAT5L has been shown to be regulated by phosphorylation of Y327. During overexpression, KAT5L (WT) localized to both the nucleus and cytoplasm, while a phospho-deficient mutant KAT5L (Y327F) localized to only the nucleus, reducing its interaction with cytoplasmic Fe65 [136]. In addition to characterizing KAT5L in the cytoplasm, several other studies have identified cytoplasm-specific functions of KAT5. Hass and Yankner found that APP, a binding partner of Fe65, recruited overexpressed KAT5α to membrane compartments in cell culture. Further, they found that KAT5α levels in the membrane fractions of mouse brains were higher in APP-overexpressing transgenic mice compared with age-matched wild-type controls, though membrane localization of KAT5α was also observed in wildtype mice, suggesting a potential physiological role for KAT5 in membrane compartments. Interestingly, the chemical inhibition of the CRM1 nuclear export protein leptomycin B reduced the ability of membranous APP to interact with KAT5α, suggesting the nuclear export of KAT5α is

required for its APP interaction [134]. Moreover, Sliva et al. showed that a single, undescribed isoform of KAT5 can interact with the interleukin-9 transmembrane receptor at the plasma membrane during overexpression [137]. In general, most studies on the localization of KAT5 rely on overexpression, and many more studies are required to distinguish the sequence and/or protein-mediated differences governing the localization of this protein and its isoforms.

Outside of the increasing complexity of distinct KAT5 isoforms and diverse reported localization patterns, KAT5 activity has also been shown to be regulated by a multitude of PTMs. Using precipitation with concanavalin A (conA), a lectin (carbohydrate binding protein) that binds to glycoproteins and protein residues that have been modified by N-glycosylation, Lee et al. found that endogenous KAT5-L (isoform 1) is N-glycosylated at N324, mediating its interaction with binding partner FE65 as well as its auto-acetylation activity. Interestingly, in confocal microscopy studies, overexpressed KAT5α localized to the cytoplasm and nucleus, while the N324A mutant localized mainly to the nucleus. Since N-glycosylation occurs in the ER, this result suggested that N-glycosylation of N324 may promote KAT5 ER retention [138]. KAT5α has also been shown to be SUMOylated at residues K430 and K451 by PIASy, which enhances the downstream K120 acetylation of p53 [139].

Phosphorylation is also a major PTM regulating KAT5 function. Glycogen synthase kinase-3 (GSK-3) [140], p38 MAP kinase [141], and CDK9 [142] have been found to phosphorylate S86, Thr158, and S90 of KAT5α, respectively, activating its transcriptional activity. Phosphorylation of KAT5α S86/S90 is required for downstream acetylation of p53 and histone 4 at the PUMA promoter, and thus the induction of apoptosis following DNA

damage [142]. Phosphorylation of KAT5L (isoform 1) at Y327 by ABL1 kinase increases the abundance of cytoplasmic KAT5 during overexpression, as a Y327F mutant was exclusively localized to the nucleus. Interestingly, the Y327 residue also facilitates KAT5L interaction with FE65, which is expressed in both the nucleus and cytoplasm [136].

KAT5 itself is also acetylated at four lysine residues – K104, K268, K282, and K327 – though this mechanism of post-translational regulation has only been studied in the context of KAT5α. Auto-acetylation at K104 increases KAT5α's HAT activity, and is essential for subsequent acetylation of p53 in response to cellular stress [143]. KAT5α K327 has been shown to be acetylated by p300 (KAT3B), enhancing its downstream acetylation of the FOXP3 transcription factor [144]. Moreover, p300 (KAT3B) and CBP (KAT3A) are responsible for acetylation of KAT5α at K282 and K268, in the context of the KAT5-HIV Tat-CBP/p300 ternary complex, which stimulates poly-ubiquitination of KAT5 and subsequent proteasomal degradation [145]. Moreover, SIRT1 [146] and HDAC3 [114] have been shown to reduce KAT5α auto-acetylation, thereby reducing its HAT activity and induction of apoptosis after DNA damage. In fact, HDAC3-mediated deacetylation of KAT5α occurs at six lysine sites, mutation of which showed complete abolishment of KAT5α auto-acetylation. Moreover, HDAC3 was shown to co-localize with KAT5α in both the nucleus and cytoplasm, suggesting the potential for HDAC3-mediated regulation of other differentially-localized KAT5 isoforms.

1.2.3.3 KAT5 and its role in viral infection

While KAT5 has not been shown to directly acetylate any viral protein, it has been implicated in some viral infections, either by regulating antiviral gene expression, acetylating histones of viral DNA, or acetylating antiviral cellular targets.

In terms of regulating gene expression, HIV-1 infection was shown to inhibit KAT5α-mediated transcriptional activation of the *mn-sod* promoter, responsible for expressing the antiviral Mn-SOD protein, which inhibits HIV-1 replication [147]. Additionally, the human t-lymphotropic virus 1 (HTLV-1) p30 protein, critical for HTLV-1 latency and immune evasion, was shown to bind to and recruit KAT5α to the *myc*-responsive element for KAT-dependent transcriptional activation. This function is likely to play a major role in the proviral transformation of T cells during HTLV-1 infection, as *myc* is a well-established oncogene [148]. Further, KAT5α was found to negatively regulate p73-mediated p21 $^{(Waf1/Cip1)}$ expression, a cyclin dependent kinase inhibitor upstream of p53, resulting in proviral G1 arrest during human cytomegalovirus (HCMV) infection. Later in the replication cycle, the HCMV kinase pUL97 was found to be responsible for binding to and targeting KAT5α for proteasomal degradation in order to inhibit KAT5α-mediated G1 repression [149].

In regards to direct viral DNA acetylation, KAT5 has been shown to promote latency of HIV by acetylating the H4 histone of the HIV provirus, recruiting Brd4 to inhibit Tat-transactivation [150]. Moreover, KAT5-mediated repression of HPV replication occurs through acetylation of histone H4 at the HPV promoter. In turn, HPV E6 was shown to target KAT5α for proteasomal degradation in order to reduce KAT5-mediated acetylation of the HPV genome [151].

Finally, KAT5 has been implicated in direct acetylation of downstream players in the antiviral innate immune response. IAV infection has been shown to upregulate total KAT5 mRNA and KAT5α protein expression, resulting in a slight repression of IAV replication. In accord, overexpression of KAT5α slightly enhanced the phosphorylated

state of endogenous TBK1 and IRF3 during IAV infection. Interestingly, overexpressed KAT5α was also found to co-localize with viral NP during infection [152], though direct KAT5α-mediated acetylation of NP has not been reported.

In addition to KAT5α-mediated TBK1 and IRF3 phosphorylation during viral infection, overexpression of KAT5α enhanced ISRE responses mediated by the cytoplasmic DNA sensor cGAS and cytokine expression during HSV-1 infection [153]. Knockdown of KAT5 reduced cytokine expression during HSV-1 infection. This effect was linked to reduced cGAMP synthesis induced by HSV-1 infection during KAT5 silencing. Moreover, overexpressed KAT5α interacted with overexpressed cGAS and enhanced cGAS acetylation. This acetylation was shown to slightly enhance cGAS binding to viral DNA. In accord, transcription of cytokines in CRISPR knock-in mice encoding a KAT5α phosphorylation-defective mutant was reduced in response to HSV, allowing for enhanced viral replication. Interestingly, cGAShad previously been found to be kept in an inactive state by acetylation, due to reduced DNA binding and sensing capability [154]. It is currently unclear whether the specific acetylation sites, the stimulus, or another factor can explain this discrepancy between stimulatory or inhibitory acetylation of cGAS.

CHAPTER 2

ACETYLATION OF ZIKV NS3 AT K389 CONTROLS NS3'S RNA BINDING AND UNWINDING ACTIVITIES AND REGULATES ZIKV REPLICATION

This chapter is adapted from: Serman, T.; Chiang, C.; Acharya, D.; Pandey, S.; Muppala, S.; Liu, G.; Gack, M.U. Acetylation of the flavivirus NS3 helicase by KAT5γ is essential for virus replication. (Manuscript under review, 2022).

Attributions: TS performed and analyzed all experiments with the following exceptions: CC performed and analyzed Figures 2.6E, 2.8B and C.

2.1 Abstract

Successful replication of flaviviruses such as Zika virus (ZIKV) requires a highly coordinated replication cycle involving various interactions with host enzymes. We show herein that the NS3 protein of ZIKV is acetylated in human cells during protein overexpression and authentic infection. The acetylated state of the ZIKV NS3, specifically at residue K389 within its helicase domain, was found to regulate its RNA binding and unwinding capacity. The dynamic regulation of the acetylated state of ZIKV NS3 was required to achieve efficient viral replication in several cell types. Our study provides molecular insight into host-mediated post-translational regulation of the ZIKV NS3 protein, revealing a potential new therapeutic avenue for antiviral drug development.

2.2 Introduction

Flavivirus NS3 protein is a large, multi-functional protein that is highly conserved between mosquito-transmitted flaviviruses and is essential for viral replication. NS3 contains an N-terminal serine protease domain, required for cleavage of the polyprotein precursor and a C-terminal SF2-family helicase domain, required for unwinding dsRNA intermediates during viral replication. The NS3 helicase domain also possesses nucleoside triphosphatase (NTPase) and 5′-RNA triphosphatase (RTPase) activities that share an active site. These activities allow for ATP hydrolysis to power helicase unwinding and removal of the γ-phosphate on nascent tri-phosphorylated viral RNA (vRNA) prior to capping by NS5, respectively [155].

During viral infection, the incoming positive-stranded genomic RNA is directly translated into a single polyprotein. Proteolytic cleavage of the polyprotein by NS3 requires interaction with the hydrophobic core of its transmembrane cofactor NS2b,

which connects to NS3 by a flexible, soluble linker. This complex is often referred to as “NS2b3” and can partake in self-cleavage during infection and *in vitro* [156]. The NS2b3 protease complex is essential for flavivirus replication and virion assembly, as inactivating mutations within the conserved catalytic triad of the NS3 protease domain prevent production of viral RNA and infectious virions [157].

After viral entry, incoming vRNAs are trafficked to ER-membrane derived replication organelles (ROs), where ZIKV NS proteins assemble to form the replication complex (RC). During replication, NS3 remains bound to RO membranes via the integral membrane domain of NS2b. Within the RC, NS3 serves as a central hub for mediating replication, binding directly to the viral RNA-dependent RNA polymerase NS5 and indirectly to ER-membrane modulatory nonstructural proteins NS2a, NS4a, and NS4b via its NS2b cofactor [158]. Within the RC, NS5 generates negative strand RNA, which is utilized as a template for synthesis of positive strand genomic RNA. The NS3 helicase is involved in unwinding dsRNA intermediates during positive strand synthesis. In a mutational study of DENV NS3 helicase domains, mutant viruses were not able to replicate properly, indicating that NS3 helicase activity is essential for virus replication [159]. Additionally, the enzymatic activities of ZIKV NS3 have been shown to be enhanced by binding to NS5 [23]. Moreover, NS3 has also been implicated in innate immune evasion, providing a competitive interaction between the antiviral signaling molecules RIG-I and MDA5 with their respective 14-3-3 chaperone proteins [46, 47], as well as in fatty acid metabolism, binding to and redistributing fatty acid synthase (FASN) to sites of viral replication [14].

Due to its important role in viral replication, NS3 is a major target for drug design. Currently, all NS3 inhibitors in development are designed to target the NS2b3 protease. Specifically, these inhibitors aim to compete with substrate binding or to disrupt the NS2b-NS3 interaction. However, several factors make targeting this complex difficult, including the shallow and largely solvent-exposed binding pocket and the dibasic nature of native substrates, resulting in low permeability of peptide-mimetic inhibitors. There are currently no drugs in clinical trials that target the NS3 helicase domain, as high structural similarity of this domain to cellular helicases results in a lack of unique targets [160]. Moreover, despite its myriad functions during the viral lifecycle, a mechanism for regulation and coordination of these various activities has not been fully elucidated. Understanding the host regulation of NS3 activity can potentially lead to new drug development avenues.

2.3 Results

2.3.1 Identification of ZIKV NS3 PTMs by MS analysis

Since post-translational modifications (PTMs) are a major vehicle for diversifying protein functions, we questioned whether the multifunctional roles of NS3 were regulated by PTMs. As such, we tested whether ZIKV NS3 is post-translationally modified by host enzymes using two parallel mass spectrometry (MS) approaches. ZIKV NS3 was ectopically-expressed, affinity-purified, and subjected to SDS-PAGE separation, alongside an additional ZIKV multi-functional NS protein, NS1, under exogenous treatment with IFN-β to mimic an infected state (**Fig. 2.1A, B).** In parallel, SVGA (human fetal astrocyte) cells were infected with ZIKV, harvested at multiple time-points post-infection, tandem mass tag (TMT)-labeled, fractionated, then immuno-enriched with anti-pan-acetyllysine (anti-acK) antibodies to assess the viral acetylome during authentic

infection by MS (**Fig. 2.1C**). In general, TMT labeling allows for samples from multiple conditions (ie, time points) to be mixed prior to a single run on the Mass Spectrometer, reducing run-to-run variance.

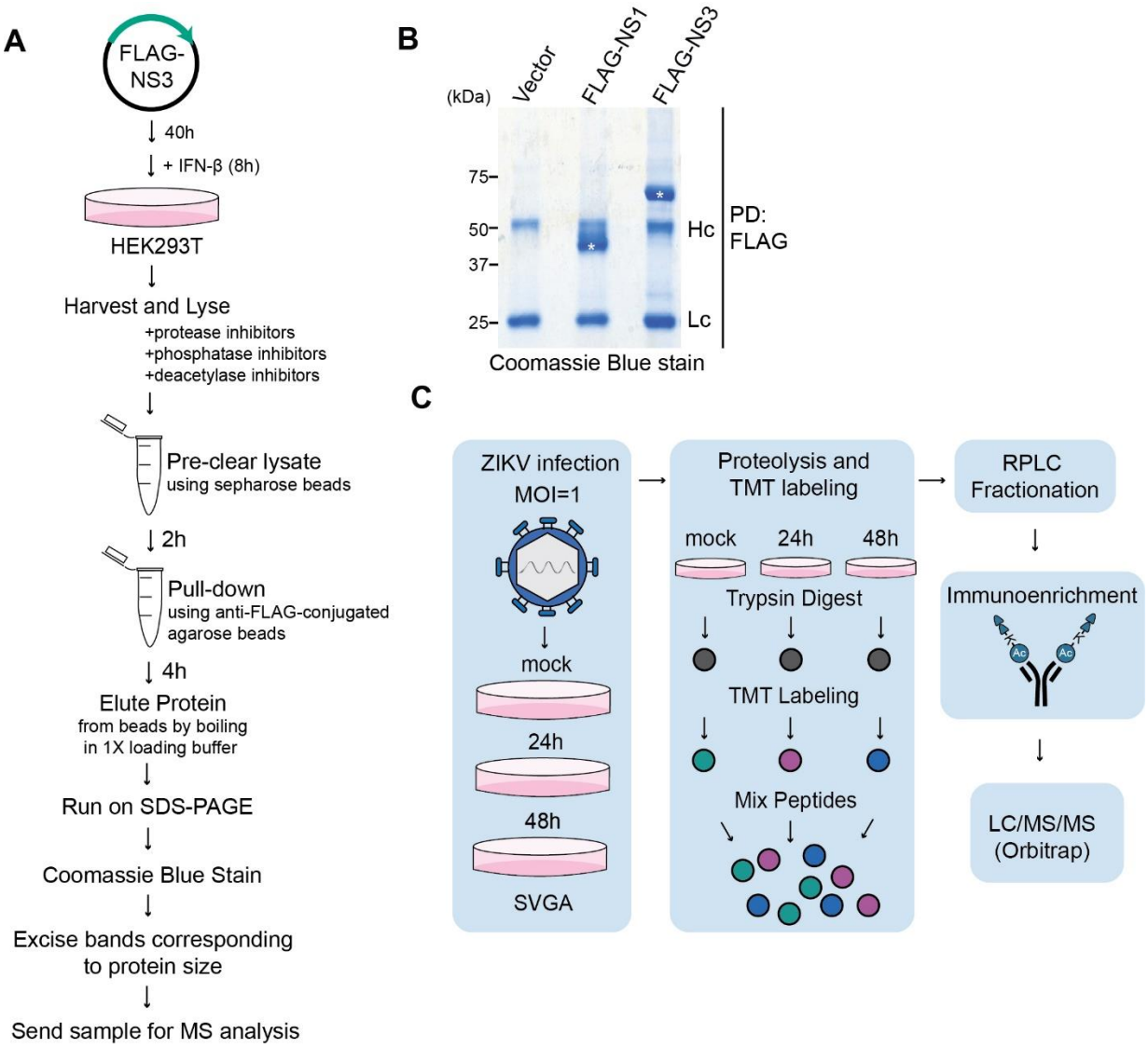

Figure 2.1 Workflows for sample preparation for Mass Spectrometry (MS) analysis of post-translational modifications of ZIKV proteins

(A) Schematic representation of the workflow for mass spectrometry (MS) analysis of FLAG-tagged ZIKV NS3 affinity-purified from HEK293T cells that were transfected for 40 h to express this construct, with stimulation with IFN-β for 8 h pre-harvest. Proteins were pulled down using anti-FLAG agarose and run on an SDS-PAGE gel prior to excision for MS analysis. FLAG-tagged ZIKV NS1 was used as a control (not shown).

Figure 2.1 *(continued)* Workflows for sample preparation for Mass Spectrometry (MS) analysis of post-translational modifications of ZIKV proteins

(B) Coomassie-stained SDS-PAGE gel showing the affinity-purified FLAG-tagged ZIKV NS3 and NS1 (control) proteins used for the MS analysis that identified the six acetylation sites in NS3. FLAG-tagged ZIKV NS1 and NS3 were purified as described in (A). Lc, antibody light chain. Hc, antibody heavy chain. PD, pulldown. Asterisks indicate NS3 and NS1 proteins.

(C) Schematic representation of the workflow for assessing global acetylome changes during ZIKV infection by MS analysis. SVGA cells were mock treated or ZIKV infected for 24 and 48 h, followed by lysis, trypsin digestion, TMT labeling, RPLC fractionation, and immuno-enrichment with anti-pan-acetyl-lysine (anti-acK) antibodies. Immuno-enriched fractions were subjected to MS analysis for detection of acetylated viral proteins.

MS analysis of the affinity-purified ZIKV NS3 revealed post-translational acetylation of six lysine residues spanning both domains of the protein (**Fig. 2.2A**). Interestingly, five of the six acetylated lysines identified by overexpression of ZIKV NS3 were within the SF2-helicase domain of the ZIKV NS3 protein. Two of these five acetylated lysines within the helicase domain, K389 and K431, were also identified by MS during authentic infection (**Fig. 2.2A (red))**. The mass spectra revealing the post-translational acetylation of K389 and K431 during ZIKV NS3 overexpression are presented in **Fig. 2.2B and C**. Interestingly, analysis of a previously-characterized crystal structure of the NS3 helicase revealed that both K389 and K431 are within the RNA binding tunnel of the NS3 helicase domain (**Fig 2.2D**). Further, introduction of a K431A mutation in ZIKV NS3 has been shown to reduce RNA binding by fluorescent polarization and NS3 helicase activity by an *in vitro* unwinding assay [23]. Meanwhile, the K389 site is near to the cognate R387 residue in DENV NS3 that has been predicted to bind the RNA phosphate backbone by molecular dynamic simulations [25]. Moreover, mutation of residues nearby the K389 site in WNV NS3 (R388) [28] and HCV NS3 (Y392/R393) [30] have both been shown to reduce viral RNA binding and unwinding.

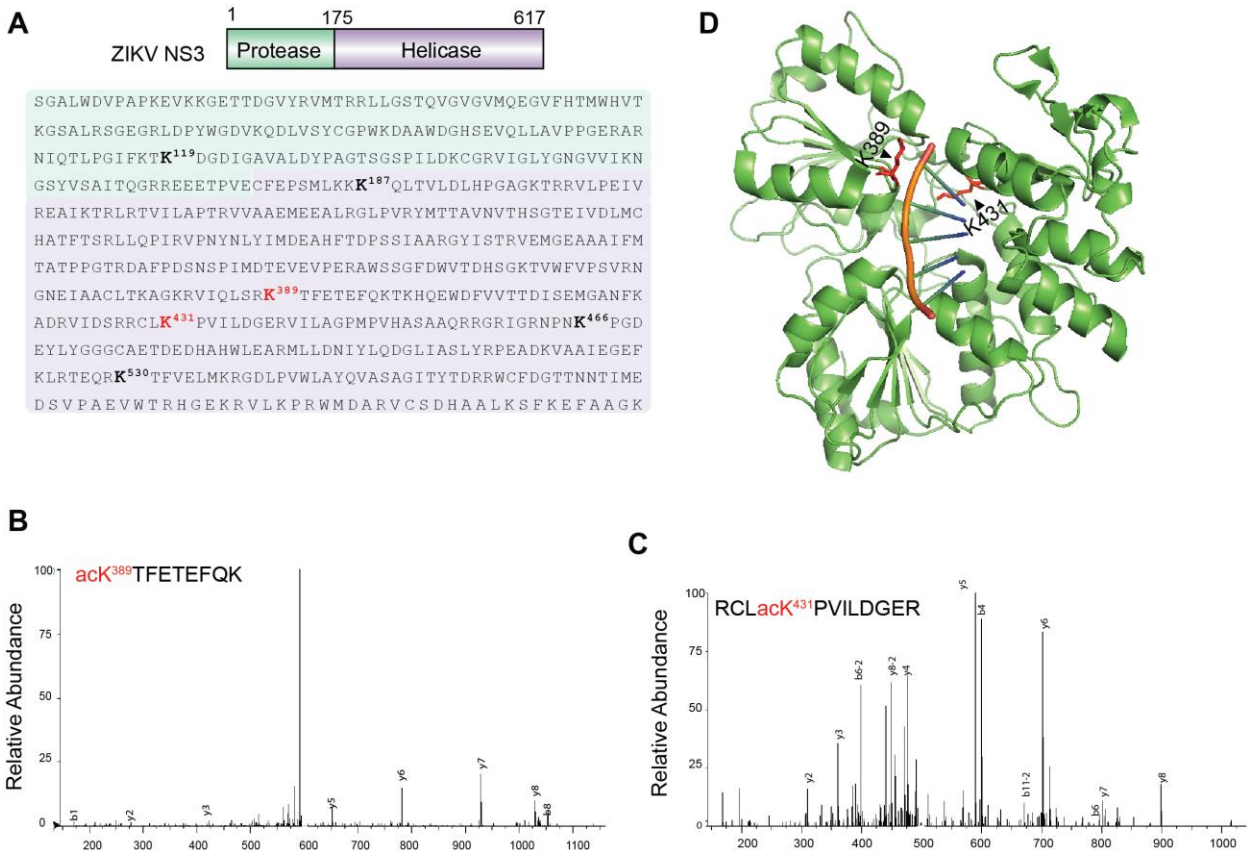

Figure 2.2 Identification of ZIKV NS3 acetylation by Mass Spectrometry (MS) analysis

(A) ZIKV NS3 domain organization and amino acid sequence. Black lysine residues (bold) indicate the acetylated residues identified by MS analysis of purified FLAG-NS3. Red lysine residues (bold) indicate acetylation sites identified by both MS approaches.

(B-C) Tandem mass spectra of the tryptic peptides acK$_{389}$TFETEFQK (B) and RCLacK$_{431}$PVILDGER (C) of affinity purified ZIKV NS3 by anti-FLAG pulldown (PD) from HEK293T cells that were transiently transfected for 40 h with this plasmid. Mass spectra identified acetylation at K389 and K431. b- and y-ion designations are shown.

(D) Ribbon representation of the crystal structure of ZIKV NS3 bound to a synthetic ssRNA substrate (orange) (Protein Data Bank, accession no. 5GJB). K389 and K431 are indicated in red.

2.3.2 ZIKV NS3 undergoes robust acetylation at K389

To validate the results of the MS analysis, all six acetylated lysine residues were mutated to arginine, a positively-charged residue that cannot be acetylated, and probed for acetylation by Western blot (WB), revealing a near-complete loss of the acetylated

signal (**Fig. 2.3A**). To confirm acetylation of ZIKV NS3 under native conditions, NS3 was purified from ZIKV-infected SVGA cells and analyzed for acetylation by WB, revealing robust ZIKV NS3 acetylation during authentic infection (**Fig. 2.3B**). ZIKV NS3 was also found to be acetylated during infection of human lung epithelial (A549) and IFN-deficient African green monkey (Vero) cells (**Fig. 2.3C, D**). Biochemical analysis of NS3 acetylation over a time-course of infection revealed that NS3 acetylation increased over time, which correlated with the increased expression of NS3 (**Fig. 2.3E**).

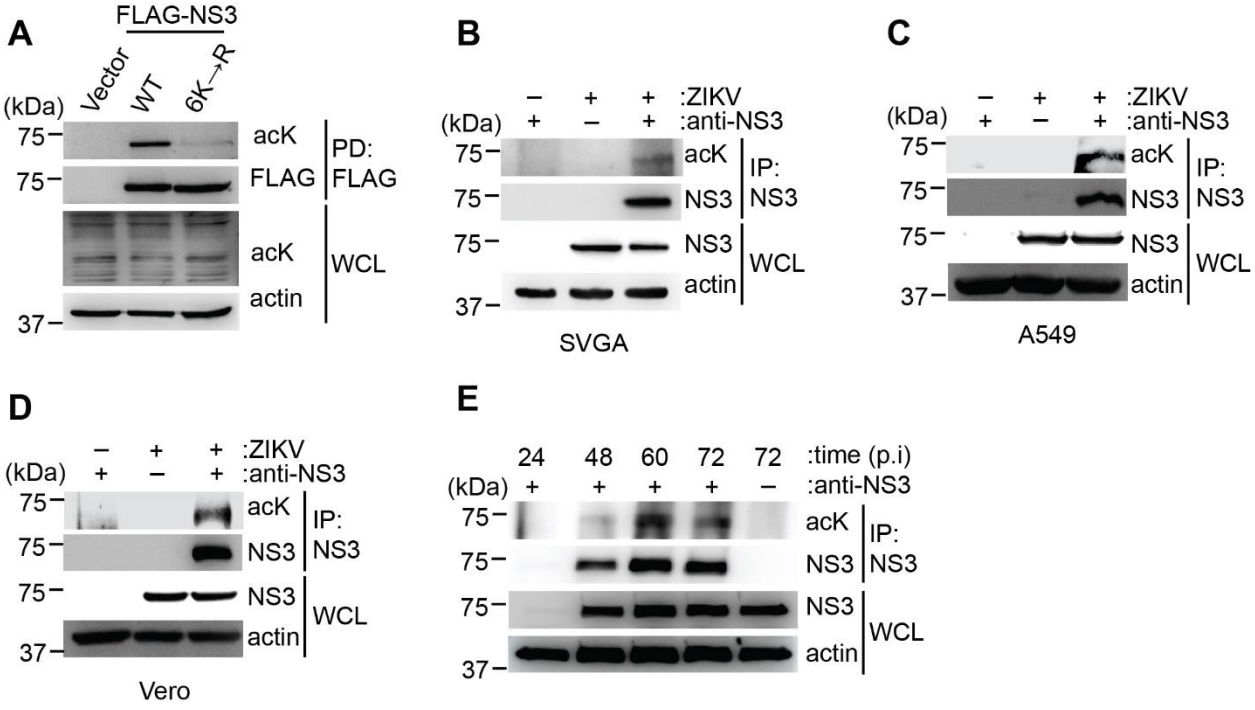

Figure 2.3 Biochemical analysis of ZIKV NS3 acetylation.

(A) Acetylation of FLAG-tagged ZIKV NS3 WT or 6K→R mutant in HEK293T cells that were transfected for 40 h to express these constructs, determined by anti-FLAG pull-down (PD: anti-FLAG) and immunoblot (IB) with anti-acK. Whole cell lysates (WCLs) were probed by IB with anti-acK and anti-Actin (loading control).

(B-D) Acetylation of ZIKV NS3 in (B) SVGA, (C) A549, or (D) Vero cells that were infected with ZIKV (strain BRA/2015, MOI 0.5) for 60 h, determined by immunoprecipitation (IP) using anti-NS3(ZIKV) and IB with anti-acK or anti-NS3. WCLs were immunoblotted with the indicated antibodies

(E) Acetylation of ZIKV NS3 in SVGA cells that were infected with ZIKV (strain BRA/2015, MOI 1) for the indicated times, determined as in (B).

Interestingly, neither exogenous IFN-β treatment nor infection with SeV (also a potent activator of the IFN response [161]) affected the acetylated state of ectopically-expressed ZIKV NS3 as measured by WB (**Fig. 2.4A, B**), suggesting that acetylation is not induced by IFN.

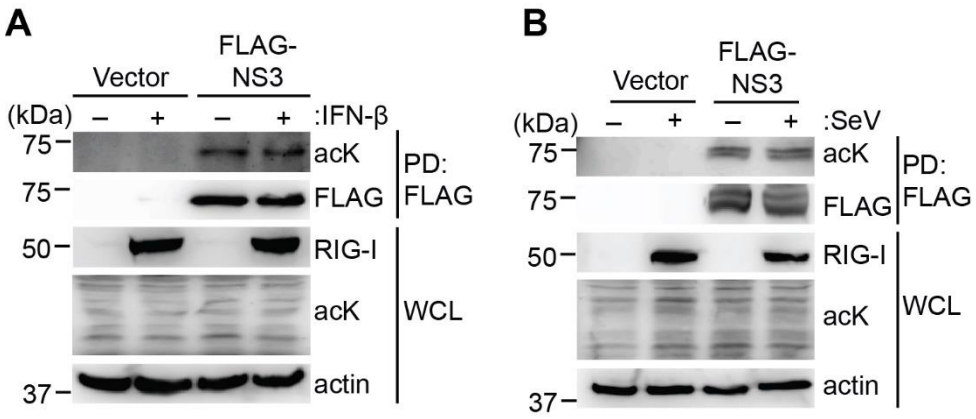

Figure 2.4 Acetylation of NS3 is not enhanced by IFN-β stimulation or Sendai virus (SeV) infection.

(A) Acetylation of FLAG-tagged ZIKV NS3 in transiently transfected HEK293T cells that were stimulated with 1000 U/mL IFN-β for 24 h or that remained untreated, determined by anti-FLAG PD and immunoblot (IB) with anti-acK. Whole cell lysates (WCLs) were probed by IB with anti-acK, and anti-Actin (loading control). WCLs were further immunoblotted for endogenous RIG-I, which is an IFN-stimulated gene and thus served as a control for effective IFN stimulation.

(B) Acetylation of FLAG-tagged ZIKV NS3 in transiently transfected HEK293T cells that were infected with 100 HAU/mL SeV for 24 h or that remained untreated, determined as in (A).

Single site mutational analysis of each of the acetyl-lysine residues identified by MS to arginine (mimicking non-acetylated lysine) showed that only mutation of K389 markedly reduced the acetylation signal of ZIKV NS3 during overexpression (**Fig. 2.5A**), suggesting that this lysine residue is the major acetylation site in the NS3 protein. In turn, ZIKV NS3 was purified from infected SVGA cells and immunoblotted using a validated, custom-

made acetyl-K389-NS3(ZIKV)-specific antibody (**Fig 2.5B, C**), revealing that K389 is acetylated during native infection of a cell type physiologically relevant to ZIKV infection.

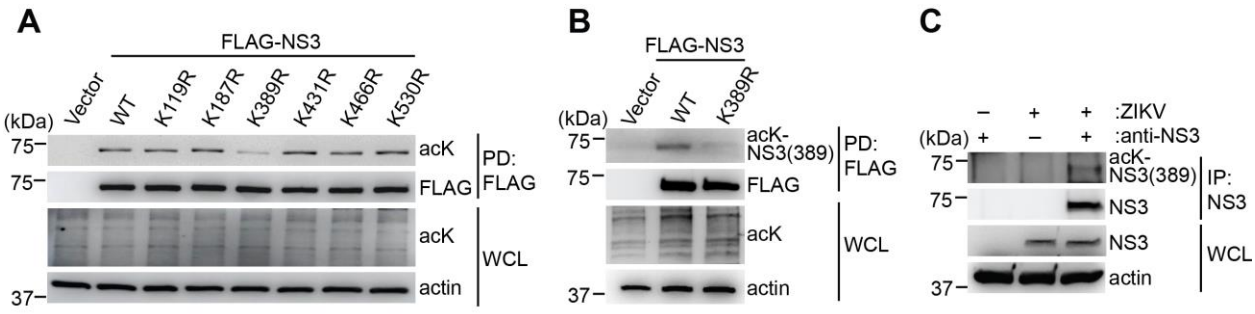

Figure 2.5 ZIKV NS3 residue K389 is robustly acetylated during overexpression and authentic viral infection.

(A) Acetylation of FLAG-tagged ZIKV NS3 WT and the indicated single K→R mutants in transiently transfected HEK293T cells, determined by anti-FLAG pull-down (PD: anti-FLAG) and immunoblot (IB) with anti-acK. WCLs were probed by IB with anti-acK and anti-Actin (loading control).

(B) Acetylation of FLAG-tagged NS3 WT or K389R mutant in HEK293T cells that were transfected for 40 h to express these constructs, determined by anti-FLAG PD and IB with an acetyl-K389-NS3(ZIKV)-specific antibody. WCLs were probed with the indicated antibodies.

(C) Acetylation of ZIKV NS3 in SVGA cells that were infected with ZIKV (strain BRA/2015, MOI 0.5) for 60 h and assessed by IP with anti-NS3 and IB with an acetyl-K389-NS3(ZIKV)-specific antibody. WCLs were probed by IB with anti-NS3 and anti-Actin.

2.3.3 *Acetylation of ZIKV NS3 at K389 controls the RNA binding and unwinding capacities of the helicase*

Since residue K389 acts as a major site for acetylation of the NS3 protein, the functional relevance of the acetylated state of this residue was investigated. Given the crystal structure that positions K389 within the RNA binding groove of the helicase domain [29] and the previous characterization of the RNA-binding ability of neighboring residues in other flavivirus NS3 proteins [25, 28, 30], we hypothesized that K389 acetylation plays

a role in RNA binding. As K389 is a positively charged residue that becomes neutralized by acetylation, we hypothesized that acetylation of K389 would reduce its ability to bind the negatively-charged backbone of ZIKV RNA. To directly test whether the RNA binding capacity of NS3 was modulated by mutation of K389, a WT NS3 construct or those encoding K389R, K389Q, or a previously-characterized RNA binding-deficient mutation, D410A [23], were purified from human cells, incubated with a biotinylated ZIKV single-stranded RNA substrate, pulled down by streptavidin-conjugated beads, and subjected to SDS-PAGE and Western blot to measure the amount of NS3 protein bound to ZIKV RNA (**Fig. 2.6A**). The result of this assay shows that the NS3 K389R protein can bind RNA with a greater affinity than the WT NS3, while K389Q reduces the RNA binding capacity, even more so than the previously-characterized RNA-binding-deficient D410A mutant (**Fig. 2.6B**). Importantly, the purified NS3 used in this assay retained its acetylation pattern after lysis and incubation in the RNA binding buffer, with reduced acetylation of the K389R mutant compared with WT NS3 (**Fig. 2.6C**). These results suggest that neutralization of the positive K389 residue through mutation to a glutamine (mimicking hyper-acetylation) reduces the NS3 RNA binding capacity, while maintaining a positively charged arginine residue at position 389 (mimicking non-acetylation) slightly enhances the NS3 RNA binding capacity. To test the downstream effect of RNA binding modulation by acetylation, HEK293T-purified NS3 WT or mutants were subjected to an *in vitro* helicase assay using a dsRNA substrate, consisting of a fluorescent (Cy3)-labeled 5′-RNA strand and its 3′ quencher (BHQ2)-bound complement, in the presence of ATP (**Fig. 2.6D)**. Interestingly, both non-acetylated (K389R) and hyper-acetylated (K389Q) NS3 mutants were deficient in this assay in their ability to unwind the dsRNA substrate

compared to WT NS3 (**Fig. 2.6E**), suggesting that both too tight and abrogated RNA binding reduce the RNA unwinding capacity of the NS3 helicase. Together, these results suggest that regulation of NS3 acetylation at residue K389 is important for the RNA binding and unwinding activities of the NS3 helicase domain.

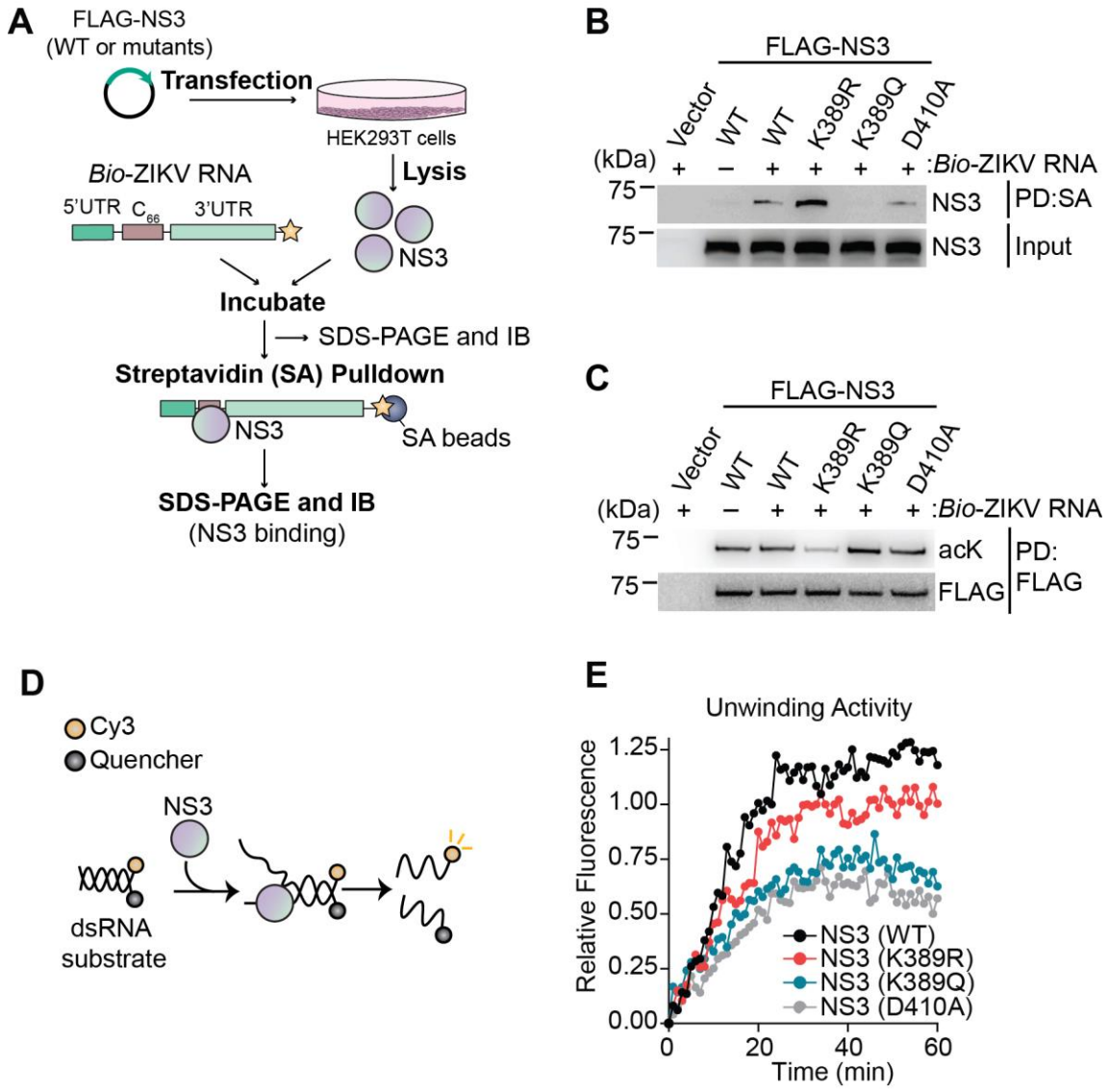

Figure 2.6 Mutation of NS3 K389 modulates the RNA binding and unwinding capacity of the helicase domain.

(A) Schematic of the experimental approach to examine the *in vitro* RNA-binding capacity of ZIKV NS3 WT and mutant proteins purified from transiently transfected HEK293T cells. Synthetic ZIKV RNA substrate used in this assay comprises ZIKV 5′UTR, the first 66 nucleotides of the Capsid protein (C66), and the ZIKV 3′UTR. See also Methods.

(B) RNA-binding ability of ZIKV NS3 WT and indicated mutants purified from HEK293T cells, determined by Streptavidin-pulldown (PD: SA) of biotinylated ZIKV RNA (*Bio*-RNA (ZIKV)) and IB with anti-NS3(ZIKV). Input amounts of ZIKV NS3 WT and mutant proteins were determined by IB with anti-NS3(ZIKV).

(C) Representative acetylation of purified FLAG-tagged ZIKV NS3 WT and mutants for the experiment in (B), determined by anti-FLAG PD and IB with anti-acK and anti-FLAG.

Figure 2.6 *(continued)* Mutation of NS3 K389 modulates the RNA binding and unwinding capacity of the helicase domain.

(D) Schematic representation of the molecular beacon helicase assay used to measure real-time unwinding kinetics of a Cy3-labeled dsRNA bound to a BHQ (Quencher)-labeled complement.

(E) In vitro RNA unwinding activity of ZIKV NS3 WT or mutants purified from HEK293T cells, measured as depicted in (D). The fluorescent (F) signal was measured every minute and is presented as $(F_t-F_0)/F_0$.

2.3.4 *NS3 K389R/Q mutant recombinant viruses have attenuated replication capacities*

To test the effect of NS3's modulated RNA binding and unwinding capacity on viral replication, recombinant ZIKV(K389R) and ZIKV(K389Q) were generated by reverse genetics using a full-length infectious cDNA plasmid (ICD) [162]. These viral plasmids were transfected into SVGA cells followed by assessment of viral titers by plaque assay. Interestingly, in accord with the data from the *in vitro* helicase assay, both ZIKV K389 mutants were attenuated in replication compared to the parental virus (WT) as determined by plaque assay, with ZIKV(K389Q) being significantly more attenuated than ZIKV(K389R) (**Fig. 2.7A**). These results were consistent when measuring viral RNA by qRT-PCR for the *ZIKV envelope (E)* gene (**Fig. 2.7B**), suggesting the observed attenuation in viral titer is due to attenuated viral RNA replication. Attenuation of the two mutant viruses was also observed in two other cell types in which ZIKV NS3 is acetylated during infection: A549 cells (**Fig. 2.7C**) and Vero cells (**Fig. 2.7D**). Interestingly, after three consecutive passages in Vero cells, recombinant viruses harboring the K389R or K3898Q mutations reverted back to ZIKV (WT), correlative with restored growth capacity (**Fig. 2.7E**).

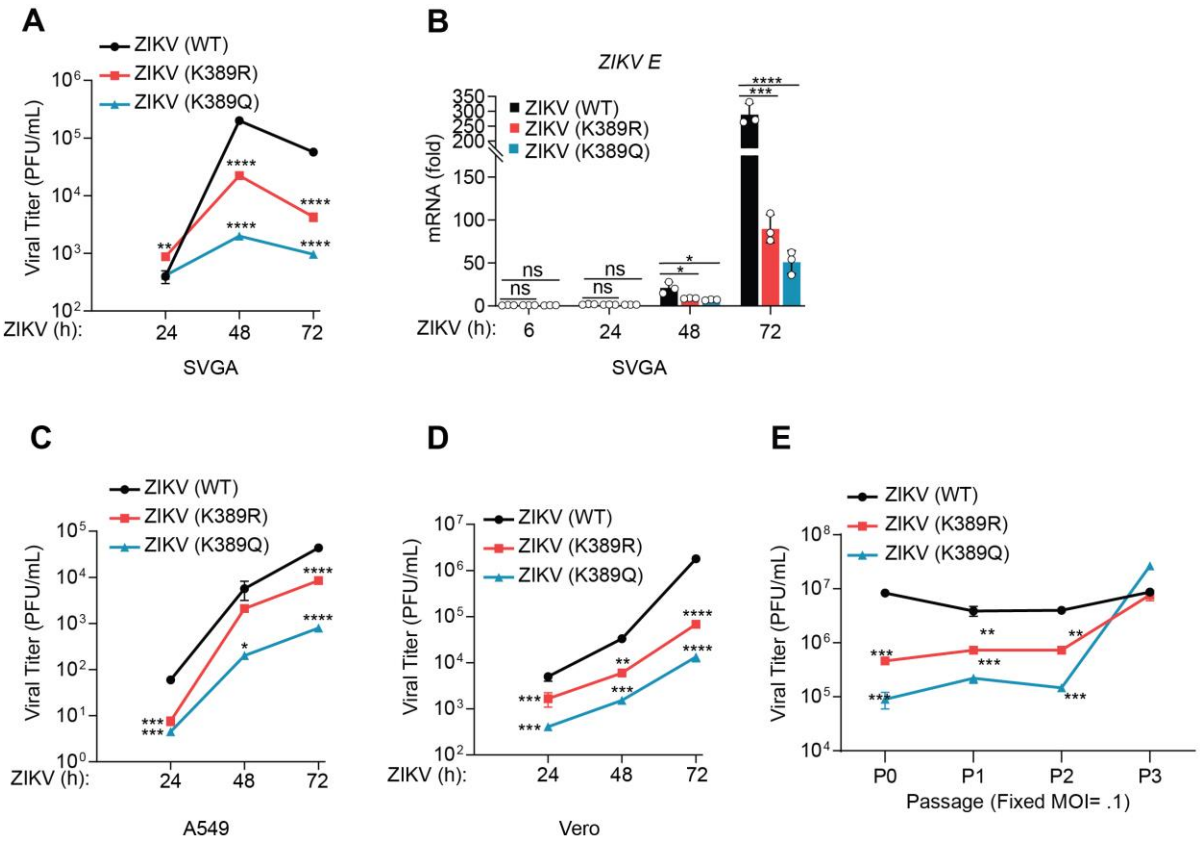

Figure 2.7 Regulation of the acetylated state of K389 in ZIKV NS3 is required for successful viral replication

(A) Viral titers in the supernatant of SVGA cells transfected with infectious cDNA clones of ZIKV(WT), ZIKV (K389R), or ZIKV (K389Q) (strain Paraiba_01/2015) for the indicated times, determined by plaque assay and presented as PFU/mL. Limit of detection: 10^2.

(B) qRT-PCR analysis of *ZIKV E* mRNA in SVGA cells transfected as in (A).

(C-D) Viral titers in the supernatant of A549 (C) and Vero (D) cells transfected as in (A).

(E) ZIKV titers across three passages at a fixed MOI (0.1) in Vero cells transfected with infectious cDNA clones of ZIKV(WT), ZIKV(K389R), or ZIKV(K389Q) (strain Paraiba_01/2015). Reversion of introduced mutations to the K389 codon was confirmed after each passage by sequencing. Unpaired Student's *t* test between indicated sample groups. ns, not significant; *p < 0.05, **p < 0.01, ***p < 0.001, **** p < 0.0001.

The growth attenuation of both recombinant viruses, and the reversion back to K389 over several passages, suggest that there is strong selective pressure for a lysine residue at position K389. In all, these results suggest that ZIKV NS3 K389 is acetylated

during infection likely in a regulatory manner, since both recombinant viruses (that mimic hyper- and non-acetylated NS3 K389) conferred a growth defect. In other words, locking the ZIKV NS3 K389 site in one regulatory state through mutation is deleterious for viral replication, suggesting that acetylation of ZIKV NS3 K389 is a pro-viral, regulatory mechanism through which the virus achieves efficient RNA replication.

2.3.5 *Acetylation of ZIKV NS3 at K389 does not affect NS3's protease activity, IFN antagonism, or NS5 binding*

To ensure that mutation of K389 did not abrogate other essential roles of NS3 that may explain the attenuated viral replication phenotypes, we mutated K389 in an NS2b3 construct, which encodes the NS2b cofactor required for protease activity of the NS3 protein. As a control, we also used a protease enzymatically-inactive mutant NS2b3 (S135A), in which the serine of the catalytic triad is mutated to an uncharged alanine. Plasmid constructs encoding NS2b3 K389R or NS3b3 K389Q did not show any change in protease self-cleavage activity compared with WT NS2b3, while NS2b3 S135A was unable to cleave itself as expected (**Fig 2.8A)**. Moreover, GST-fused NS3 mutant proteins encoding K389R or K389Q bound to FLAG-tagged NS5 as efficiently as WT NS3 by co-immunoprecipitation (co-IP) (**Fig. 2.8B**). As NS3 is capable of inhibiting RIG-I-mediated type I IFN induction by binding competitively to the RIG-I cofactor 14-3-3ε, the inhibition of RIG-I-mediated IFN-β promoter activation by WT NS3 and the K389R/Q NS3 mutants was tested by luciferase assay. In this assay, we used a construct expressing the constitutively-active CARD signaling domains of RIG-I, referred to as "RIG-I-2C". Both NS3 mutants were able to inhibit RIG-I-2C-mediated stimulation of the IFN-β promoter to a similar degree as the WT NS3 construct (**Fig. 2.8C**). These results show that mutation

of K389 did not affect other major activities of NS3 that may account for the observed attenuation in viral replication.

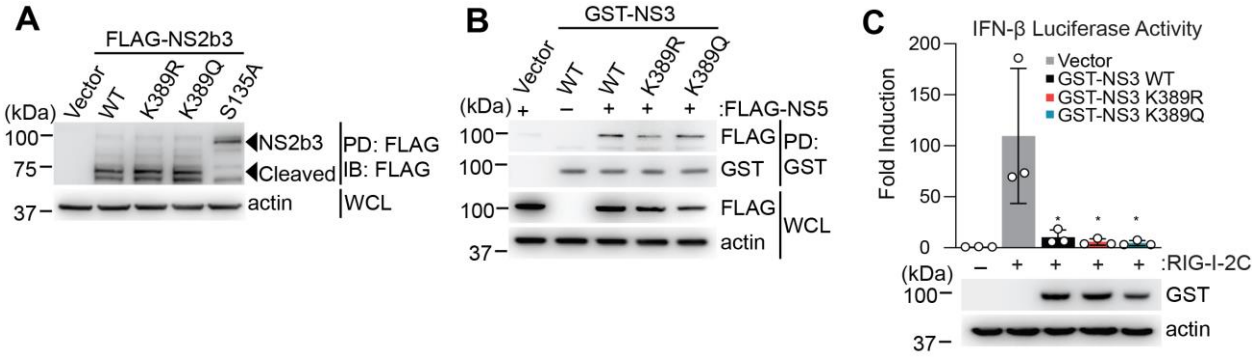

Figure 2.8 K389 mutation does not affect NS3's protease, immunodulatory, or NS5-binding abilities.

(A) Self-cleavage activity of FLAG-tagged ZIKV NS2b3 WT, its K389R and K389Q mutants, or the catalytically-inactive S135A mutant (control), in transiently transfected HEK293T cells, determined by anti-FLAG PD and IB with anti-FLAG. WCLs were probed by IB with anti-Actin (loading control). Black arrows indicate full-length NS2b3 and its cleavage product.

(B) Binding of GST-fused ZIKV NS3 WT and mutants to FLAG-tagged ZIKV NS5 in HEK293T cells that were transfected for 40 h with GST-NS3 (WT or mutants) together with either empty vector or FLAG-NS5, determined by anti-GST PD and IB with anti-FLAG and anti-GST. WCLs were probed by IB with anti-FLAG and anti-Actin (loading control).

(C) IFN-β luciferase reporter activity in HEK293T cells that were transfected for 40 h with an IFN-β luciferase reporter plasmid and RIG-I-2CARD ("RIG-I-2C") together with either vector control or the indicated GST-fused ZIKV NS3 proteins. Luciferase values were normalized to values of co-transfected β-galactosidase activity and presented relative to vector-transfected cells. WCLs were probed by IB with anti-GST (NS3) and anti-Actin (loading control). One way ANOVA between indicated sample groups. *$p < 0.05$, **$p < 0.01$, ***$p < 0.001$, **** $p < 0.0001$.

2.4 Discussion

Though the molecular mechanisms of flavivirus replication are highly characterized, most studies have focused on determining the myriad functions of

individual viral proteins. However, how these single viral proteins function as a unit, and moreover, how their dynamic roles are regulated and coordinated, is less well-understood in the field. Here, we questioned for the first time whether flavivirus NS3, specifically that of ZIKV, is post-translationally regulated by the host. Our work found that six lysine residues are acetylated during overexpression, and two of these residues are acetylated during ZIKV infection. However, as the peptide coverage of NS3 captured by MS was much lower during authentic infection than during NS3 overexpression, there may be even more sites acetylated during infection that were not detected in our analysis. Regardless, we found that one site, K389, located within the RNA-binding tunnel of the NS3 helicase domain, functions as a major site of acetylation in ZIKV NS3.

The mutation of K389 to arginine (positively-charged, mimicking non-acetylation) strikingly reduced the acetylation of the NS3 protein upon overexpression. This abrogated acetylation ignites two hypotheses for how K389 can act as a “major” acetylated site. The first hypothesis is that K389 acts as the most abundantly-acetylated lysine residue within the pool of NS3 protein purified for acetyl-lysine analysis by biochemistry. In this case, a mutation of K389 to glutamine (mimicking hyper-acetylation) would reduce the acetylated signal similar to the K389R mutation, since both mutations remove the “acetylatable” lysine residue at position 389 (**Fig 2.9A**). On the other hand, K389 may act as a priming site, whereby its acetylation allows for the subsequent acetylation of one or more of the remaining five lysine residues, either by recruiting the responsible acetyltransferase enzyme(s) or by inducing a conformational change that exposes these additional lysine residues to the acetyltransferase. In this case, a mutation of K389 to glutamine may simulate this acetyltransferase recruitment/conformational change, thus maintaining or

enhancing the native acetyl-lysine signal (**Fig. 2.9B**). While we have not specifically experimentally assessed these two hypotheses, mutational analysis pointed towards K389 serving more likely as a priming site, because the degree of acetylation of the NS3 K389Q mutant was similar to that of WT NS3 (**Fig 2.6C**).

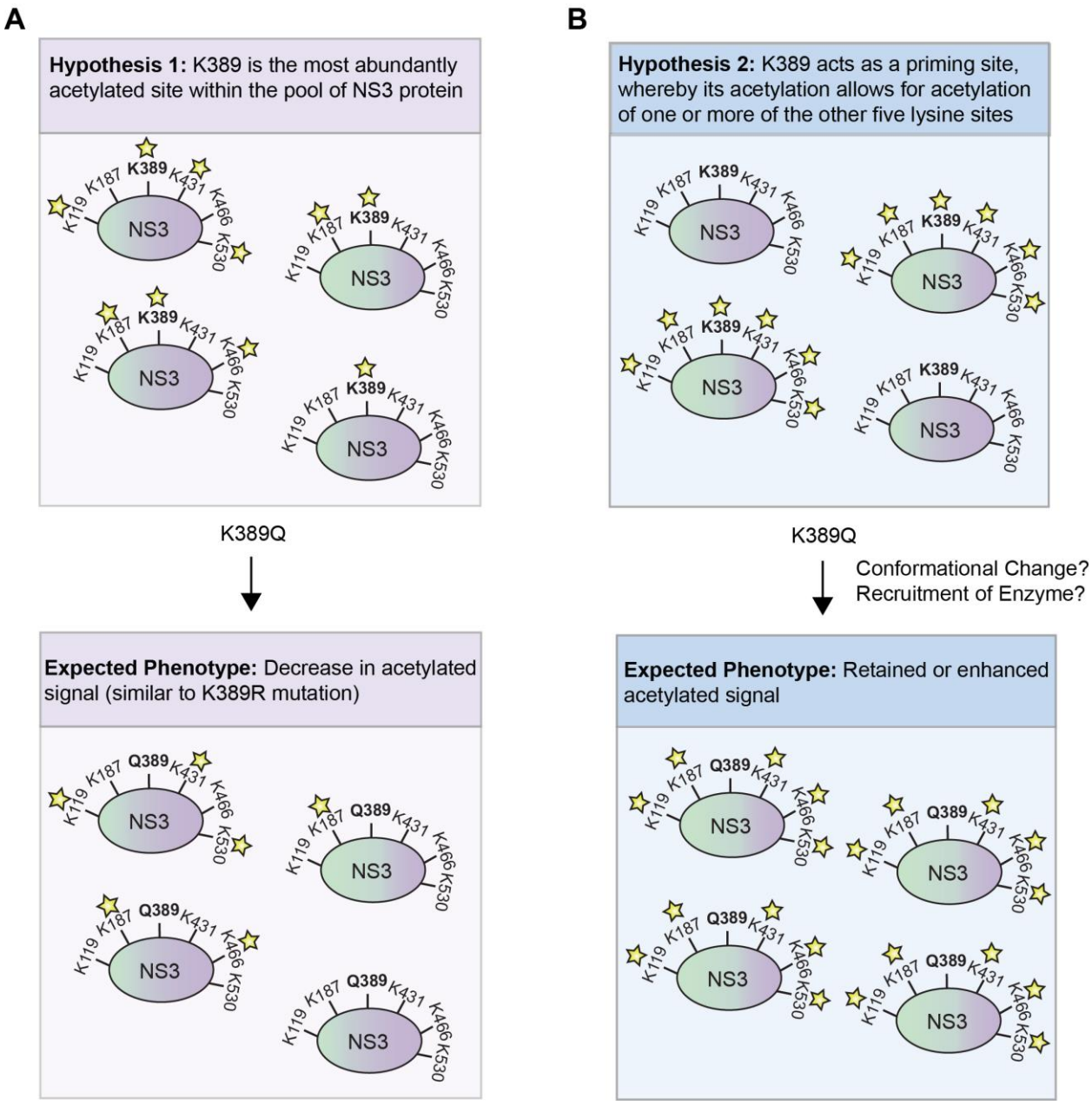

Figure 2.9 Two hypotheses explaining how K389 may act as a major site for NS3 acetylation.

(A) Schematic depiction of the acetylated state of ZIKV NS3 if the K389 acts as the most abundant site for acetylation, and how K389Q mutation would affect the overall acetylation signal detected in biochemical assays.

(B) Schematic depiction of the acetylated state of ZIKV NS3 if the K389 acts as a priming site for acetylation, and how K389Q mutation would affect the overall acetylation signal detected in biochemical assays.

While the current data point towards K389 likely serving as a priming site, more investigation is required to distinguish between these possibilities. Furthermore, since K431 has been previously shown to act as an RNA binding residue in the ZIKV NS3 helicase [23], it would be interesting to test if K389 is a priming site for K431. This could be investigated by assessing the acetylation of an NS3(K389/K431only) construct, in which the remaining four acetyl-lysine residues are mutated to arginine, compared to an NS3(K389Q, K431only) construct. If the acetylation of the NS3(K431only, K389Q) construct shows enhanced acetylation compared to the NS3(K389, K431only) construct, this would suggest that K389 acts as a priming site for the K431 residue, as only this site would be available for acetylation in the mutant background. Moreover, whether indirect modulation of the K431 acetylated state may contribute to the phenotypes we observed for RNA binding and unwinding is a subject for further research.

We show herein that acetylation is a negative regulator for NS3's helicase function. Therefore, in order to significantly impact viral replication, it is likely that a relatively abundant portion of NS3 is regulated by acetylation within the host cell. While assessing the stoichiometry of the NS3 acetylation would be desirable and informative, this determination is technically challenging given the low abundance of viral protein within an infection setting.

Our data suggest that even though the post-translational acetylation of NS3 K389 acts to negatively regulate the RNA binding and unwinding activity of the viral helicase, this PTM is ultimately proviral, as the capability for dynamic regulation of this site is required for efficient viral replication. If the replication of ZIKV(K389R) was enhanced compared with its ZIKV(WT) counterpart, this would have suggested that acetylation is a

strictly antiviral mechanism, as the K389R mutation would prevent the antiviral addition of an acetyl group. However, the attenuated replication of both the ZIKV(K389R) and ZIKV(K389Q) viruses suggested that dynamic regulation of the acetylated state of ZIKV NS3 K389 is required for successful viral replication (**Fig. 2.7, Fig. 2.10**).

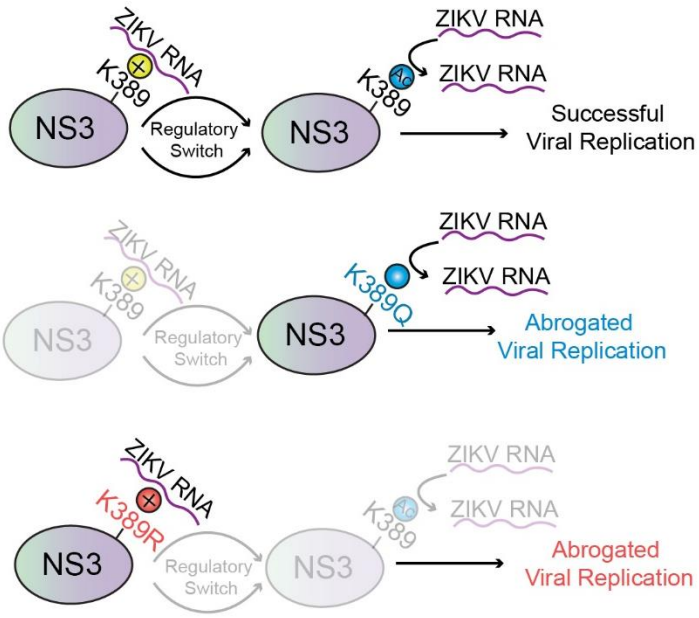

Figure 2.10 Recombinant ZIKV replication results suggesting proviral control of ZIKV replication by NS3 acetylation.
Schematic depiction of K389 acetylation as a proviral mechanism mediating optimal virus replication. This model is in line with our data showing both ZIKV(K389Q) and ZIKV(K389R) are attenuated compared with ZIKV(WT), as both mutations disrupt the ability to regulate the acetylated state of the K389 site.

Further, although our data support that ZIKV NS3 acetylation represents a proviral mechanism by modulating the RNA binding and unwinding capacity of the NS3 protein, it is unclear exactly the manner in which this regulation is achieved. For example, regulation by acetylation may be a stoichiometric or spatiotemporal form of regulation. In the case

of stoichiometric regulation, the NS3-specific acetyltransferase may acetylate only a portion of the NS3 protein pool, while the remaining protein remains non-acetylated, perhaps due to higher abundance of NS3 protein than acetyltransferase protein in the infected cell. This would allow for a fraction of the total NS3 pool to bind to viral RNA, while the remaining portion could perform other NS3 protein functions. Alternatively, the NS3 protein may be acetylated in a spatiotemporal fashion during the viral replication cycle, whereby the acetylation status is determined by the step of the viral lifecycle. In this scenario, virus-induced changes in host cell dynamics may allow for re-localization of the NS3-specific acetyltransferase at a certain step of the lifecycle, allowing for a regulatory switch from RNA binding and unwinding towards other NS3 functions. While these hypotheses are valid, mutation of K389 to Q or R did not influence NS3's protease, immunomodulatory, and NS5 binding capabilities, suggesting that the acetylation state of K389 in NS3 does not control these other functions of NS3. Therefore, the acetylation of K389 is likely an incredibly dynamic process, with both an acetyltransferase and deacetylase at play on the same NS3 molecule to manipulate its function. In this scenario, the NS3 helicase is finely-tuned by acetylation to bind and unwind viral RNA within the replication complex (**Fig. 2.11**). While deacetylation of total NS3 protein was not observed during a time-course of infection (**Fig. 2.3E**), a dynamic acetylation and deacetylation of NS3 during the replication cycle would be detected as a steady-state acetylation when analyzing the NS3 protein pool in bulk. Despite the multiple ways in which NS3 acetylation may be regulated during infection, our data supports that this PTM functions in a proviral manner, and can therefore be targeted to reduce viral replication.

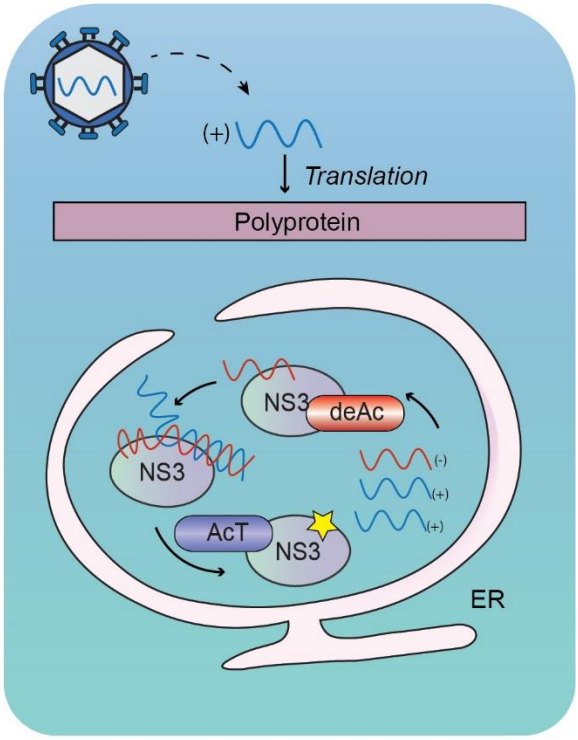

Figure 2.11 Model for how acetylation serves as a dynamic, proviral regulatory switch controlling the RNA binding and unwinding activity of the NS3 helicase. Our data suggests that NS3 is regulated by acetylation (at K389) through a dynamic regulatory switch, in which NS3 when acetylated releases replicated viral RNA, and when deacetylated restarts the RNA binding and unwinding process.

2.5 Methods

Cell lines. HEK 293T (human embryonic kidney cells, female), Vero (African Green monkey kidney epithelial, female) (ATCC), and A549 (human lung epithelial cells, male, age 58) were purchased from American Type Culture Collection (ATCC) and cultured in Dulbecco's Modified Eagle's Medium (DMEM, Gibco) supplemented with 10% (v/v) fetal bovine serum (FBS, Gibco) and 1% (v/v) penicillin-streptomycin (Gibco). SVGA cells (human fetal astrocyte, embryonic, sex unidentified) (provided by Ellen Cahir-McFarland; Cambridge, MA [163]) were cultured in Minimum Essential Medium (Gibco) supplemented with 10% (v/v) FBS and 1% (v/v) penicillin-streptomycin. All cell cultures

were maintained at 37 °C in a humidified 5% CO2 incubator. Purchased cell lines were authenticated by the respective vendor and were not validated further in our laboratory. Cell lines obtained and validated by other groups were not further authenticated.

Viruses. Sendai virus (strain Cantell) was purchased from Charles River. ZIKV (strain BRA/2015) [46, 164] was kindly provided by Michael Diamond (Washington University St. Louis). The infectious cDNA clone (ICD) of ZIKV (strain Paraiba 2015) was kindly provided by Alexander Pletnev (NIH) [162].

Plasmids and Reagents. ZIKV NS3 (strain H/PF/2013) was subcloned using as templates a plasmid encoding GST-fused ZIKV NS3 [46] into the pcDNA3.1+ vector together with an N-terminal FLAG-tag using the restriction sites Nhe1 and BamH1. FLAG-tagged NS1 (strain H/PF/2013) and NS2b3 were kindly provided by Tom Hobman (University of Alberta) [165]. Site-directed mutagenesis was performed using 'Round-the-Horn' cloning. cDNA encoding ZIKV NS3 6K→R (K119R, K187R, K389R, K431R, K466R, K530R) was purchased as a G-block from IDT and cloned into the pcDNA3.1+ vector using Kpn1 and Xho1 restriction sites and Gibson assembly. GST-fused ZIKV NS3 (strain BRA/2015) was described previously [46]. For luciferase assays, the IFN-β luciferase reporter plasmid and β-galactosidase-expressing plasmid (pGK-β-gal) have been described previously [46]. The plasmid encoding GST-RIG-I-2CARD has been published previously [161]. All constructs were validated by sequencing. Transfections were performed using linear polyethylenimine (1 mg/mL solution in 20 mM Tris pH 6.8; Polysciences), Lipofectamine and Plus reagent (Life Technologies), or Lipofectamine 2000 (Life Technologies) following the manufacturer's instructions.

Anti-FLAG M2 agarose affinity gel (Sigma), magnetic A/G beads (Pierce) or agarose A/G beads (Pierce) were used for respective pull down and immunoprecipitation assays. Protease inhibitor cocktail (Sigma; #P2714) was added at a concentration of 1:50 to cell lysates for all pull down and immunoprecipitation assays. Deacetylase inhibitor cocktail (Santa Cruz; sc-362323) was diluted in media at a concentration of 1:200 and added to cells 12 h pre-harvest and to cell lysis buffer at the same concentration for all biochemical assays analyzing NS3 acetylation. Human IFN-β (Beta 1a, Mammalian Expressed) was purchased from PBL Biomedical Laboratories.

Virus Propagation

ZIKV was propagated in Vero cells based on a protocol described in [166]. Briefly, 4xT175 flasks of Vero cells were seeded ($1x10^5$ cells/mL) and infected 24 h later with a small amount (MOI=.001) of stock virus in 8 mL of ZIKV growth medium (DMEM, 10mM HEPES, 1% NEAA, 1% penicillin-streptomycin, 1mM sodium pyruvate) for 2 h followed by replacement with 8 mL ZIKV growth medium supplemented with 2% FBS (v/v). Supernatants were harvested on 48 h and 72 h post-infection and aliquoted for storage at -80°C. After freezing, ZIKV stocks were titered using a standard plaque assay (described in detail below) on a confluent Vero cell layer.

Viral Infection Assays. Infection experiments were performed and processed as described previously [166]. Briefly, Vero, A549, or SVGA cells were counted during seeding and plated in triplicate. The next day, the MOI was calculated using the stock titer and assuming double the seeding density. The viral stock was thawed at RT and the corresponding amount of virus was resuspended in the final seeding volume of FBS-free media. Cells were incubated with virus (ZIKV) in serum-free media for 2 h, followed by

incubation in complete media until harvest at the indicated time points. For plaque assay, 100-250 μl of supernatant was removed and stored immediately at -80°C. For qRT-PCR analysis, media was removed and cells were washed 1X with RT PBS and lysed immediately in 350 μl GTC lysis buffer (Omega RNA Kit 1). For downstream biochemical analysis, cells were washed 1X in cold PBS and harvested using a cell scraper in cold PBS.

Viral Titrations. Plaque assays were performed as described previously [46, 166]. Briefly, 20 μl of supernatants of infected cells were serially diluted in 180 μl serum-free media and 100 μl was incubated on a confluent monolayer of Vero cells in 900 μl for 2 h, followed by removal of infection media and addition of 1% (w/v) low melting agarose (Lonza, #50101) mixed 1:1 with 2X MEM. Plaques were analyzed after 3-5 days by removing the agar overlay and fixing cells with 2% PFA in PBS for 30 min at room temperature, followed by staining with crystal violet in 20% (v/v) methanol. Plaques were stained for 15min then washed 3 times with ddH_2O. Plaques were counted and reported as PFU/mL, calculated as number of (plaques/well) x (dilution factor)/(infection volume).

Generation of recombinant Zika viruses. For the generation of recombinant viruses, a ZIKV (strain Paraiba_01/2015) full-length infectious cDNA clone (ICD) was used, which was kindly provided by the Alexander Pletnev (NIH). Cloning of the ZIKV ICD was carried out by Kas1 and EcoN1 restriction digest of the parental plasmid followed by Gibson Assembly-mediated insertion of the Geneblock (IDT) encoding K389R/Q mutations. Cloned plasmids were transformed into the MC106 bacterial strain and propagated in Luria broth at 30°C for 30 h, followed by DNA isolation. Clones were screened by sequencing using a primer spanning the chimeric intron region of the ICD backbone (5'-

TCCACAGCCGTCTCTGCTGAT-3'), where high homologous recombination rates occur. Positive clones that had intact sequences across this region were subjected to full-length sequencing using a Sanger sequencing primer library. Those with 100% sequence identity to the parental ICD (excluding the K389 mutation) were used for viral replication experiments.

Recombinant ZIKV infectious cDNA clone (ICD) assays. Viral replication assays using the ICD clones were carried out by seeding cells in triplicate ($1x10^5$ cells/mL) in 12-well plates. The next day, media was replaced with warm Opti-Mem and cells were transfected with 300 ng of ICD plasmid using the Transit-LT1 transfection reagent (Mirus; MIR2304), per manufacturer's instructions. Eight hours post-transfection, media was removed and replaced with Dulbecco's Modified Eagle's Medium (DMEM, Gibco. Cell supernatants were harvested at the indicated time points, and kept frozen at -80C until viral titering.

Cell Lysis and Co-immunoprecipitation. HEK293T, SVGA, Vero, or A549 cells were lysed in Nonidet P-40 (NP-40) buffer (50 mM HEPES pH 7.4, 150 mM NaCl, 1% (v/v) NP-40, 1 mM EDTA, 1:50 protease inhibitor cocktail (Sigma)) and then centrifuged at 21,000 x g for 20 min at 4°C. WCLs were taken post lysate clearance and the remainder was used to perform GST or FLAG pull downs, immunoprecipitation, or co-immunoprecipitation assays following protocols as previously described [161]. Briefly, lysates were incubated with GST or FLAG beads for 4 h at 4°C, or incubated with specific antibodies overnight at 4°C followed by pulled down with magnetic/agarose A/G beads for 2 h at 4°C. Following pull-down or (co)immunoprecipitations, proteins were eluted from beads either by heating samples in Laemmli SDS sample buffer at 95°C for 5 min. For experiments in which FLAG-tagged NS3 was analyzed by IB with anti-acK, beads were

or by incubated in 100 μg/mL FLAG peptide (Sigma; F3290) in TBS (10mM Tris HCL, 150mM NaCl, ph 7.4) for 1 h at 4°C.

Large-scale pull-down for ZIKV NS3 mass spectrometry analysis. To identify post-translational modifications of ZIKV NS3, HEK293T (~12 x 10^7) cells were transfected with 20 μg of empty vector, FLAG-tagged ZIKV NS1 (strain H/PF/2013), or FLAG-tagged ZIKV NS3 (strain H/PF/13) for 48 h. At 8 h pre-harvest, cells were treated with exogenous recombinant IFN-β (1000 units/mL) to mimic an infected state. Post-harvest, cells were lysed with 1% Nonidet P-40 buffer (50 mM HEPES pH 7.4, 150 mM NaCl, 1% (v/v) NP-40, 1 mM EDTA, 1:50 protease inhibitor cocktail (Sigma), 1:100 phosphatase inhibitor (Sigma), 1:200 deacetylase inhibitor cocktail (Santa Cruz)), clarified by centrifugation at 21,000 x g for 20 min at 4°C, and incubated with anti-FLAG M2 agarose beads at 4°C for 4 h. Pulldown samples were washed harshly with 1 M RIPA buffer (1 M NaCl, 1% (v/v) NP-40, 1% (w/v) deoxycholic acid, 0.01% (w/v) SDS, 20 mM Tris (pH 8.0)) and resolved by SDS-PAGE. The protein gel was subsequently stained with GelCode Blue Stain Reagent (Thermo Fisher) for 1 h at room temperature, and destained with UltraPure water for 4 h at room temperature. The band corresponding to the size of ZIKV NS3 was excised and analyzed by ion-trap MS at the Harvard Taplin Biological Mass Spectrometry Facility, Boston.

Large-scale sample preparation for MS analysis of viral acetylation analysis during infection. SVGA cells (~1 x 10^8) were mock-treated or ZIKV-infected (MOI 1) in duplicates for 24 h and 48 h. After infection, cells were harvested, washed, and lysed in 150 mM RIPA buffer (150 mM NaCl, 1% (v/v) NP-40, 1% (w/v) deoxycholic acid, 0.01% (w/v) SDS, 20 mM Tris (pH 8.0)) containing 1:50 protease inhibitor (Sigma), 1:100

phosphatase inhibitor (Sigma), and 1:200 deacetylase inhibitor (Santa Cruz)) and then bead beat with 1mm silicone beads three times for 40s, resting on ice for 1 min between each burst. The lysate was cleared by centrifugation and the protein concentration measured by BCA assay (Pierce). A 100 μg aliquot of each sample was mixed with fresh urea acid buffer (8 M Urea, 0.1M triethylammonium bicarbonate (TEAB) (Thermo Scientific; #90114), 5 mM DTT) and transferred onto a Microcon-10 kDa Centrifugal Filter Unit (Millipore; #MRCPRT010). The samples were processed using the previously-described Filter Aided Sample Preparation (FASP) protocol [167]. Samples were alkylated by the addition of 0.05M iodoacetamide in urea acid buffer and trypsinized on the column overnight at 37°C in a wet chamber using 1:100 MS-grade trypsin (Pierce) in TEAB. Peptides were collected in TEAB by centrifugation, precipitated with 0.5M NaCl, and acidified to pH 3 with formic acid. Samples were subjected to TMT-labeling and anti-acetyllysine enrichment using anti-acK (CST; #9814) and anti-acetyllysine antibody agarose (ImmuneChem; #ICP0388) at the Mass Spectrometry Core of the University of Illinois at Chicago, followed by analysis of the viral acetylome.

Immunoblot Analysis and Antibodies Purified proteins or whole cell lysates were resolved on 8.5% or 10% Tris-Glycine-SDS PAGE gels (pH8) and then transferred onto a polyvinylidene difluoride (PVDF) membrane (Bio-Rad) for 1h using a Wet Transfer Chamber (Bio-Rad). Membranes were blocked in 5% (w/v) non-fat dry milk in PBS-T (0.05% (v/v) Tween-20 in PBS) for 1h at room temperature, followed by primary antibody incubation O/N at 4C overnight. Following primary antibody incubation, blots were probed with HRP-conjugated secondary antibody (7074S and 7076S; CST) for 1 h at room temperature. Proteins were visualized using SuperSignal West Pico or Femto (Thermo

Scientific) and imaged using either an ImageQuant LAS 4000 Chemiluminescent Image Analyzer (General Electric) or Amersham ImageQuant 800 (Cytiva). Primary antibodies used (at a 1:1000 dilution unless otherwise indicated) for immunoblot include: anti-FLAG (1:2000; Sigma; #F1804), anti-GST (1:2000, Sigma; #G1160), anti-β-actin (1:5000, GeneTex; #GTX629630), anti-AcK (Cell Signaling Technology; #9814), anti-ZIKV(NS3 K389) (Custom-made; this paper), anti-ZIKV NS3 (Custom-made; [46]), anti-ZIKV NS3 (GeneTex; #GTX133309), anti-RIG-I (Adipogen; AG-20B-000).

Generation of 5'UTR-C66-3'UTR ZIKV RNA. A GeneBlock ("Gblock") encoding the minimum T7 promoter 5'TAATACGACTCACTATAGG3' and the 5'UTR, the first 66nt of the capsid protein, and the 3'UTR of ZIKV was ordered from IDT. Upon receipt, the GBlock was resuspended to 100ng/μl. Next, 5ng of the Gblock was PCR amplified using High Fidelity PCR Master Mix with primers from IDT (Forward: 5'-TAATACGACTCACTATAGGAGTTGTTGATCTGTGTG-3'; Reverse: 5-AGACCCATGGATTTCCCCACACC-3') using a 55'C annealing temperature and a 40 s extension time. The PCR reaction was resolved on a 1% agarose gel by electrophoresis and the 620 bp product was gel purified using an Omega BioTek Gel purification kit (eluted in 30μl). The concentration of the PCR product was measured by nanodrop (20ng/ μl) and .1μg of product was used in a 2.5 h *in vitro* transcription reaction at 37°C using the Invitrogen MEGAscript kit. After IVT, the product was treated with Turbo DNase for 15 min x 37°C. Next, the reaction was stopped by the addition of nuclease-free water and lithium chloride (Invitrogen). The RNA was precipitated at -20°C for 1 hand the pellet resuspended in 50 μl of nuclease-free water. An aliquot of the RNA (5μl) was immediately heated at 85°C for 8 minutes to resolve secondary structures, then moved into an

overnight 3′ end biotinylation reaction (Pierce) at 16°C, while the remainder was frozen at -80°C.

RNA pulldown assay. HEK293T cells (~1x10^7) were transfected with FLAG-NS3 WT or mutants for 48 h, and treated with deacetylase inhibitor at 16 h pre-harvest. Cells were lysed in NT2 buffer (50 mM Tris-HCl, pH 7.0, 150 mM NaCl, 1 mM $MgCl_2$, 0.05% [vol/vol] NP-40, SUPERase·In [Thermo Fisher], protease inhibitor, and deacetylase inhibitor). 30% of the lysate was pulled down using FLAG beads for 4 h to determine the acetylated state of the purified NS3 proteins. The remaining lysate was incubated with 1 pmol of biotinylated ZIKV RNA (described above) for 3 h, followed by pull-down with streptavidin beads for 2 hours. Following pull-down, streptavidin beads were gently washed with NT2 buffer and resuspended in 2X Laemmli buffer for subsequent SDS-PAGE to determined pull-downed FLAG-NS3 protein.

NS3 Helicase Assay. FLAG-tagged ZIKV NS3 WT and mutants, or FLAG-tagged ZIKV NS3 WT co-transfected with increasing amounts of HA-tagged KAT5γ, were affinity-purified from ~1 x 10^8 transiently transfected HEK293T cells, and eluted with FLAG peptide as described above. FLAG peptide was removed from the elution using a Microcon centrifugal Ultracel filter with a 30 kDa cutoff. Subsequently, purified FLAG-NS3 protein concentrations were determined by BCA assay (Pierce). Equal amounts (2.6 μM) of NS3 WT or mutant proteins were incubated in a black 96-well plate (Nunc; #165305) with 1 μM of annealed, complementary synthetic RNAs (generated by IDT) encoding a fluorescent 5′-Cy3-label (with a 3′ overhang to allow helicase loading) and a quenching 3′-BHQ2-label in the presence of 16.5 mM ATP (Abcam; #ab146525) in helicase reaction buffer (20 mM Tris–HCl (pH 7.0), 10 mM NaCl, 0.1 mg/mL BSA, 5 mM MgCl2, 2 mM DTT)

for 60 min. The release and subsequent fluorescence of the Cy3-labeled RNA substrate was measured using a BioTek Syngery Neo2 Plate reader with settings Ex 540nm and Em 579nm. Unwinding activity was calculated by subtracting the baseline reading at time = 0 (F_0) from each time point reading (F_t) and dividing by F_0. The RNA sequences used were: ZIKV Cy3-RNA (5′-Cy3-GCGUCUUUACGGUGCUUAAAACAAAACAAAACAAAACAAAA-3′; 5′-AGCACCGUAAAGACGC-3′-BHQ2). Annealing of the synthetic RNA strands for the Molecular Beacon Assay was carried out by mixing 100 μM of each fragment in 5X annealing buffer (50 mM Tris (pH 7.5), 250 mM NaCl, 5 mM EDTA) at 95°C for 5 min and cooling down slowly to RT.

RNA purification and qRT-PCR. For viral transcript analyses and knockdown efficiency determination, total cellular RNA was purified using an RNA extraction kit (OMEGA Bio-Tek) per the manufacturer's instructions. Equal amounts of RNA (25–500 ng) were used in a one-step qRT-PCR reaction using the SuperScript III Platinum One-Step qRT-PCR kit with ROX (Invitrogen) and commercially-available FAM reporter dye primers (IDT) for the analyzed transcripts. Gene expression was normalized to that of house-keeping gene *18S* (for SVGA cells). The comparative CT method (ΔΔCT) was used to measure the transcript levels of each target gene. ZIKV genomic RNA was analyzed using a previously described primer for ZIKV E: 5′-CCACTAACGTTCTTTTGCAGACAT-3′ (forward), 5′-CCGCTGCCCAACACAAG-3′ (reverse), 5′-/56-FAM/AGCCTACCT/ZEN/TGACAAGCAATCAGACACTCAA/3IABkFQ/-3′ (probe) (*11*). All qRT-PCR reactions were performed using a 7500 FAST Real-time PCR machine

(Applied Biosystems) or QuantStudio 6 Pro Real-Time PCR Machine (Applied Biosystems).

Sequencing and determination of ZIKV revertants. Viral supernatants from Vero cells transfected with ZIKV ICD WT or K389 mutants were harvested and half of the aliquot was subjected to plaque assay to measure viral titer (P0). The other half was used to infect Vero cells at a fixed MOI (.001), and supernatants were harvested at 72h p.i (P1). The P1 supernatants were used to infect P2 and P3. After 3 fixed-MOI passages, the supernants were plaqued to determine titer as well as sequenced across the K389 site. and processing with the Omega BioTek RNA Kit 1. The purified RNA was then reverse transcribed using the SuperScript First-strand synthesis kit (Invitrogen) with gene-specific primers covering the NS3 K389 region of the ZIKV genome. The resultant cDNA was further amplified by PCR using the same primer set and subsequently Sanger-sequenced to track the reversion.

Quantification and Statistical Analysis. All data were presented as means ± SD and analyzed using GraphPad Prism software (version 7). An unpaired two-tailed Student's *t*-test or one-way ANOVA (with Tukey's HSD) ($P < 0.05$ was considered statistically significant) was used as indicated in the legends. Pre-specified effect sizes were not assumed and three biological replicates (n) for each condition were used within each individual experiment. Data were reproduced in independent experiments as indicated in the legends for each figure.

CHAPTER 3

HUMAN KAY5γ ACETYLATES ZIKV NS3 AND PROMOTES VIRUS REPLICATION

This chapter is adapted from: Serman, T.; Chiang, C.; Acharya, D.; Pandey, S.; Muppala, S.; Liu, G.; Gack, M.U. Acetylation of the flavivirus NS3 helicase by KAT5γ is essential for virus replication. (Manuscript under review, 2022).

Attributions: TS performed and analyzed all experiments with the following exceptions: SP performed and analyzed Figures 3.1D, 3.9C and D. GL performed and analyzed Figures 3.4E-H. SM performed and analyzed Figures 3.4A and 3.7C. CC performed and analyzed Figure 3.8E.

3.1 Abstract

Lysine acetyltransferases are a class of enzymes that reversibly transfer an acetyl group from the cofactor acetyl-CoA onto the ε-amino group of a lysine residue within a target protein. The addition of the acetyl group neutralizes the positive charge of the lysine residue, and can have myriad downstream consequences for protein function. Herein, we took an RNAi approach to identify the host acetyltransferase responsible for lysine acetylation of the ZIKV NS3 K389 residue. Our efforts discovered that KAT5γ, a hitherto uncharacterized, replication complex-localized isoform of the host lysine acetyltransferase 5 (KAT5), is required for NS3 K389 acetylation and regulation of ZIKV replication.

3.2 Introduction

Since its discovery, TIP60/KAT5α has been shown to function in host cells within a large multiprotein complex that acts largely as a transcriptional co-regulator at the chromatin level by acetylating histones [168]. Additionally, TIP60/KAT5α plays an important nuclear role within the DNA damage response, apoptosis, and cell cycle regulation by acetylating diverse downstream protein substrates [169]. However, nearly every study characterizing these KAT5 protein functions have focused on only one of its four encoded isoforms, namely KAT5α, which localizes almost exclusively to the nucleus [132, 170]. The remaining three splice isoforms of KAT5 – KAT5-Long (KAT5L), KAT5β, and KAT5γ – are less well studied [131, 133, 136]. While a few studies have characterized the cytoplasmic and nuclear localization patterns of KAT5L and KAT5β isoforms [133, 136], KAT5γ has only been characterized at the genomic level, as a distinct isoform that

encodes an alternate intron (also encoded by KAT5L) but lacks the exon 5. Notably, these two distinguishing features of the KAT5 isoforms have not been functionally characterized.

In the previous chapter, we identified ZIKV NS3 K389 as a major site for post-translational acetylation. The functional consequence of acetylation was tested using non-acetylated and hyper-acetylated mimicking amino acids, arginine (R) and glutamine (Q), respectively, introduced into the NS3 protein and recombinant virus context. Using this mutational approach, we uncovered that acetylation modulates the RNA binding capacity of the NS3 helicase domain, with the NS3 K389R mutant showing enhanced RNA binding and the NS3 K389Q mutant showing reduced RNA binding compared with the WT NS3 protein. Moreover, we found that the downstream consequence of too tight or too weak RNA binding was impairment of helicase unwinding activity, as both NS3 K389 mutants showed reduced RNA unwinding abilities compared with the WT NS3 protein. Finally, recombinant viruses ZIKV(K389R) and ZIKV(K389Q) were both attenuated compared with the parental virus, suggesting that acetylation is a required regulatory mechanism determining successful replication of the virus. While point mutations of the ZIKV NS3 K389 residue suggest that acetylation is important for these key functions of the viral helicase, the assessment of viral replication during bonafide loss of K389 acetylation would confirm the importance of this PTM for ZIKV replication.

3.3 Results

3.3.1 Identification of human acetyltransferases that modulate ZIKV replication through an RNAi screen

To determine the effect of reduced acetylation of the ZIKV NS3 protein during replication, we first designed a candidate acetyltransferase screen to identify the

acetyltransferase required for NS3 K389 acetylation. To this end, we selected a panel of acetyltransferases previously identified as cellular candidates for modulating flavivirus replication to test their effect on ZIKV replication during siRNA-mediated silencing. This panel included KAT2A and KAT2B, the cofactors (TAF5, 6, and 12) of which were identified as WNV antiviral factors in a genome-wide screen [171]; KAT3A and KAT3B, the cofactor (CITED2) of which was identified as a WNV host susceptibility factor in a genome-wide screen [172]; and KAT5, which was previously functionally validated as a WNV antiviral factor in insect cells [171]. Given its structural similarity to KAT5, KAT8 was also included in this candidate screen [173]. Interestingly, three of the six screened acetyltransferases – KAT3B, KAT5, and KAT8 – reduced viral replication by both qRT-PCR (**Fig. 3.1A**) and plaque assay (**Fig. 3.1B**) when silenced (**Fig. 3.1C**), suggesting a proviral role during ZIKV replication, akin to that of NS3 acetylation as determined by recombinant virus experiments (**Fig. 2.7**). Since multiple proviral acetyltransferases were identified in this candidate screen, we decided to expand our screen to include the full panel of human acetyltransferases (28 total genes) to ensure that the NS3 acetyltransferase was not missed by our original, candidate approach. Therefore, we silenced all 23 identified human acetyltransferases in addition to 5 putative acetyltransferases, which have no yet identified substrates but encode an acetyltransferase domain, and assessed the effect of silencing on ZIKV replication by qRT-PCR. Through this approach we found that 9 acetyltransferases (KAT 1, 3B, 5, 7, 8, 12, and GCN5I1, ELP4 and METTL8), when silenced, significantly reduced ZIKV replication (**Fig. 3.1D**).

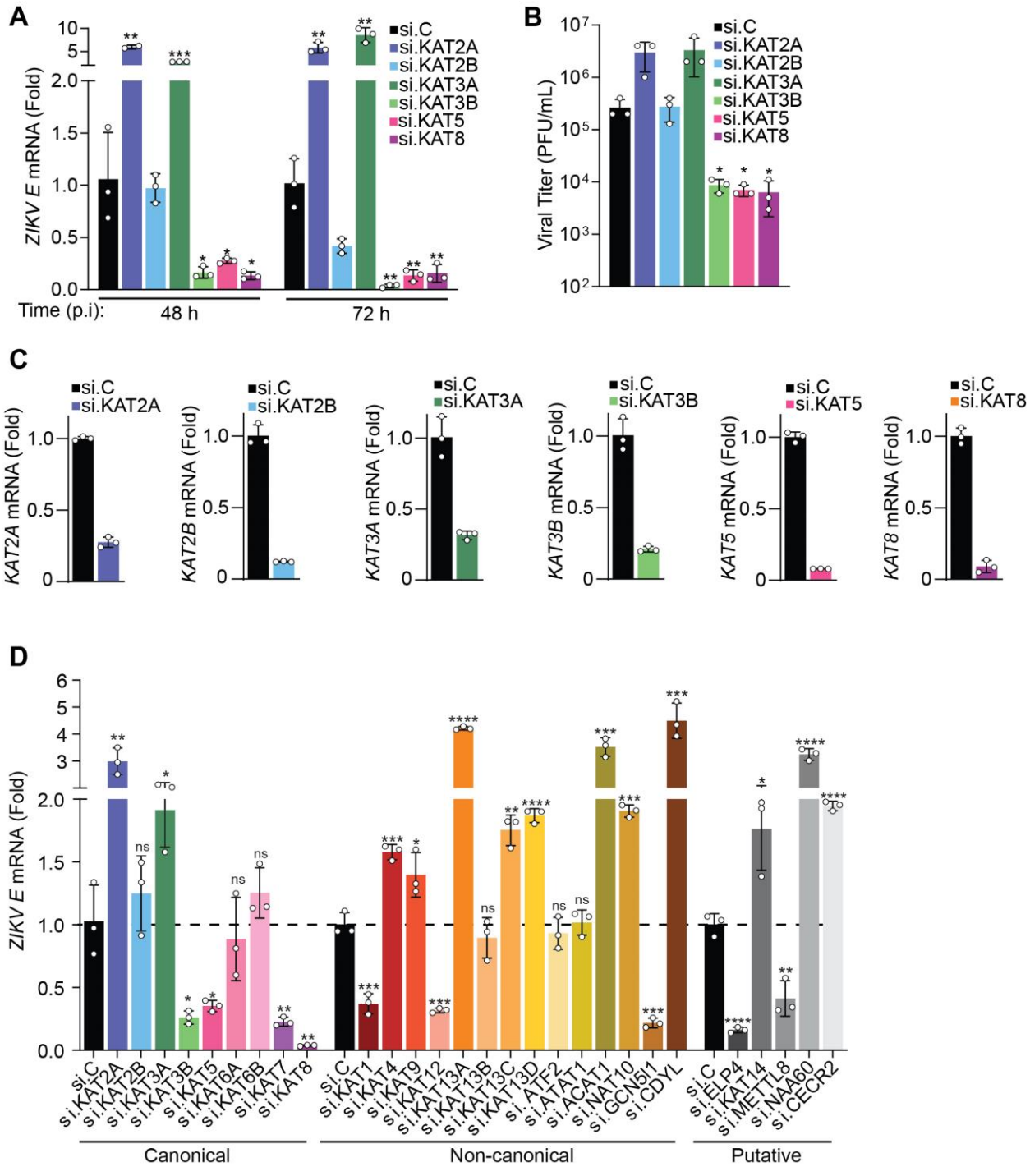

Figure 3.1 RNAi screen of human lysine acetyltransferases (KATs) for their effect on ZIKV replication.

Figure 3.1 *(continued)* RNAi screen of human lysine acetyltransferases (KATs) for their effect on ZIKV replication.

(A) qRT-PCR analysis of *ZIKV E* mRNA in A549 cells that were transfected for 16 h with either non-targeting control siRNA (si.C) or siRNAs targeting the indicated human acetyltransferases, and then infected with ZIKV (BRA/2015, MOI 0.001) for 48 h and 72 h, determined by qRT-PCR analysis

(B) Viral titers in the supernatant of A549 cells transfected as in (A) and then infected with ZIKV (strain BRA/2015, MOI 0.001) for 72 h, determined by plaque assay and presented as PFU/mL. Limit of detection: 10^2.

(C) Knockdown efficiency of the indicated genes in A549 cells that were transfected as in (A), analyzed by qRT-PCR.

(D) qRT-PCR analysis of *ZIKV E* mRNA in A549 cells that were transfected for 30 h with either non-targeting control siRNA (si.C) or siRNAs targeting the indicated human acetyltransferases, and then infected for 48 h with ZIKV (BRA/2015, MOI 0.001).

Unpaired Student's *t* test between indicated sample groups. ns, not significant; *p < 0.05, **p < 0.01, ***p < 0.001, **** p < 0.0001.

To confirm whether this proviral role was due to direct acetylation, an NS3 mutant encoding the K389 site with the remaining five acetylated lysine residues mutated to arginine, called "NS3(K389only)", was ectopically expressed in cells transfected with individual siRNAs targeting each of the proviral candidate KATs and subsequently assessed for acetylation by Western blot (WB). As a result, siRNA-mediated knockdown of KAT5, but not the other proviral acetyltransferases, reduced acetylation of NS3(K389only) compared to the non-targeting control siRNA (**Fig. 3.2A**). Additionally, RNA was purified from an aliquot of these samples for validation of efficient gene silencing (**Fig. 3.2B**).

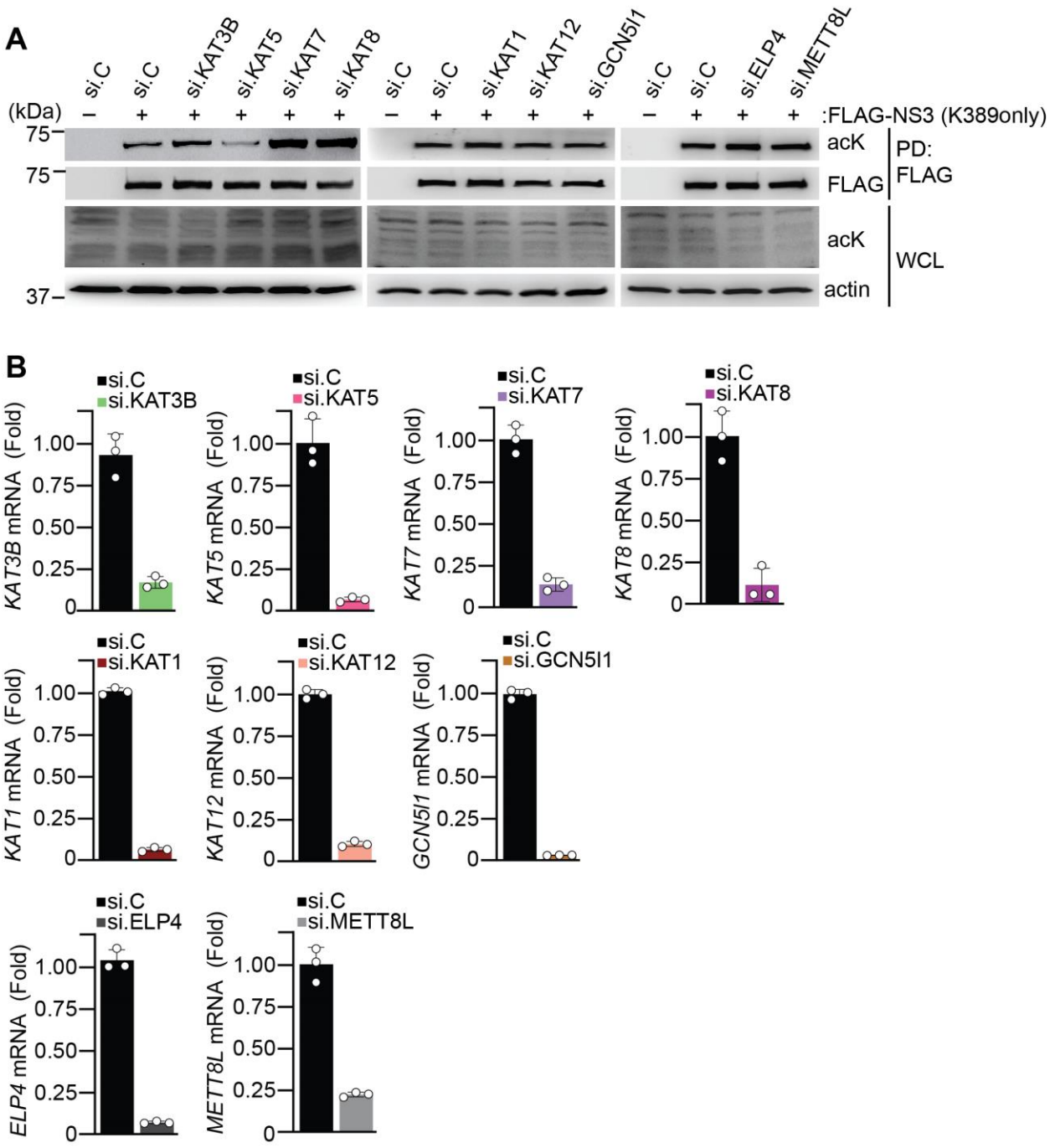

Figure 3.2 Screening proviral KAT candidates for their role in direct acetylation of ZIKV NS3 at residue K389.

(A) Acetylation of FLAG-tagged ZIKV NS3(K389only) in HEK293T cells that were transfected for 16 h with either si.C or siRNAs targeting the indicated genes and then co-transfected with FLAG-NS3(K389only) for 30 h, assessed by PD with anti-FLAG and IB with anti-acK.

(B) Knockdown efficiency for silenced genes determined in parallel in (B) by qRT-PCR.

3.3.2 Acetylation of ZIKV NS3 at K389 and regulation of viral replication by host enzyme KAT5

In accord with the results of the screen, we also found that silencing of KAT5, but not KAT3B, reduced the acetylation of WT ZIKV NS3 (**Fig. 3.3A, B**). Moreover, the reduced acetylation signal observed with the anti-pan-acK antibody in the original screen (**Fig. 3.2A**) was also reproduced using a custom-made acetyl-K389-NS3(ZIKV)-specific antibody (**Fig. 3.3C**). Further, ectopically-expressed NS3 bound to endogenous KAT5, but not to endogenous KAT3B (**Fig 3.3D**). Importantly, NS3 also co-immunoprecipitated with endogenous KAT5 during authentic ZIKV infection of A549 cells (**Fig 3.3E**). Combined, these results suggest that KAT5 is the direct acetyltransferase for NS3 K389 acetylation.

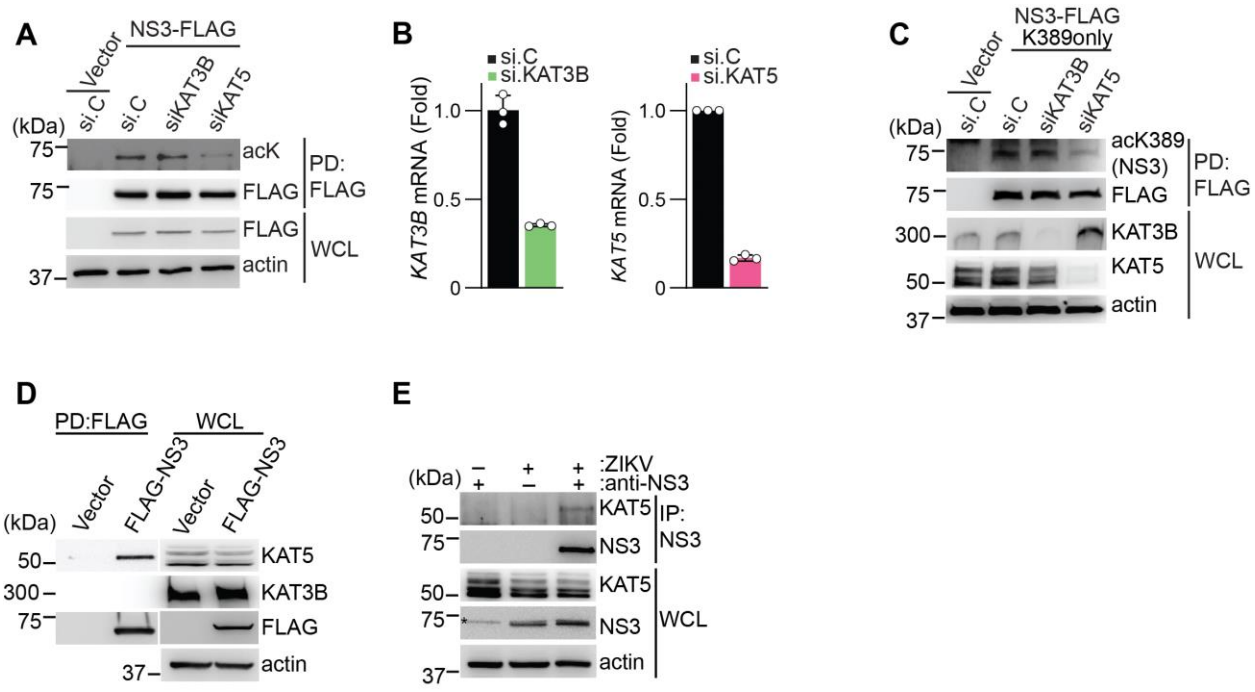

Figure 3.3 KAT5 binds and acetylates ZIKV NS3.

(A) Acetylation of FLAG-tagged ZIKV NS3 in HEK293T cells that were transfected for 40 h with either si.C or siRNAs targeting KAT3B or KAT5, determined by anti-FLAG PD and IB with anti-acK and anti-FLAG. WCLs were probed by IB with anti-FLAG and anti-Actin (loading control).

(B) Representative knockdown efficiency of the indicated genes, determined by qRT-PCR.

(C) Acetylation of FLAG-tagged ZIKV NS3(K389only) in HEK293T cells that were transfected for 40 with si.C or siRNAs targeting KAT3B or KAT5, determined by anti-FLAG PD and IB with an acetyl-K389-NS3(ZIKV)-specific antibody. WCLs were probed by IB with the indicated antibodies.

(D) Binding of endogenous KAT5 or KAT3B (negative control) and ZIKV NS3 in HEK293T cells that were transfected for 40 h with either empty vector or FLAG-NS3 (ZIKV), determined by PD with anti-FLAG and IB with anti-KAT5 or anti-KAT3B.

(E) Binding of endogenous KAT5 and NS3 in A549 cells that were mock-treated or infected with ZIKV (BRA/2015, MOI 1) for 48 h, assessed by IP with anti-NS3 and IB with anti-KAT5. Asterisk denotes unspecific band.

To further assess the proviral role of KAT5 for ZIKV replication, KAT5 (all four isoforms) was silenced in Vero cells and viral replication was assessed by plaque assay (**Fig. 3.4A**), revealing a striking reduction in ZIKV replication. This reduction was also

observed during KAT5 silencing in HMC3 (microglial) cells, by both qPCR and plaque assay (**Fig. 3.4B-D**). Moreover, KAT5 silencing reduced ZIKV replication in A549 cells to a similar or even greater extent than a previously-identified proviral host factor, TMEM41B [174], by qPCR and plaque assay (**Fig. 3.4E-H**). In all, these results support that KAT5 is a proviral factor for ZIKV replication in a variety of cell types.

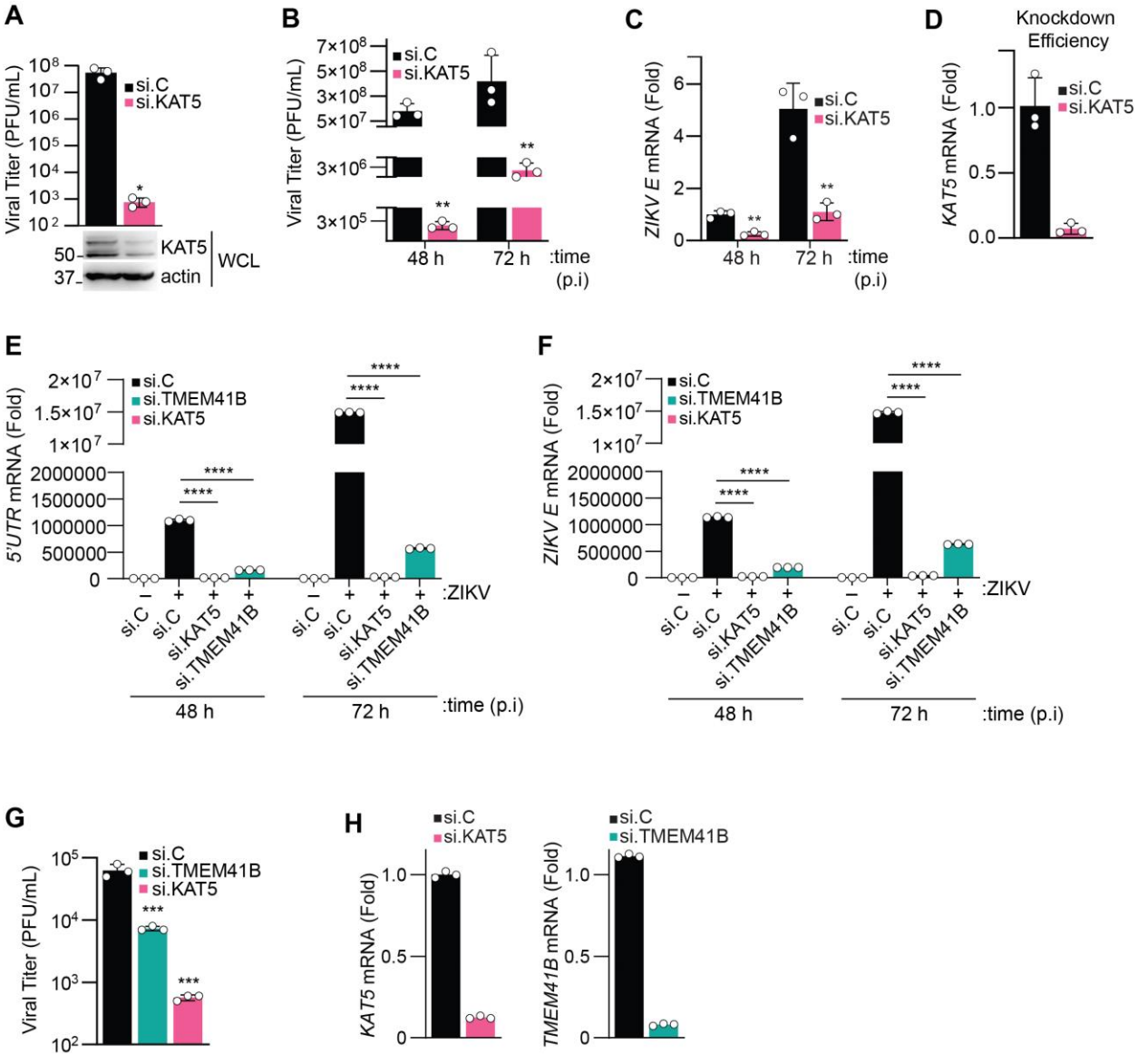

Figure 3.4 Knockdown of KAT5 reduces ZIKV replication in several different cell types.

Figure 3.4 *(continued)* Knockdown of KAT5 reduces ZIKV replication in several different cell types.

(A) Upper: ZIKV replication in Vero cells that were transfected for 30 h with either si.C or KAT5-specific siRNA (si.KAT5) and then infected with ZIKV (BRA/2015, MOI 0.001) for 48 h, determined by plaque assay. Lower: Representative knockdown efficiency of endogenous KAT5, determined in the WCLs by IB with anti-KAT5 and anti-Actin (loading control).

(B) ZIKV replication in HMC3 cells that were transfected for 30 h with either si.C or si.KAT5 and then infected with ZIKV (BRA/2015, MOI 0.001) for the indicated times, determined by plaque assay and presented as PFU/mL. Limit of detection: 10^2.

(C) ZIKV *E* transcripts in HMC3 cells that were transfected as in (B), determined by qRT-PCR.

(D) Representative knockdown efficiency of *KAT5* in HMC3 cells transfected for 30 h with si.C and si.KAT5, determined by qRT-PCR.

(E,F) ZIKV *5'UTR* **(E)** or ZIKV *E* **(F)** transcripts in A549 cells that were transfected for 30 h with either si.C, si.KAT5, or TMEM41B-specific siRNA (si.TMEM41B) and then either mock-treated or infected with ZIKV (BRA/2015, MOI 0.001) for the indicated times, determined by qRT-PCR.

(G) ZIKV replication in A549 cells that were transfected as in (E,F) and infected with ZIKV (BRA/2015, MOI 0.001) for 48 h, determined by plaque assay and presented as PFU/mL. Limit of detection: 10^2

(H) Representative knockdown of the indicated genes for the experiments in (E-G).

Unpaired Student's *t* test between indicated sample groups. *p < 0.05, **p < 0.01, ***p < 0.001, **** p < 0.0001.

In addition to siRNA-mediated silencing of KAT5, we also took a small molecule inhibitor approach towards targeting of KAT5. Several small molecule inhibitors have been characterized in the literature to bind to the catalytic or Ac-CoA pocket of KAT5 and thereby reduce its acetyltransferase activity [175, 176]. One of these inhibitors, anacardic acid, was found to strikingly reduce ZIKV virus replication at a 10μM concentration, which did not reduce cell viability (**Fig. 3.5A, B**), suggesting that KAT5's catalytic activity contributes to ZIKV replication. However, given anacardic acid's broad effects on several cellular pathways, in addition to its inhibition of the enzymatic activities of other KATs, this molecule was not further utilized in this study [176].

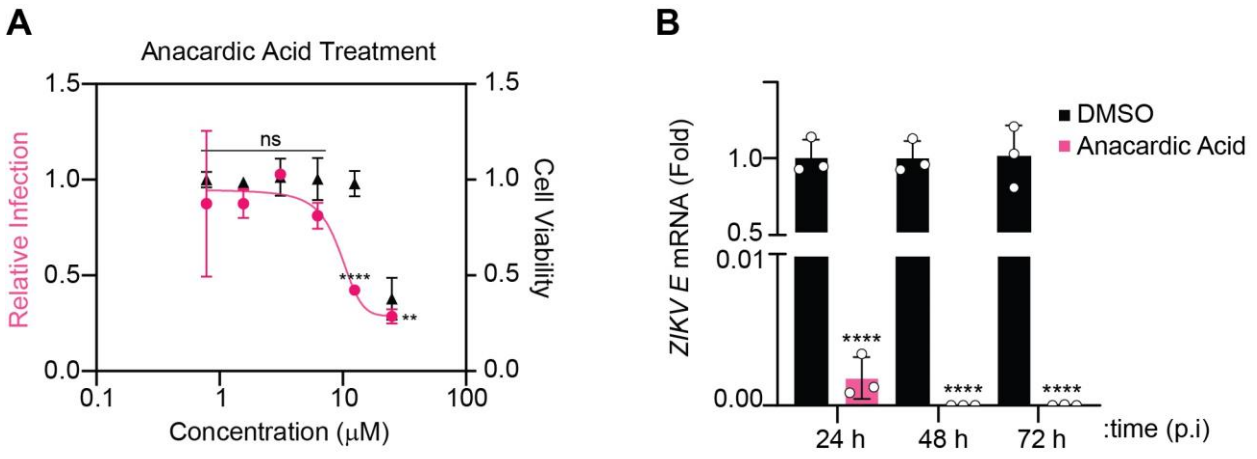

Figure 3.5 Anacardic acid treatment restricts ZIKV replication.

(A) ZIKV replication measured by qRT-PCR of the *ZIKV E* gene in A549 cells that were treated with increasing doses of anacardic acid for 2 h prior to infection with ZIKV (BRA/2015, MOI 0.001) for 48 h. Cell viability was measured by luminescence after incubation with Cell Titer Glo (See Methods).

(B) ZIKV replication measured by qRT-PCR in A549 cells that were treated with 10 μM anacardic acid (or DMSO control) for 2 h prior to infection as in (A).

Unpaired Student's *t* test between indicated sample groups. ns, not significant; **p < 0.01, **** p < 0.0001.

3.3.3 A specific isoform of KAT5, KAT5γ, controls ZIKV NS3 acetylation and viral replication

Human endogenous KAT5 is transcribed as four unique isoforms: KAT5L, KAT5α, KAT5β, and KAT5γ [131, 177]. These four isoforms differ by the inclusion or splicing of two encoded features: intron 1 and exon 5 (**Fig. 3.6A**). The differential splicing of these isoforms produces four uniquely-sized proteins that can be distinguished WB (**Fig. 3.6B**).

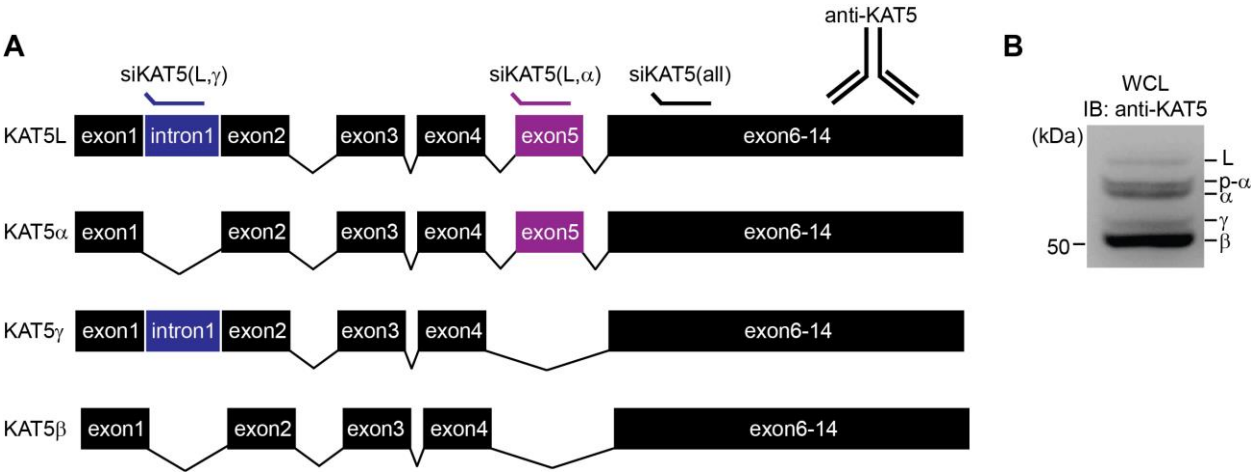

Figure 3.6 Schematic representation of the KAT5 gene organization and Western blot of the four human KAT5 isoforms.

(A) Schematic representation of the KAT5 gene organization as well as strategy for pairwise silencing of the four KAT5 splice isoforms in human cells. The antibody used for KAT5 detection by IB detects a protein region conserved in all four isoforms.

(B) Representative WB showing the individual KAT5 isoforms (L, α, γ and β) in HEK293T cells, determined in the WCLs by IB with anti-KAT5. p-α indicates the phosphorylated form of KAT5α.

Interestingly, when endogenous KAT5 was co-immunoprecipitated by FLAG-tagged NS3 or NS3 purified from ZIKV-infected cells, only one band was detected by the anti-pan-KAT5 antibody (**Fig. 3.3D,E**), which corresponded to the size of the KAT5γ isoform. To assess whether this specific isoform of KAT5 was responsible for acetylation of ZIKV NS3 K389, and thus, modulation of viral replication, KAT5 isoforms were pair-wised silenced using siRNAs targeting either (1) intron 1 (shared by KAT5L and KAT5γ) or (2) exon 5 (shared by KAT5L and KAT5α), in addition to the control siRNA that targets a region conserved in all four isoforms (**Fig. 3.6A**). Using this approach, NS3 acetylation was found to be reduced only under conditions of KAT5γ silencing (during intron or "KAT5(all)" silencing), while cells silenced for the two other isoforms, KAT5L and KAT5α, showed no change in NS3 acetylation compared to transfection of a non-targeting control

siRNA (**Fig. 3.7A**). Likewise, ZIKV replication was only attenuated after silencing of KAT5γ by the intron-targeting or total KAT5-targeting siRNA (**Fig. 3.7B**). Although KAT5γ could only be silenced along with KAT5L (intron silencing), silencing of KAT5L along with KAT5α (exon silencing) did not reduce NS3 acetylation nor attenuate viral replication, suggesting that KAT5γ is the specific isoform responsible for regulating NS3 acetylation and subsequent ZIKV replication. To test the specificity of the proviral role of KAT5γ during ZIKV replication, replication of a positive sense RNA picornavirus (EMCV) and a negative sense RNA rhabdovirus (VSV) were assessed during KAT5γ silencing by plaque assay, in parallel with assessing ZIKV replication in these cells. Silencing of KAT5γ reduced only ZIKV replication, but had no effect on EMCV or VSV replication (**Fig. 3.7C**), suggesting that the proviral role of KAT5γ is likely specific for ZIKV or, more generally, flaviviruses (ie, mediated through acetylation of the flavivirus NS3 protein). Similar to total KAT5 silencing, silencing of KAT5γ (intron silencing) in SVGA cells reduced ZIKV replication similar to the previously-characterized proviral factors TMEM41B andEMC2 [178] (**Fig. 3.7D**).

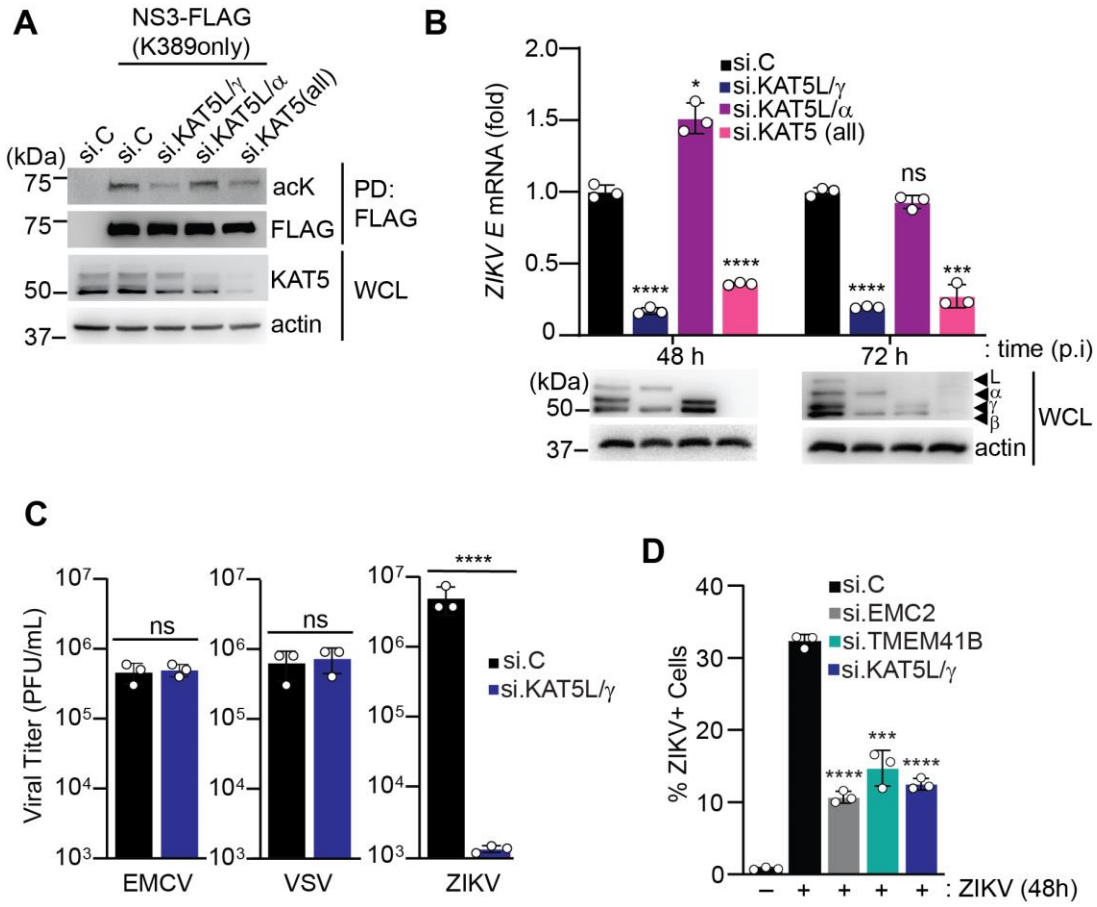

Figure 3.7 KAT5γ is required for ZIKV NS3 K389 acetylation and viral replication.

(A) Acetylation of FLAG-tagged ZIKV NS3(K389only) in HEK293T cells that were transfected for 16 h with either si.C or siRNAs targeting the indicated KAT5 isoforms and then co-transfected with FLAG-NS3 for 30 h, determined by PD with anti-FLAG and IB with anti-acK. Knockdown of the individual KAT5 isoforms was confirmed in the WCLs by IB with anti-KAT5 and anti-Actin (loading control).

(B) *ZIKV E* transcripts in A549 cells that were transfected for 16 h with the indicated siRNAs and then infected with ZIKV (BRA/2015, MOI 0.001) for the indicated times, determined by qRT-PCR. Representative knockdown efficiency of the individual KAT5 isoforms was determined in the WCLs by IB with anti-KAT5.

(C) EMCV, VSV and ZIKV titers in the supernatants from A549 cells that were transfected for 30 h with either si.C or siRNA targeting the KAT5 intron (siKAT5L/γ) and then infected with EMCV (MOI 0.1) for 12 h, VSV (MOI 0.001) for 24 h, or ZIKV (BRA/2015, MOI 0.001) for 48 h, determined by plaque assay and presented as PFU/mL.

(D) Frequency of ZIKV-positive A549 cells that were transfected with si.C or siRNAs targeting EMC2, TMEM41B, or KAT5L/γ and then infected for 48 h with ZIKV (BRA/2015, MOI 0.05), determined by viral E protein staining and flow cytometric analysis.

Unpaired Student's *t* test between indicated sample groups. ns, not significant; *p < 0.05, ***p < 0.001, **** p < 0.0001.

Conversely to KAT5γ silencing, a KAT5γ plasmid construct was designed by introducing a silent mutation at Q37 (125-CAG-127→ 125-CAA-127) at the guanine splice acceptor site of the KAT5 intron, preventing further splicing of KAT5γ to KAT5β during overexpression, as validated by Western blot (**Fig. 3.8A**). Using this construct, we found that overexpression of KAT5γ enhanced acetylation of ZIKV NS3(K389only) in a dose-dependent fashion (**Fig 3.8B**). On the other hand, overexpression of a dominant-negative KAT5γ mutant (Q377E/G380E), previously characterized for its abrogated KAT activity [179], reduced acetylation of NS3 at residue K389 (**Fig. 3.8C**). Moreover, expression of this dominant-negative mutant construct abrogated ZIKV infection, measured by flow cytometry, in a dose-dependent manner (**Fig. 3.8D).** Finally, ZIKV NS3-mediated RNA unwinding was shown to be reduced during overexpression of WT KAT5γ, in a dose-dependent manner, corresponding to increased acetylation of the NS3 protein, suggesting that acetylation directly modulates this key NS3 protein function (**Fig. 3.8E**).

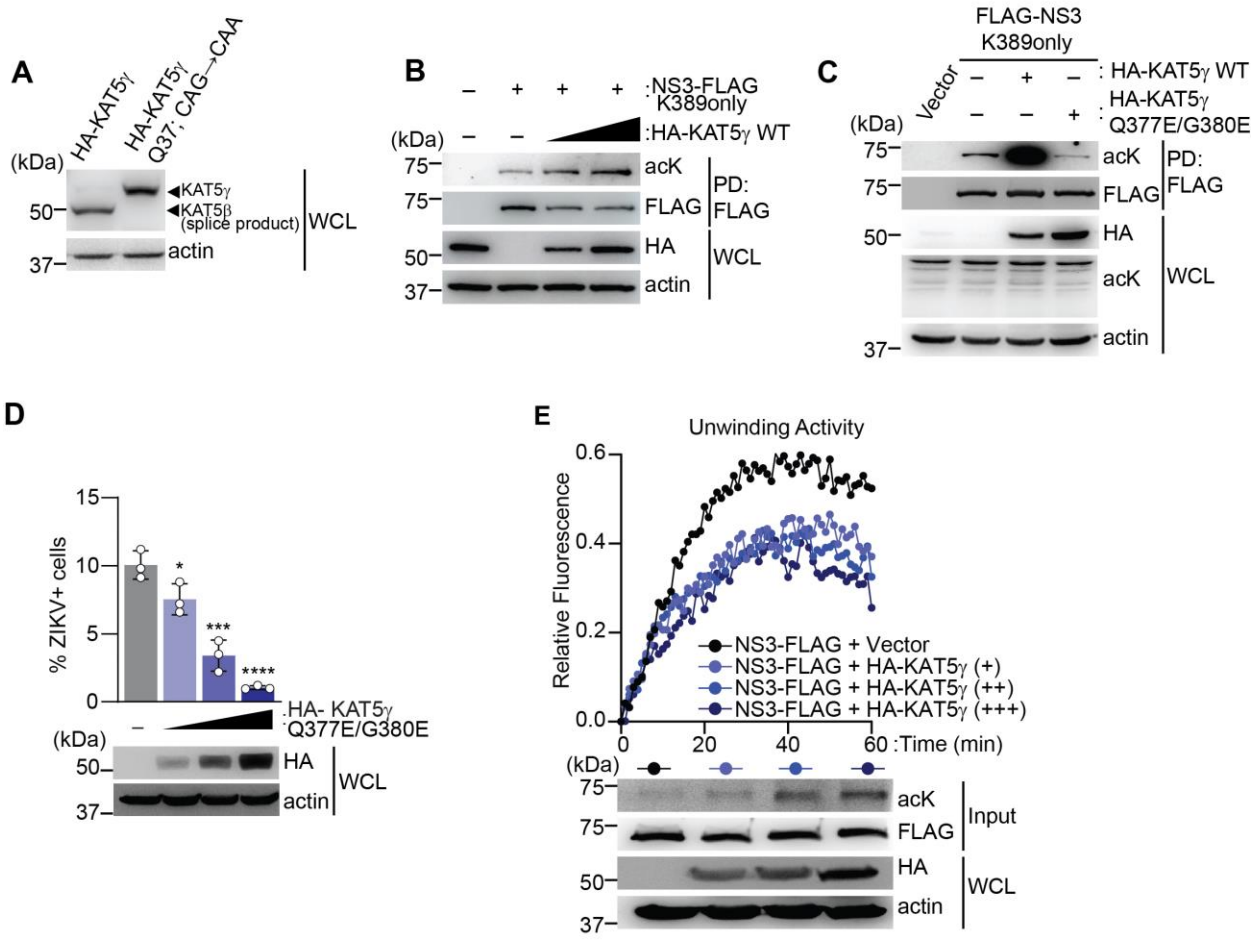

Figure 3.8 Ectopic expression KAT5γ modulates ZIKV NS3 acetylation, ZIKV replication, and RNA unwinding by NS3.

(A) Representative WB showing overexpression of HA-tagged KAT5γ WT and KAT5γ harboring a silent splice site mutation (Q37; CAG→ CAA), determined in the WCLs by IB with anti-HA.

(B) Acetylation of FLAG-tagged ZIKV NS3(K389only) in HEK293T cells that were co-transfected for 40 h with increasing amounts of HA-tagged KAT5γ, determined by anti-FLAG PD and IB with anti-acK and anti-FLAG. WCLs were probed with anti-HA and anti-Actin (loading control).

(C) Acetylation of FLAG-tagged ZIKV NS3(K389only) in A549 cells that were co-transfected for 40 h with either empty vector or HA-tagged KAT5γ WT or dominant-negative mutant (Q377E/G380E), determined by PD with anti-FLAG and IB with anti-acK. WCLs were probed by IB the indicated antibodies.

(D) Frequency of ZIKV-positive A549 cells that were transfected for 24 h with either empty vector (-) or increasing amounts of HA-KAT5γ Q377E/G380E and then infected with ZIKV (BRA/2015; MOI 001) for 48 h, determined by staining of the viral E protein (anti-4G2) and flow cytometry. Expression of HA-KAT5γ was confirmed in the WCLs by IB with anti-HA. Unpaired Student's *t* test between indicated sample groups. ns, not significant; *p < 0.05, ***p < 0.001, **** p < 0.0001.

Figure 3.8 *(continued)* Ectopic expression KAT5γ modulates ZIKV NS3 acetylation, ZIKV replication, and RNA unwinding by NS3.
(E) FRET-based molecular beacon helicase assay measuring the dsRNA-unwinding capacity of FLAG-tagged ZIKV NS3 purified from HEK293T cells that were transiently transfected with NS3 together with empty vector or increasing amounts of HA-KAT5γ. Equal input amounts of FLAG-NS3 as well as its acetylation level were confirmed by IB with anti-FLAG and anti-acK, respectively. Expression of HA-KAT5γ was confirmed by IB with anti-HA.

Despite the observation of KAT5γ, and not the other KAT5 isoforms, as a proviral factor supporting ZIKV replication, the KAT5γ isoform does not possess any unique structural features compared with other KAT5 isoforms that may explain its specificity for acetylation of ZIKV NS3. Therefore, we tested whether the KAT5γ isoform was transcriptionally induced by ZIKV infection. However, qRT-PCR analysis revealed that total KAT5 gene expression in both A549 cells (**Fig. 3.9A**) and SVGA cells (**Fig. 3.9B**) was unaffected by ZIKV infection. Further, gene expression profiling showed that KAT5 mRNA and protein were not exclusively expressed in ZIKV-permissive cells but widely abundant in human tissues and cell types, albeit to varying levels (**Fig 3.9C, D**).

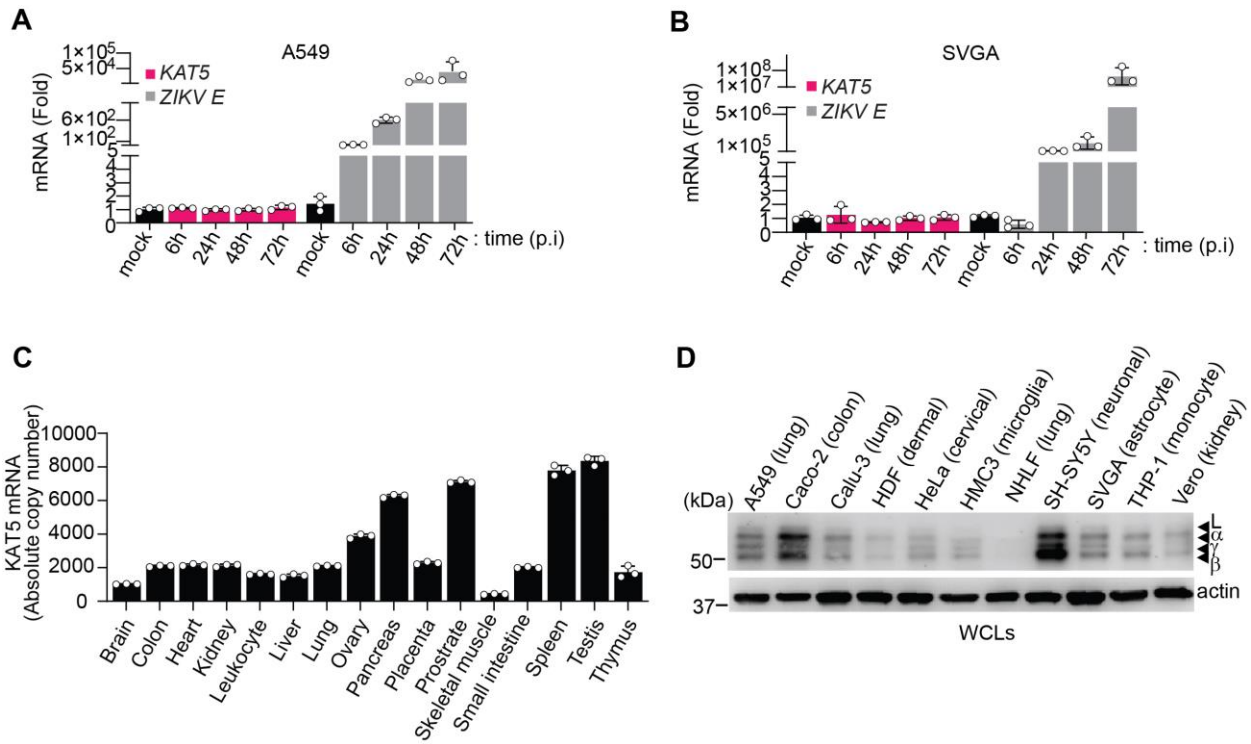

Figure 3.9 KAT5 expression is not induced by ZIKV infection nor specific to ZIKV-permissive cell types.

(A-B) *KAT5* and *ZIKV E* transcript levels in A549 (A) and SVGA (B) cells that were infected with ZIKV (strain BRA/2015, MOI 0.5) for the indicated times, determined by qRT-PCR.

(C) Absolute *KAT5* transcript numbers in the indicated human tissues, measured by qRT-PCR.

(D) Endogenous KAT5 protein expression in the indicated cell lines or primary cells, determined in the WCLs by IB with anti-KAT5. WCLs were further probed with anti-Actin (loading control).

Therefore, it was tested whether KAT5γ has a specific localization within ZIKV-infected cells. Unfortunately, endogenous KAT5 is notoriously difficult to detect by IF using available antibodies [135]. Therefore, the localization of endogenous KAT5 was determined by a membrane flotation assay during ZIKV infection, which showed that KAT5γ specifically localized to ER-derived membranes containing ZIKV NS3 and NS4b (ie, the viral replication complex) during infection (**Fig 3.10**). In summary, these data

support a role of KAT5γ-mediated acetylation of ZIKV NS3 K389 during infection. Our results further suggest that KAT5γ acetylates NS3 at the virus replication complex.

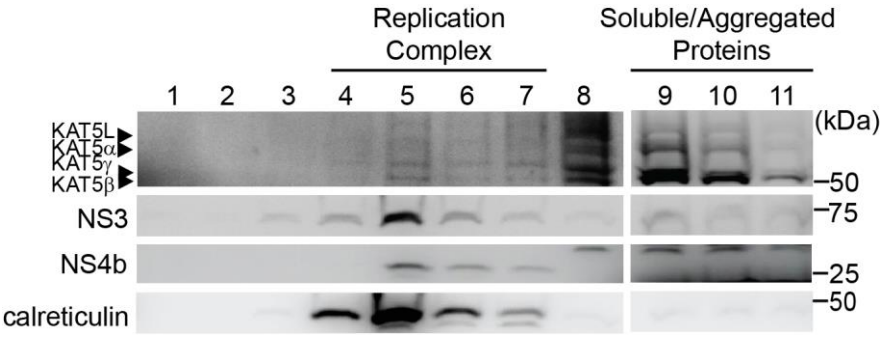

Fig 3.10 KAT5γ localizes to the replication complex during ZIKV infection.
Protein abundance of endogenous KAT5 isoforms, viral NS3 and NS4b, and calreticulin (ER-marker protein) in indicated fractions of A549 cells that were infected with ZIKV (BRA/2015, MOI 1) for 48 h, determined by membrane flotation assay and IB with the indicated antibodies.

3.4 Discussion

The data presented herein strongly supports a proviral role for KAT5, specifically KAT5γ, in NS3 acetylation and viral replication. The required role for KAT5 during ZIKV replication reflects the proviral role of NS3 K389 acetylation in mediating ZIKV replication, shown in Chapter 2 by the attenuation of both ZIKV(K389R) and ZIKV(K389Q) recombinant viruses compared to the parental virus. To further link these two parallel phenotypes, the replication of ZIKV(WT), ZIKV(K389R), and ZIKV(K389Q) could be tested in KAT5γ–depleted cells. Our results suggest that the replication of ZIKV(WT) would be attenuated in KAT5γ–depleted cells, compared with non-targeting control cells. In contrast, the replication phenotype of the two recombinant K389 mutant viruses would not be further attenuated by KAT5γ silencing, if the major role of KAT5γ in supporting ZIKV replication is through acetylation of K389 in NS3. This experiment would control for

other potential proviral roles mediated by KAT5γ outside of direct acetylation of ZIKV NS3 K389.

Previous studies of KAT5 have revealed that this enzyme often functions as part of a larger, transcriptionally-active complex called NuA4 [118]. While only KAT5α and KAT5β have been characterized within this complex, it is possible that KAT5γ also assembles into a larger complex and/or has additional binding partners. It is possible that binding proteins, or other chaperone proteins, facilitate NS3 binding or ER localization of KAT5γ and thereby ZIKV NS3 acetylation. However, future interaction studies are required to identify KAT5γ-binding proteins and their potential involvement in ZIKV NS3 acetylation.

Moreover, several upstream activating and deactivating proteins of KAT5 enzymatic function have been identified [114, 121, 140, 142-144]. While these upstream mediators are typically studied in the context of KAT5α-mediated transcriptional activation, it is possible that some of these factors could also regulate KAT5γ-mediated acetylation of ZIKV NS3. Since our data showed that KAT5 itself was not upregulated at the gene or protein expression level, perhaps upstream activators of KAT5 are upregulated during ZIKV infection, allowing for ZIKV-induced activation of KAT5γ. For example, upregulation of PTMases specific for KAT5, such as the kinases responsible for the activating KAT5α S86/90 phosphorylation [140, 142], or the activating K104 acetylation of KAT5α [143], may allow for enhanced KAT5γ–mediated NS3 acetylation during ZIKV infection. Supporting the potential for upstream mediators of KAT5 in regulating NS3 acetylation, our preliminary data suggest that KAT3B may act as one of these mediators. A previous study found that KAT3B interacts with KAT5 and promotes

KAT5 auto-acetylation at residue K327, thereby enhancing its stability, acetyltransferase activity, and interaction with downstream substrate FOXP3, ultimately enhancing its acetylation [144] (**Fig. 3.11A**). In accord, when both KAT3B and KAT5 were knocked down in the same cells, near complete loss of NS3(K389only) acetylation was observed (**Fig. 3.11B**). Further, overexpression of myc-tagged KAT3B enhanced ZIKV NS3 acetylation in a dose-dependent manner (**Fig 3.11C**), while a negative control, KAT8, did not show any enhancement (**Fig. 3.11D**), suggesting that KAT3B may be an upstream regulator of KAT5γ–mediated acetylation. However, further investigation characterizing this interaction and its potential role in NS3 acetylation, such as the loss of KAT3B-mediated enhancement of ZIKV NS3 acetylation in the absence of KAT5, is required to ensure its physiologically-relevant role as a KAT5γ upstream mediator. In terms of negative regulators, HDAC3 has been identified to inhibit KAT5α auto-acetylation, reducing enzymatic activity of its KAT domain [114]. Perhaps deacetylation of KAT5 by HDAC3, or by another HDAC enzyme, could also play a role in the regulatory switch governing NS3 acetylation and its RNA binding dynamics.

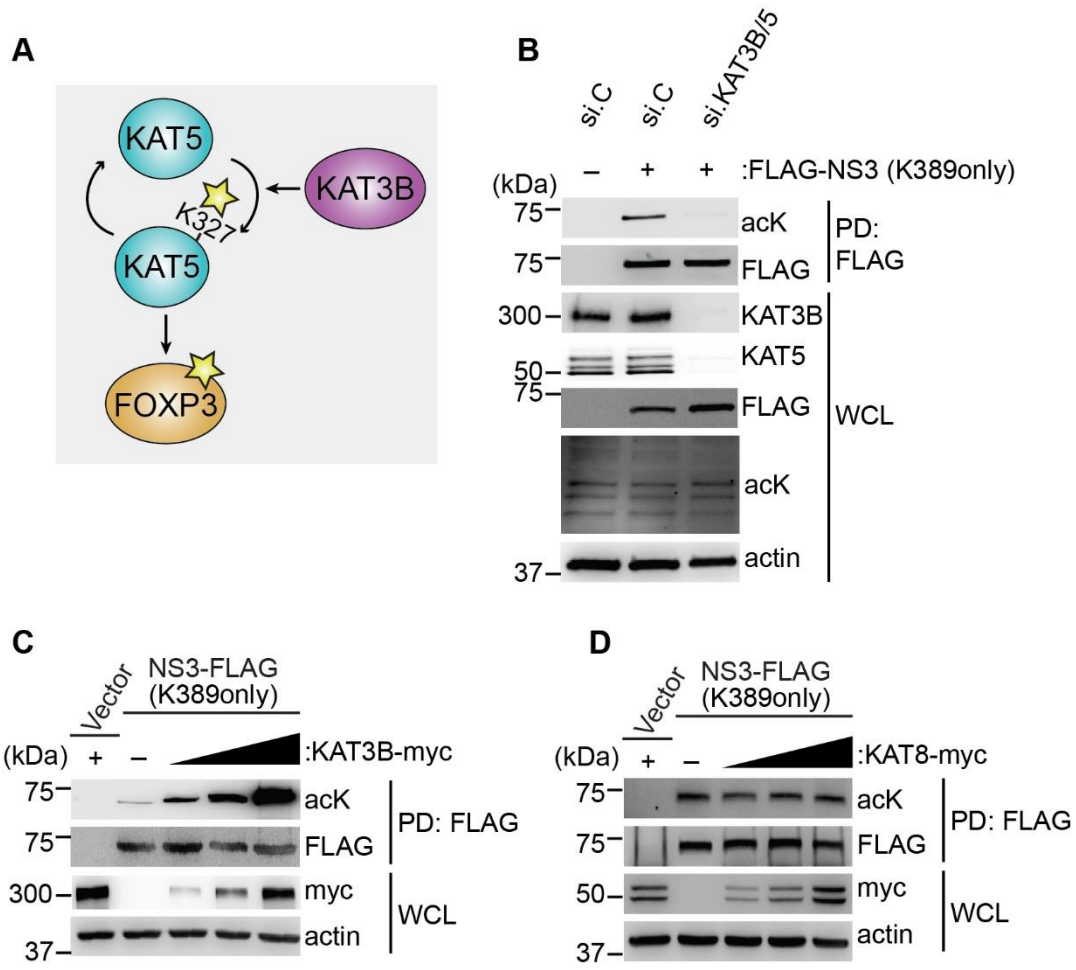

Figure 3.11 Potential role for KAT3B in enhancement of ZIKV NS3 acetylation by KAT5γ

(A) Schematic depicting a previously-identified role for KAT3B-mediated KAT5 auto-acetylation at residue K327, resulting in enhanced downstream KAT5-mediated acetylation of FOXP3.

(B) Acetylation of FLAG-tagged ZIKV NS3(K389only) in HEK293T cells that were transfected for 16 h with either si.C or siRNAs targeting KAT3B and KAT5 and then co-transfected with FLAG-NS3(K389only) for 30 h, determined by PD with anti-FLAG and IB with anti-acK. Knockdown of KAT3B and KAT5 was confirmed in the WCLs by IB with anti-KAT3B, anti-KAT5 and anti-Actin (loading control).

(C) Acetylation of FLAG-tagged ZIKV NS3(K389only) in HEK293T cells that were co-transfected for 40 h with either empty vector or increasing amounts of myc-tagged KAT3B, determined by anti-FLAG PD and IB with anti-acK and anti-FLAG. WCLs were probed with anti-myc and anti-Actin (loading control).

(D) Acetylation of FLAG-tagged ZIKV NS3(K389only) in HEK293T cells that were co-transfected for 40 h with either empty vector or increasing amounts of myc-tagged KAT8, determined by anti-FLAG PD and IB with anti-acK and anti-FLAG. WCLs were probed with anti-myc and anti-Actin (loading control).

Interestingly, our data shows that only KAT5γ binds to ZIKV NS3. As previously mentioned, KAT5γ does not have any unique structural features compared with the other isoforms, as KAT5L also encodes the KAT5 intron that sets KAT5γ apart from KAT5α and KAT5β. Therefore, the specific localization of KAT5γ to ER-derived membranes cannot be explained simply by the presence of the KAT5 intron. It is, however, possible that the additional KAT5 exon encoded by KAT5L, but not by KAT5γ, retains KAT5L within the nucleus, while the absence of exon 5 allows for KAT5γ ER localization. However, our membrane flotation assay shows that KAT5β, which lacks both the KAT5 intron 1 and exon 5, is also present in some RC fractions. This may suggest that exon 5 is the distinguishing feature preventing localization to the ER membrane, by retaining KAT5L and KAT5α in the nucleus. Interestingly, while a nuclear localization signal (NLS) has been predicted for KAT5 [136], these signals are not isoform-specific, and are shared with all four isoforms. In addition, using the WOLF PSORT II software, a potential ER retention signal (541-KRGK-546) is present in the C-terminus of the KAT5 protein. Like the NLS, however, this ER retention signal is present in the sequence of all four KAT5 isoforms. It is possible that the folding of the different isoforms allows for differential exposure and/or shielding of the potential NLS and ER retention signal in different KAT5 isoforms. Alternatively, PTMs in the NLS or ER sites may shield these signals and allow for regulated subcellular localizations. However, more structural information and localization studies are required to make any conclusions regarding these hypotheses.

Since both KAT5γ and KAT5β, which lack the potential nuclear-retaining exon 5, are present in some RC fractions by membrane flotation, the specificity for KAT5γ in binding to ZIKV NS3 may be mediated by the KAT5 intron region. Mapping studies of the

interaction between KAT5γ and ZIKV NS3 would be required to conclude this. Moreover, the intron region may not only directly bind to ZIKV NS3 during infection, but potentially mediate interaction with other proteins that allow for the ZIKV NS3 and KAT5γ interaction. Finally, as KAT5 has been shown to be regulated by its own PTMs, it is possible that only KAT5γ is post-translationally modified in a way that allows for ER localization/NS3 binding. Several lipid-based PTMs have been shown to mediate interaction with membranous compartments, though KAT5 has not yet been identified as a substrate for these PTMs [70].

Overall, more in-depth localization studies may elucidate why only KAT5γ binds to and acetylates ZIKV NS3 during infection. However, the available anti-pan-KAT5 antibodies are poor detectors of endogenous KAT5 expression in cells by IF. While overexpression of tagged KAT5 proteins and IF detection using tag-specific antibodies has been achieved in previous studies, these methods are not reliable for discerning endogenous or isoform-specific localization, as many of these published studies show differential localization of the KAT5 isoforms depending on tags and cell types used [133, 136, 137]. Therefore, a more robust approach may be to use endogenous tagging of KAT5 at the genomic level. However, since all of the KAT5 isoforms are encoded by the same gene, this approach would limit isoform-specific detection. One could foresee a potential in CRISPR-mediated fluorescent-tagging [180] of only KAT5L and KAT5γ by introducing a fluorescent molecule within the KAT5 intron. Moreover, a potential for KAT5γ-specific tagging could be achieved by introducing a fluorescent tag in the KAT5 intron and its quencher within the KAT5 exon 5 region. This would allow for only KAT5γ, which encodes the fluorescent intron but splices out the quencher in the exon 5, to be detected by IF. However, more

intricate design and trouble-shooting are required to ensure the feasibility of this approach.

Our characterization of the localization of KAT5γ within the ZIKV replication complex supports the hypothesis that NS3 is dynamically regulated by acetylation (**Fig 2.11**). This proposed scenario for NS3 regulation by acetylation leaves room for a yet identified deacetylase as a major player in NS3-mediated RNA binding and unwinding dynamics. To identify the NS3-specific deacetylase, and thus extend the functional understanding of the mechanism for regulation of ZIKV replication by acetylation, a candidate or unbiased screen could be designed similar to the acetyltransferase screens shown in **Fig. 3.1**. In this case, it would be expected that silencing of the deacetylase would reduce ZIKV replication, similar to silencing of the acetyltransferase, since silencing of either class of enzymes will disrupt the finely-tuned regulation of NS3 acetylation. These deacetylases could then be biochemically characterized during silencing or gene-editing for their effect on ZIKV NS3 acetylation at K389 and on ZIKV replication.

The data presented herein also suggest that KAT5 and KAT5γ are widely expressed in various cell types (**Fig. 3.9C, D**). As expected, KAT5γ protein expression as well as KAT5γ's proviral role was found to be conserved in Vero (African Green Monkey) cells (**Fig. 3.4A**). It will be an interesting future direction to test whether KAT5γ expression and NS3 acetylation is also conserved in mosquito cells, the main vector for ZIKV transmission. Moreover, our data shows that KAT5 is highly expressed in the neuronal cell type SH-SY-5Y (**Fig 3.9D**), stimulating the hypothesis that enhanced KAT5/KAT5γ expression may account for the neuronal tropism of ZIKV during *in vivo* infection. More

characterization is required to conclude whether KAT5γ expression may contribute to the infectivity of ZIKV-permissive cell types/organs.

3.5 Methods

Cell lines. HEK 293T (human embryonic kidney cells, female), Vero (African Green monkey kidney epithelial, female) (ATCC), A549 (human lung epithelial cells, male, age 58) and SH-SY5Y (human neuroblastoma cells) were purchased from American Type Culture Collection (ATCC) and cultured in Dulbecco's Modified Eagle's Medium (DMEM, Gibco) supplemented with 10% (v/v) fetal bovine serum (FBS, Gibco) and 1% (v/v) penicillin-streptomycin (Gibco). SH-SY5Y were further supplemented with 1 mM sodium pyruvate. SVGA cells (human fetal astrocyte, embryonic, sex unidentified) (provided by Ellen Cahir-McFarland; Cambridge, MA; [163]) HMC3 (human embryonic microglial cell, sex unidentified) (ATCC), and Calu-3 (human lung cancer cells, male) (ATCC) cells were cultured in Minimum Essential Medium (Gibco) supplemented with 10% (v/v) FBS and 1% (v/v) penicillin-streptomycin. Caco2 (colon epithelial cells, white male age 72 with colorectal carcinoma) (ATCC) were cultured in Minimum Essential Medium (Gibco) supplemented with 20% (v/v) FBS and 1% (v/v) penicillin-streptomycin. The NHLF (normal human lung fibroblasts) (Lonza) and hTERT-immortalized HDF (human dermal fibroblasts; kindly gifted by Patrick Hearing [181] cells were cultured in DMEM medium supplemented with 10% (v/v) FBS, 1 mM sodium pyruvate (Gibco) and 1% (v/v) penicillin-streptomycin. The THP-1 cells (human leukemia monocytic cell lines) (ATCC) were cultured in suspension in Roswell Park Memorial Institute (RPMI 1640, Gibco) medium supplemented with 10% (v/v) FBS, 1% (v/v) penicillin-streptomycin, 1 mM sodium pyruvate, 10 mM HEPES, 1x non-essential amino acids and 0.05 mM β-mercaptoethanol.

All cell cultures were maintained at 37 °C in a humidified 5% CO2 incubator. Purchased cell lines were authenticated by the respective vendor and were not validated further in our laboratory. Cell lines obtained and validated by other groups were not further authenticated.

Viruses. ZIKV (strain BRA/2015) [46, 164] was kindly provided by Michael Diamond (Washington University St. Louis) and propagated in Vero cells as previously described [166]. Sendai virus (strain Cantell) was purchased from Charles River. EMCV (strain EMC) was purchased from ATCC and propagated in HEK293T cells [182]. VSV-eGFP was provided by Sean Whelan (Washington University St. Louis).

Plasmids and Reagents. ZIKV NS3 (strain H**/**PF**/**2013) was subcloned using as a templates a GST-fused construct plasmid [46] into the pcDNA3.1+ vector together with an N-terminal FLAG-tag using the restriction sites Nhe1 and BamH1. cDNA encoding ZIKV NS3 6K→R (K119R, K187R, K389R, K431R, K466R, K530R) was purchased as a G-block from IDT and cloned into the pcDNA3.1+ vector using Kpn1 and Xho1 restriction sites and Gibson assembly. The K389R site was reverted back to K389 in the ZIKV NS3 6K→R backbone using 'Round-the-Horn cloning. Myc-DDK-tagged KAT5γ (transcript 4) was purchased from Origene (#RC234280) and subcloned into the pcDNA3.1+ vector together with an N-terminal HA**-**tag using BamHI and Nhe1 restriction sites. Importantly, an additional silent mutation at the splice acceptor site of the KAT5 intron (Q37; 125-CAG-127 to 125-CAA-127) was introduced into HA-tagged KAT5γ by 'Round-the-Horn' cloning, preventing the further splicing of overexpressed KAT5γ to KAT5β, which was validated by Western blot. KAT5γ (Q377E/G380E) was generated by site-directed mutagenesis using 'Round-the-Horn' cloning using HA-KAT5γ plasmid as template.

Transfections were performed using linear polyethylenimine (1 mg/mL solution in 20 mM Tris pH 6.8; Polysciences), Lipofectamine and Plus reagent (Life Technologies), or Lipofectamine 2000 (Life Technologies) following the manufacturer's instructions.

Anti-FLAG M2 agarose affinity gel (Sigma), Glutathione Sepharose 4B resin (GE Life Sciences), magnetic A/G beads (Pierce) or agarose A/G beads (Pierce) were used for respective pull down and immunoprecipitation assays. Protease inhibitor cocktail (Sigma; #P2714) was added at a concentration of 1:50 to cell lysates for all pull down and immunoprecipitation assays. Deacetylase inhibitor cocktail (Santa Cruz; sc-362323) was diluted in media at a concentration of 1:200 and added to cells 12 h pre-harvest and to cell lysis buffer at the same concentration for all biochemical assays analyzing NS3 acetylation.

Cell Lysis and Co-immunoprecipitation. Cells were lysed in Nonidet P-40 (NP-40) buffer (50 mM HEPES pH 7.4, 150 mM NaCl, 1% (v/v) NP-40, 1 mM EDTA, 1:50 protease inhibitor cocktail (Sigma)) and then centrifuged at 21,000 x g for 20 min at 4°C. WCLs were taken post lysate clearance and the remainder was used to perform GST or FLAG pull downs, immunoprecipitation, or co-immunoprecipitation assays following protocols as previously described [161]. Briefly, lysates were incubated with GST or FLAG beads for 4 h at 4°C, or incubated with specific antibodies overnight at 4°C followed by pulled down with magnetic/agarose A/G beads for 2 h at 4°C. Following pull-down or (co)immunoprecipitations, proteins were eluted from beads either by heating samples in Laemmli SDS sample buffer at 95°C for 5 min. For experiments in which FLAG-tagged

NS3 was analyzed by IB with anti-acK, beads were or by incubated in 100 μg/mL FLAG peptide (Sigma; F3290) in TBS (10mM Tris HCL, 150mM NaCl, ph 7.4) for 1 h at 4°C.

Immunoblot Analysis and Antibodies. Purified proteins or whole cell lysates were resolved on 8.5% or 10% Tris-Glycine-SDS PAGE gels (pH 8) and then transferred onto a polyvinylidene difluoride (PVDF) membrane (Bio-Rad) for 1 h using a Wet Transfer Chamber (Bio-Rad). Membranes were blocked in 5% (w/v) non-fat dry milk in PBS-T (0.05% (v/v) Tween-20 in PBS) for 1 h at room temperature, followed by primary antibody incubation overnight at 4°C. Following primary antibody incubation overnight at 4°C, blots were probed with HRP-conjugated secondary antibody (CST; #7074S and #7076S) for 1 h at room temperature. Proteins were visualized using SuperSignal West Pico or Femto (Thermo Scientific) and imaged using either an ImageQuant LAS 4000 Chemiluminescent Image Analyzer (General Electric) or Amersham ImageQuant 800 (Cytiva). Primary antibodies used (at a dilution of 1:1000 unless otherwise indicated) for immunoblot include: anti-FLAG (1:2000; Sigma; #F1804), anti-β-actin (1:5000; GeneTex; #GTX629630), anti-HA (Sigma; H3663), anti-acetyl-lysine (acK) (CST; #9814), anti-ZIKV NS3 (custom-made; [46]), anti-acetyl-K389-NS3(ZIKV) antibody (custom-made; this paper), anti-ZIKV NS3 (GeneTex; #GTX133309), anti-ZIKV NS4b (GeneTex; #GTX133311), anti-Calreticulin (CST; #12238), anti-p300 (Santa Cruz Biotech; #sc-48343), anti-KAT5 (Santa Cruz Biotech; #sc-166323).

NS3 Helicase Assay. FLAG-tagged ZIKV NS3 WT co-transfected with increasing amounts of HA-tagged KAT5γ, were affinity-purified from ~1 x 10^8 transiently transfected HEK293T cells, and eluted with FLAG peptide as described above. FLAG peptide was removed from the elution using a Microcon centrifugal Ultracel filter with a 30 kDa cutoff.

Subsequently, purified FLAG-NS3 protein concentrations were determined by BCA assay (Pierce). Equal amounts (2.6 μM) of proteins were incubated in a black 96-well plate (Nunc; #165305) with 1 μM of annealed, complementary synthetic RNAs (generated by IDT) encoding a fluorescent 5′-Cy3-label (with a 3′ overhang to allow helicase loading) and a quenching 3′-BHQ2-label in the presence of 16.5 mM ATP (Abcam; #ab146525) in helicase reaction buffer (20 mM Tris–HCl (pH 7.0), 10 mM NaCl, 0.1 mg/mL BSA, 5 mM MgCl2, 2 mM DTT) for 60 min. The release and subsequent fluorescence of the Cy3-labeled RNA substrate was measured using a BioTek Syngery Neo2 Plate reader with settings Ex 540nm and Em 579nm. Unwinding activity was calculated by subtracting the baseline reading at time = 0 (F_0) from each time point reading (F_t) and dividing by F_0. The RNA sequences used were: ZIKV Cy3-RNA (5′-Cy3-GCGUCUUUACGGUGCUUAAAACAAAACAAAACAAAACAAAA-3′; 5′-AGCACCGUAAAGACGC-3′-BHQ2). Annealing of the synthetic RNA strands for the Molecular Beacon Assay was carried out by mixing 100 μM of each fragment in 5X annealing buffer (50 mM Tris (pH 7.5), 250 mM NaCl, 5 mM EDTA) at 95°C for 5 min and cooling down slowly to RT.

Membrane Flotation Assay. A549 cells (~4 x 10^8) were mock-treated or infected with ZIKV (strain BRA/2015; MOI 1) for 48 h and harvested by trypsinization. Samples were processed following an established protocol for membrane flotation of flavivirus replication vesicles (*47*). Briefly, pellets were resuspended in 3.5 mL PBS containing 0.25 M sucrose (PBS/sucrose) and freshly-added protease inhibitor cocktail (1:100, Sigma; #P2714). Cells were lysed with a tight-fitting dounce homogenizer on ice for 200 passages and clarified by centrifugation at 2500 x g for 10 min at 4°C. An aliquot of this

WCL was saved and added to 2X Laemmli buffer for downstream SDS-PAGE analysis. Equal amounts of lysate from mock or infected samples were adjusted to 2 mL and added to 2 mL of 60% iodixanol (OptiPrep). This 4 mL of iodixanol/lysate mixture was added to a 12-mL polypropylene centrifuge tube (Beckman Coulter) and carefully overlayed with a 4 mL 30% (v/v) and 20% (v/v) iodixanol layer diluted in PBS/sucrose. Tubes were balanced using 10% (v/v) iodixanol in PBS/sucrose and spun in an ultracentrifuge (Thermo Fisher Scientific; Sorvall WX) at 35,000 rpm overnight at 4°C in a TH-641 rotor (Thermo Fisher Scientific). Eleven 1 mL fractions were taken off the top of the sucrose density gradient and a 100 uL aliquot of each fraction was added 1:1 to 2X Laemmli buffer and resolved on an SDS-PAGE gel for IB analysis as indicated using primary antibodies described above.

Virus infections and Titer analyses. Infection experiments were performed and processed as described previously (*42*). Briefly, Vero, A549, SVGA, or HMC3 cells were incubated with virus (ZIKV, WNV, EMCV, or VSV) at the indicated MOI in serum-free media for 2 h, followed by incubation in complete media for the indicated times. Plaque assays to determine viral titers were performed as described previously (*42*). Briefly, supernatants of infected cells were serially diluted in serum-free media and incubated on a confluent monolayer of Vero cells for 2 h, followed by removal of infection media and addition of 1% (w/v) low melting agarose (Lonza; #50101) mixed 1:1 with 2X MEM (described in detail in (*42*)). Plaques were analyzed after 3-5 days by removing the agar overlay and fixing cells with 2% (w/v) PFA in PBS for 30 min at room temperature, followed by staining with crystal violet in 20% (v/v) methanol. Plaques were counted and

reported as PFU/mL, calculated as number of (plaques/well) x (dilution factor)/(infection volume).

Anacardic Acid treatment and Cell Viability Measurement. For determination of ZIKV restriction by anacardic acid, ~1x105 A549 cells were treated in triplicate with increasing concentrations of anacardic acid (Abcam) or DMSO for two hours prior to infection with ZIKV (BR/2015, MOI= .001) for 48 hours. ZIKV infection was measured by qPCR using a primer specific for the ZIKV Envelope (E) gene. Cell viability was measured in parallel by CellTiter-Glo® Luminescent Cell Viability Assay (Promega) per the Manufacturer's Instructions.

RNA purification and qRT-PCR. For viral transcript analyses and knockdown efficiency determination, total cellular RNA was purified using an RNA extraction kit (OMEGA Bio-Tek) per the manufacturer's instructions. Equal amounts of RNA (25–500 ng) were used in a one-step qRT-PCR reaction using the SuperScript III Platinum One-Step qRT-PCR kit with ROX (Invitrogen) and commercially-available FAM reporter dye primers (IDT) for the analyzed transcripts. Gene expression was normalized to that of house-keeping genes GAPDH (HEK293T), HPRT1 (A549), and 18S (SVGA and HMC3). The comparative CT method (ΔΔCT) was used to measure the transcript levels of each target gene. ZIKV genomic RNA was analyzed using a previously described primer for ZIKV E: 5′-CCACTAACGTTCTTTTGCAGACAT-3′ (forward), 5′-CCGCTGCCCAACACAAG-3′ (reverse), 5′-/56-FAM/AGCCTACCT/ZEN/TGACAAGCAATCAGACACTCAA/3IABkFQ/-3′ (probe) (11) and for the ZIKV 5'UTR: 5′-CAGACTGCGACAGTTCGAG

-3′ (forward), 5′-AGAAACTCTCGYTTCCAAATCC-3′ (reverse), 5′-/56-FAM-CCTGTTGATACTGTTGYTAGCTYTCGCTTC-lABkFQ/-3′ (probe) [183]. All qRT-PCR reactions were performed using a 7500 FAST Real-time PCR machine (Applied Biosystems) or QuantStudio 6 Pro Real-Time PCR Machine (Applied Biosystems).

KAT5 expression in human tissues. The absolute copy number of KAT5 transcripts was determined by one-step qRT-PCR, described above, using 20 ng of the individual cDNA library samples provided in the Human Total cDNA Panel I and II (TaKaRa Biosciences). A standard of known concentration of KAT5 was serially diluted and amplified to determine the absolute numbers of KAT5 mRNA in the individual tissues.

Flow Cytometry Analysis. To determine the percentage of ZIKV-infected cells, A549 cells (1 x 10^5 cells/well) were fixed in 2% (w/v) PFA (in PBS) for 30 min at RT and then permeabilized with 1X PermWash (BD Scientific) for 30 min. Following fixation and permeabilization, cells were incubated with a PE-conjugated 4G2 antibody (Novus; #NPB2-52709PE) for 1 h at RT (1:1000 in 1X PermWash). Cells were washed three times with PBS-T (0.05% (v/v) Tween-20 in PBS) and resuspended in PBS for flow cytometry analysis using a Cytek Aurora. Data analysis was performed using FlowJo.

Gene silencing using siRNA. Transient gene silencing was achieved by reverse transfecting cells with 60-120 μM of gene-specific siGENOMe SMARTpool siRNAs (Dharmacon) using RNAiMax transfection reagent (Invitrogen), according to the manufacturer's instructions. The non-targeting siRNAs (siGENOME Non-Targeting siRNA Pool #2, D-001206–14-05 and siRNA Pool #3, D-001210-03-05) were used as controls. The following siRNAs were used to target the following respective genes: KAT2A (M-009722-01-0010), KAT2B (M-005055-00-0010), KAT3A (M-003477-02-0010), KAT3B

(M-003486-04-0010), KAT5 (M-006301-01-0010), KAT6A (M-019849-01-0010), KAT6B (M-019563-01-0010), KAT7 (M-017668-00-0010), KAT8 (M-014800-00-0010), KAT1 (M-011490-02-0010), KAT4 M-005041-01-0005), KAT9 (M-015940-01-0005), KAT12 (M-019863-01-0010), KAT13A (M-005196-03-0005), KAT13B (M-003759-02-0005), KAT13C (M-020159-01-0005), KAT13D (M-008212-00-0005), ATF2 (M-009871-00-0005), ATAT1 (M-014510-01-0005), ACAT1 (M-009408-00-0005), NAT10 (M-014402-00-0005), GCN5L1 (M-012580-00-0010), CDYL (M-008521-00-0005), ELP4 (M-016927-01-0010), KAT14 (M-008481-01-0005), METTL8 (M-014442-01-0010), NAA60 (M-014479-01-0005), CECR2 (M-024450-01-0005), TMEM41B (M-033252-01-0010), and EMC2 (L-010631-00-0010). A custom pool of African green monkey-specific KAT5-targeting siRNAs was generated by Dharmacon and used to target KAT5 in Vero cells, with sequences (1) 5'-GGACAGCUCAGAUGGAAUAUU-3′ and (2) 5′-CACAGGAGCUCACCACAUUUU-3′. A custom pool of siRNAs, generated by Dharmacon, was used to target the KAT5 exon, with sequences (1) 5′-GCGGGAAGACCTTGCCAAT-3′ (2) 5′- tCCCGGTCCAGATCACACT-3′ (3) 5′-GAGCGGGAGGCCATTCCCG-3′ (4) 5′-GCAGCCCAACCACCGCTCA-3′. A custom siRNA to target the KAT5 intron was generated by Dharmacon with the sequence: 5′-AGGGGAGGTGGGTAGAGCC-3′. Knockdown efficiency of these genes was determined by qRT-PCR at the indicated times using pre-designed primers from IDT.

Quantification and Statistical Analysis. All data were presented as means ± SD and analyzed using GraphPad Prism software (version 7). An unpaired two-tailed Student's t-test or one-way ANOVA (with Tukey's HSD) ($P < 0.05$ was considered statistically significant) were used as indicated in the respective legends. Pre-specified effect sizes

were not assumed and three biological replicates (n) for each condition. Data were reproduced in independent experiments as indicated in the legends for each figure.

CHAPTER 4

ACETYLATION OF NS3 BY KAT5γ IS CONSERVED IN WEST NILE VIRUS

This chapter is adapted from: Serman, T.; Chiang, C.; Acharya, D.; Pandey, S.; Muppala, S.; Liu, G.; Gack, M.U. Acetylation of the flavivirus NS3 helicase by KAT5γ is essential for virus replication (2022) (manuscript under review).

Attributions: TS performed and analyzed all experiments with the following exceptions: DA performed and analyzed Figure 4.3B.

4.1 Abstract

The flaviviruses are a family of vector-borne pathogens responsible for significant morbidity and mortality across the global population [184]. The mosquito-borne flaviviruses, such as ZIKV, WNV, DENV, and YFV, are the most common culprits for causing flavivirus-associated diseases in humans. Both ZIKV and WNV present with neurological symptoms during human infection given their neuronal tropism. In terms of neuropathology, ZIKV most often presents in newborn babies after crossing the trans-placental barrier and infecting neuro-progenitor cells during fetal development, while WNV infection is more commonly associated with meningoencephalitis in immuno-compromised adults [185]. Here, we show that robust acetylation of the NS3 helicase is conserved in WNV. Moreover, we found that mutation of K389 reduces acetylation of WNV NS3. In turn, we tested whether KAT5 was the enzyme responsible for acetylation of WNV NS3 and found that proviral acetylation of NS3 by KAT5/KAT5γ is a conserved mechanism controlling both ZIKV and WNV replication, providing the potential for an antiviral therapy capable of restricting multiple flaviviruses.

4.2 Introduction

Both WNV and ZIKV are mosquito-transmitted flaviviruses capable of causing neurological clinical manifestations in human patients, despite different transmission cycles. ZIKV is mainly transmitted through the *Aedes* species of mosquito, and is largely maintained in a sylvatic cycle, in which the virus transmits between non-human primates and forest-dwelling mosquito vectors, with humans as incidental hosts. However, humans are able to contribute to ZIKV transmission, as the virus can spread between humans via a mosquito vector, sexual transmission, or vertical (trans-placental) transmission. ZIKV

induced neuropathology typically presents as cranial and developmental abnormalities in babies born to infected mothers, though neurological symptoms such as acute paralysis and Guillain-Barré syndrome are also associated with ZIKV infection in adults [3].

On the other hand, the enzootic transmission cycle of WNV relies on transmission between the *Culex* species of mosquito and birds, such as crows and jays, with humans and other mammals, such as horses, as the main incidental hosts. However, these mammalian hosts are considered “dead-end” hosts, as they do not develop sufficient viremia to allow for subsequent transmission. Infection with WNV is typically asymptomatic, but a small percentage (~20%) of infected patients can develop West Nile Fever (WNF), associated with headache, tremors, numbness, and disorientation, while an even smaller percentage (~1%) develop West Nile Neuroinvasive Disease (WNND), associated with multiple syndromes such as meningitis, encephalitis, and poliomyelitis, all of which can be fatal [186]. Like ZIKV, WNV has also been found to cross placentas during infection of pregnant mice [187], and there has been one reported case of vertical transmission in humans [188], suggesting the potential for vertical transmission in other mammalian hosts.

In addition to their dissimilar transmission cycles and clinical manifestations, ZIKV and WNV infection are experimentally studied using distinct *in vivo* models. The recent emergence and rapid resolution of the ZIKV epidemic has stunted the development of a suitable mouse model. Moreover, ZIKV is readily cleared by the mouse innate immune system, as the ZIKV NS2b3 protease is unable to cleave the mouse signal transducer and activator of transcription 2 (STAT2) antiviral signaling molecule, a major way in which flaviviruses evade the host innate immune response in humans [189]. On the other hand,

STAT2$^{-/-}$ mice, or mice deficient in both subunits of the IFN receptor (IFNAR), were susceptible to ZIKV infection and showed more severe ZIKV-associated pathology, compared to wildtype (WT) mice [190, 191]. In addition, ZIKV infection of pregnant *IFNAR1*$^{-/-}$ mice led to severe fetal growth restriction and fetal demise, compared to control mice [192, 193]. Another useful mouse model for ZIKV is mice lacking *IFNAR1* or mice lacking *IRF 3*, *5*, and *7*, both of which develop more severe neurological disease compared to WT mice [194].

On the other hand, WNV, which was first isolated in 1937 and associated with human disease as early as the 1960's has more established *in vivo* models [186]. While wild mice are not susceptible to WNV infection, lab strains of mice are highly susceptible to WNV infection due to a truncation in the 2′,5′-oligoadenylate synthetase (OAS) antiviral gene family, which is functional in wild mice [195]. For example, WNV infection and immunity has been characterized extensively in the C57BL/6 (B6) mouse model, which is readily infected by the virus without any manipulation to innate immune signaling. Following subcutaneous infection in the footpad, approximately 30% of mice develop neuroinvasive disease, with clinical manifestations as human WNND, resulting in death within 10-12 days post-infection [195]. Moreover, intracranial injection of wildtype B6 mice with WNV rapidly results in neuroinvasive disease and death within 3-6 days post-infection [196]. In addition to mouse models, a WNV macaque and baboon model have been established for viral pathogenesis studies [197].

In previous chapters, we showed that ZIKV NS3 is acetylated at residue K389. Mutational analysis of K389 in ZIKV NS3 to a non-acetylated arginine or a hyper-acetylation-mimicking glutamine resulted in modulated RNA binding, unwinding, and

ZIKV replication, suggesting a proviral role for NS3 functional regulation by acetylation. An unbiased screen identified KAT5 as the host acetyltransferase responsible for ZIKV NS3 acetylation and support of ZIKV replication. In depth biochemical and virologic analyses revealed that only one isoform of KAT5, KAT5γ, mediates ZIKV NS3 acetylation and controls ZIKV replication. Here, we sought to test the conservation of the proviral regulatory role of NS3 acetylation in other related mosquito-transmitted flaviviruses.

4.3 Results

4.3.1 Acetylation of WNV, DENV, and YFV NS3 proteins

To test whether acetylation of NS3 is conserved in other flaviviruses, the NS3 proteins from WNV, DENV, and YFV were ectopically-expressed along with ZIKV NS3 and assessed for acetylation by Western blot (WB). Interestingly, all four flavivirus NS3 proteins were acetylated by WB, although the degree of acetylation varied, with only WNV NS3 being acetylated to a similar level as ZIKV NS3, while DENV and YFV NS3 proteins were much less acetylated (**Fig. 4.1A**). Interestingly, the degree of acetylation corresponded to the structural conservation between the respective NS3 proteins and ZIKV NS3 [198]. Since the major acetylation site, K389, is conserved across ZIKV and WNV strains (**Fig. 4.1.B**), we tested whether K389 is also acetylated in WNV NS3. WNV NS3 K389R showed reduced acetylation (by about 60%) compared with the WT protein (**Fig. 4.1C**), suggesting that K389 is also a dominant acetylation site in WNV NS3, and further, that likely other sites are acetylated in WNV NS3. Moreover, we showed by WB that WNV NS3 was acetylated during authentic infection of A549 cells (**Fig. 4.1D**).

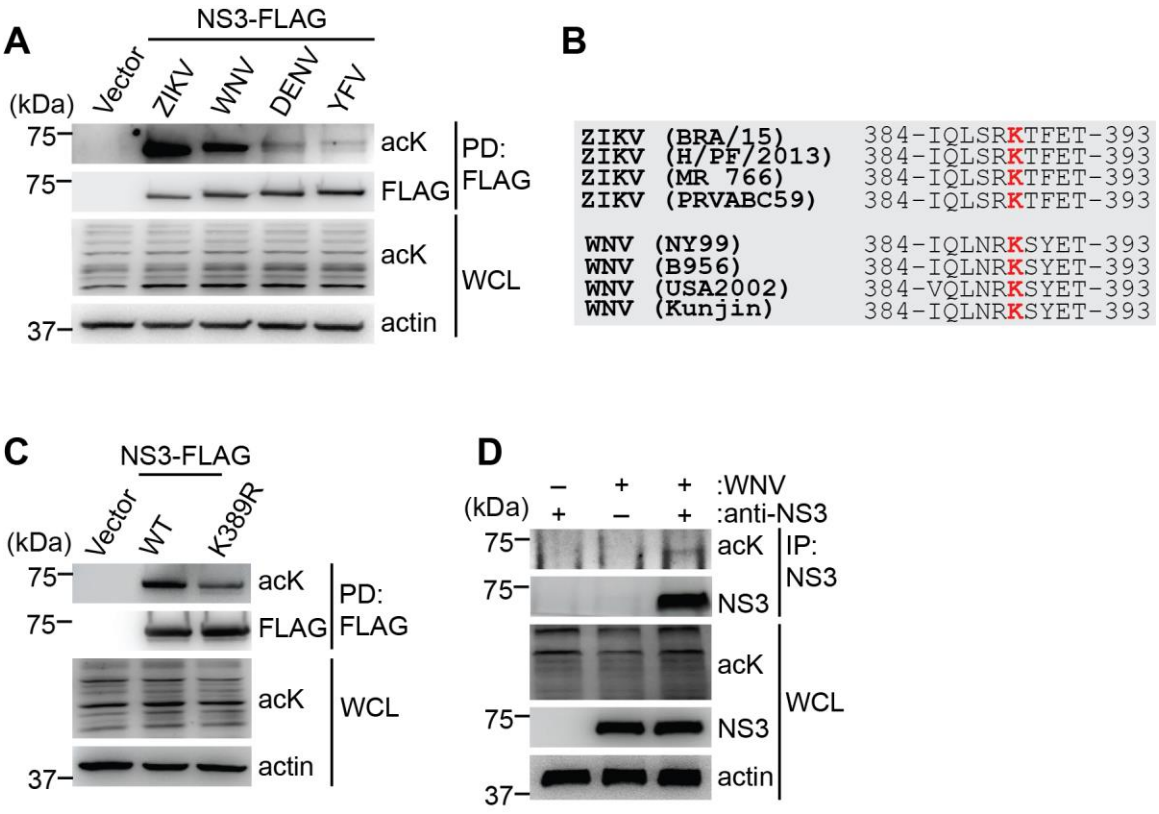

Figure 4.1 Acetylation of NS3 is conserved in West Nile Virus (WNV).
(A) Acetylation of FLAG-tagged ZIKV, WNV, DENV, and YFV NS3 in HEK293T cells that were transfected for 40 h to express those constructs, assessed by PD with anti-FLAG and IB with anti-acK. WCLs were probed with anti-acK and anti-Actin (loading control).
(B) Amino acid sequence spanning the region in NS3 that contains K389 for the indicated ZIKV and WNV strains. The conserved K389 residue is highlighted in red.
(C) Acetylation of FLAG-tagged WNV NS3 WT or K389R mutant in transiently transfected HEK293T cells, determined by PD with anti-FLAG and IB using anti-acK. WCLs were probed with the indicated antibodies.
(D) Acetylation of WNV NS3 in A549 cells that were infected with WNV (NY99, MOI 1) for 30 h, determined by IP with anti-NS3(WNV) and IB with anti-acK and anti-NS3(WNV).

4.3.2 WNV NS3 binds to KAT5γ

Since NS3 acetylation was conserved in WNV, we wanted to test the role of KAT5 in mediating this conserved PTM. To this end, we first examined KAT5-NS3 binding and found that both ZIKV and WNV NS3 bound to a single isoform of endogenous KAT5

(KAT5γ) when overexpressed in HEK293T cells (**Fig. 4.2A**). Moreover, binding of native WNV NS3 to KAT5γ during authentic infection of A549 cells was also confirmed (**Fig. 4.2B**).

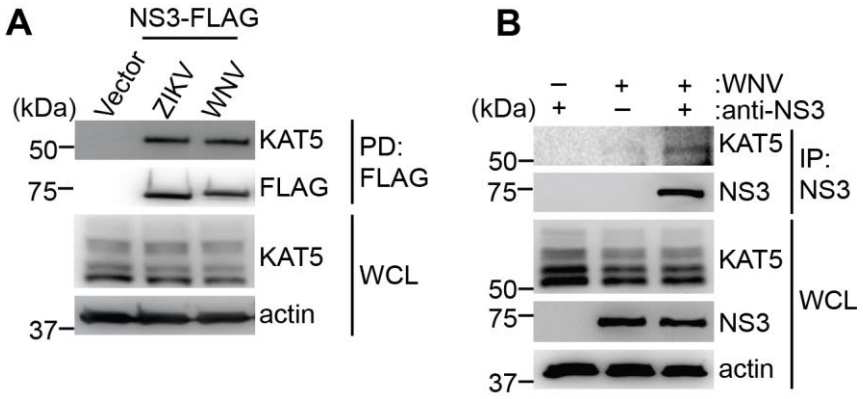

Figure 4.2 WNV NS3 binds to a single isoform of KAT5, corresponding to the size of KAT5γ.

(A) Binding of endogenous KAT5γ to FLAG-tagged NS3 from ZIKV or WNV in transiently transfected HEK293T cells, determined by PD with anti-FLAG and IB with anti-KAT5 or anti-FLAG. WCLs were probed by IB with the indicated antibodies.

(B) Binding of endogenous KAT5γ to WNV NS3 in A549 cells that were infected for 30 h with WNV (NY99, MOI 1), determined by IP with anti-NS3 and IB with anti-KAT5 or anti-NS3.

4.3.3 KAT5 controls WNV NS3 acetylation and WNV replication

To test whether KAT5 binding to WNV NS3 also resulted in acetylation of the NS3 protein, we silenced KAT5 in HEK293T cells and found that WNV NS3 acetylation was reduced in conditions of KAT5 silencing compared with control cells (**Fig 4.3A**). Likewise, we tested whether replication of WNV was controlled by KAT5. As observed during ZIKV replication, silencing of KAT5L/γ or KAT5 (all) markedly reduced WNV replication and to similar degrees, as determined by plaque assay (**Fig. 4.3B**). In contrast, knockdown of

KAT5L/α did not diminish WNV replication; titers were similar to those in cells transfected with nontargeting control siRNA (**Fig. 4.3B**). Together, these data suggest that the role for KAT5γ-mediated NS3 acetylation in promoting viral replication is conserved also in WNV.

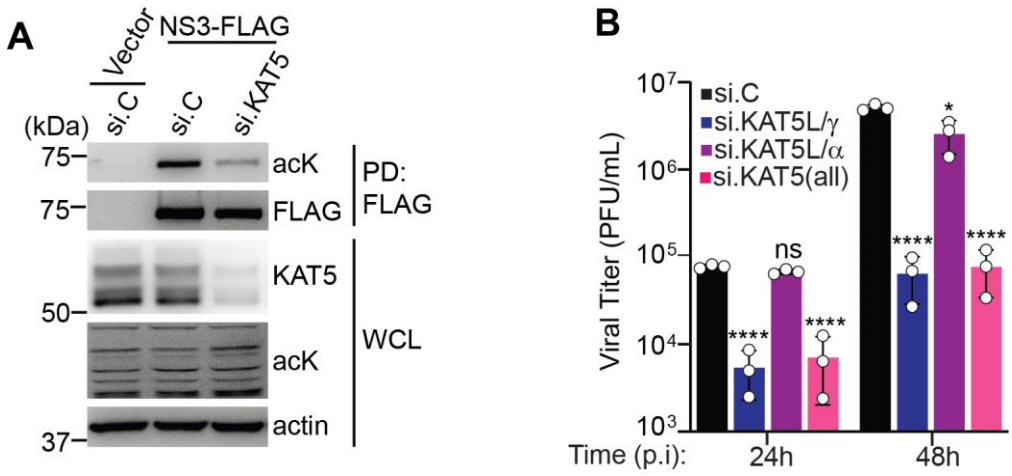

Figure 4.3. Silencing of KAT5/KAT5γ reduces WNV NS3 acetylation and viral replication.

(A) Acetylation of FLAG-tagged WNV NS3 in HEK293T cells transfected for 16 h with either si.C or KAT5-specific siRNA (si.KAT5) and then co-transfected with FLAG-NS3 for 30 h, determined by anti-FLAG PD and IB with anti-acK and anti-FLAG. WCLs were probed with anti-KAT5 to validate knockdown efficiency, anti-acK, and anti-Actin (loading control).

(B) WNV replication in A549 cells that were transfected for 30 h with the indicated siRNAs and then infected with WNV (NY99, MOI 0.001) for the indicated times, determined by plaque assay and presented as PFU/mL. Unpaired Student's *t* test between indicated sample groups. ns, not significant; *p < 0.05, **** p < 0.0001.

4.4 Discussion

Herein, we showed robust acetylation of ZIKV and WNV NS3, while the NS3 proteins from the tested strains of DENV and YFV were less acetylated under the experimental conditions and cell type used, despite the overall high structural similarity of the NS3 protein in these flaviviruses. However, as ZIKV and WNV are more highly

structurally-related to each other than to DENV and YFV, it is possible that the mechanism for regulation by acetylation diverged due to structural changes in the NS3 protein. On the other hand, this result could be explained by the technical use of an overexpression system using HEK293T cells. Perhaps under conditions of overexpression, the low level of acetylation of the NS3 protein from the representative strains of DENV and YFV NS3 cannot be detected, though regulation by acetylation may still be possible during viral replication, during which the expression of NS3 is much less than in an overexpression context. Moreover, DENV and YFV NS3 may have diverged in their utilization of KAT5 as the NS3 acetyltransferase, providing the potential for a cell type-specific unknown acetyltransferase that may not be highly expressed in HEK293T cells to mediate NS3 acetylation. In this scenario, this unknown acetyltransferase may be expressed in other DENV and YFV-permissive cell types. Outside of the technical possibilities, it is conceivable that DENV and YFV do not utilize NS3 acetylation as a regulatory mechanism for the binding, unwinding, and replication of their viral RNA genomes. It is possible that their NS3 enzymatic activities are regulated by a distinct PTM, or do not require fine-tuned regulation to achieve viral replication.

While it is tempting to speculate that the requirement for NS3 acetylation contributes to the neuronal tropism of ZIKV and WNV, our data in Chapter III does not show any neuron-specific expression of KAT5/KAT5γ, as KAT5 isoforms are expressed widely across human tissues and cell types. Moreover, NS3 regulation by KAT5γ appears to be conserved in Vero (African Green Monkey), HMC3 (microglial), SVGA (astrocytic), and A549 (epithelial) cells, as knockdown of KAT5γ reduced ZIKV replication in all of these cell types. Mutation of the major acetylation site, K389, reduced ZIKV replication in

SVGA, Vero, and A549 cells, suggesting that this phenotype is not specific to neuronal cell types. Nevertheless, it is still possible that NS3 regulation by acetylation in neuronal cell types may be important for pathogenesis of these neuroinvasive flaviviruses, despite the conserved role of NS3 acetylation in a variety of cell types. Regardless, our data support that NS3 acetylation is a fundamental regulatory mechanism for ZIKV NS3 activity in multiple target cells.

In addition to the variance in the degree of acetylation, the WNV NS3 K389 site seems to be less of a dominant site for NS3 acetylation than observed for ZIKV NS3. This could potentially be due to variation at the structural level at the RNA binding tunnel. For example, the cognate K389 site (at the structural level) is K366 in DENV NS3 [29]. While the WNV NS3 protein has not been crystallized in its RNA-bound state, or across the conserved K389 site [199], it is possible that also other sites within the RNA binding tunnel of WNV NS3 contribute to NS3 acetylation. This could be tested by overexpression of the WNV NS3, or infection with native WNV, followed by purification of the NS3 protein and MS analysis to identify potential additional acetylation sites.

Our data also showed that NS3 acetylation and successful viral replication mediated by KAT5γ are conserved in ZIKV and WNV. This provides a tool for studying the role of NS3 acetylation in an *in vivo* model, since WNV more readily infects wildtype strains of lab mice and reflects the human clinical presentations of symptoms than does ZIKV. Importantly, mice encode all four human isoforms of KAT5, and two additional truncated isoforms [131]. However, since KAT5 plays an essential epigenetic role during embryonic development, full KAT5 knockout mice are not viable. Alternatively, there is one established conditional KAT5 knockout mouse line, in which all four KAT5 isoforms

are targeted by a tamifloxin-inducible CaMKCreERT2 driver, allowing for conditional knockout in neural tissues including cortex, hippocampus, and striatum [200]. In general, neuroinvasive WNV infection in mice yields highest viral titers in the olfactory bulbs, brainstem, and mid-brain, with lower titers in the cerebral cortex and hippocampus [57]. Therefore, the feasibility of using this existing conditional KAT5 KO mouse model is still questionable for *in vivo* WNV viral replication and survival studies, as the effect of the conditional knockout in tissues that support only low WNV replication may not be significant. Another potential KAT5 knockdown model for studying WNV pathogenesis is a recently established KAT5 S86A CRISPR knock-in mouse, in which the wildtype KAT5 allele is replaced with the KAT5 S86A allele, preventing the activating phosphorylation by glycogen synthase kinase 3 (GSK3). Since these mice maintain the inactivating mutation in all cell types, this model may be more suitable for WNV pathogenesis studies [153]. However, while S86 is encoded by all four KAT5 isoforms, whether the S86A mutation reduces the enzymatic activity of KAT5γ is unknown, as this associated loss of function has only been characterized in the KAT5α isoform [140]. Therefore, alternative methods are required for studying the role of specifically KAT5γ during *in vivo* WNV infection (discussed in more detail in the next Chapter).

4.5 Methods

Cell lines. HEK 293T (human embryonic kidney cells, female) and A549 (human lung epithelial cells, male, age 58) were purchased from American Type Culture Collection (ATCC) and cultured in Dulbecco's Modified Eagle's Medium (DMEM, Gibco)

supplemented with 10% (v/v) fetal bovine serum (FBS, Gibco) and 1% (v/v) penicillin-streptomycin (Gibco).

All cell cultures were maintained at 37 °C in a humidified 5% CO2 incubator. Purchased cell lines were authenticated by the respective vendor and were not validated further in our laboratory. Cell lines obtained and validated by other groups were not further authenticated.

Viruses. West Nile virus (strain NY99) was obtained from BEI Resources (#NR-158) and propagated in Vero cells as previously described [166].

Plasmids and Reagents. ZIKV NS3 (strain H**/**PF**/**2013), DENV NS3 (strain NGC), WNV NS3 (strain NY99) and YFV NS3 (strain 17D) were subcloned using as templates plasmids expressing the respective constructs as GST-fused proteins [46, 47] into the pcDNA3.1+ vector together with an N-terminal FLAG-tag using the restriction sites Nhe1 and BamH1. FLAG-tagged WNV NS3 K389R was generated by site-directed mutagenesis using 'Round-the-horn cloning. Transfections were performed using linear polyethylenimine (1 mg/mL solution in 20 mM Tris pH 6.8; Polysciences), Lipofectamine and Plus reagent (Life Technologies), or Lipofectamine 2000 (Life Technologies) following the manufacturer's instructions.

Anti-FLAG M2 agarose affinity gel (Sigma), Glutathione Sepharose 4B resin (GE Life Sciences), magnetic A/G beads (Pierce) or agarose A/G beads (Pierce) were used for respective pull down and immunoprecipitation assays. Protease inhibitor cocktail (Sigma; #P2714) was added at a concentration of 1:50 to cell lysates for all pull down and immunoprecipitation assays. Deacetylase inhibitor cocktail (Santa Cruz; sc-362323) was

diluted in media at a concentration of 1:200 and added to cells 12 h pre-harvest and to cell lysis buffer at the same concentration for all biochemical assays analyzing NS3 acetylation.

Cell Lysis and Co-immunoprecipitation. HEK293T and A549 cells were lysed in Nonidet P-40 (NP-40) buffer (50 mM HEPES pH 7.4, 150 mM NaCl, 1% (v/v) NP-40, 1 mM EDTA, 1:50 protease inhibitor cocktail (Sigma)) and then centrifuged at 21,000 x g for 20 min at 4°C. WCLs were taken post lysate clearance and the remainder was used to perform GST or FLAG pull downs, immunoprecipitation, or co-immunoprecipitation assays following protocols as previously described [161]. Briefly, lysates were incubated with GST or FLAG beads for 4 h at 4°C, or incubated with specific antibodies overnight at 4°C followed by pulled down with magnetic/agarose A/G beads for 2 h at 4°C. Following pull-down or (co)immunoprecipitations, proteins were eluted from beads either by heating samples in Laemmli SDS sample buffer at 95°C for 5 min. For experiments in which FLAG-tagged NS3 was analyzed by IB with anti-acK, beads were or by incubated in 100 μg/mL FLAG peptide (Sigma; F3290) in TBS (10mM Tris HCL, 150mM NaCl, ph 7.4) for 1 h at 4°C.

Immunoblot Analysis and Antibodies. Purified proteins or whole cell lysates were resolved on 8.5% or 10% Tris-Glycine-SDS PAGE gels (pH 8) and then transferred onto a polyvinylidene difluoride (PVDF) membrane (Bio-Rad) for 1 h using a Wet Transfer Chamber (Bio-Rad). Membranes were blocked in 5% (w/v) non-fat dry milk in PBS-T (0.05% (v/v) Tween-20 in PBS) for 1 h at room temperature, followed by primary antibody incubation overnight at 4°C. Following primary antibody incubation overnight at 4°C, blots were probed with HRP-conjugated secondary antibody (CST; #7074S and #7076S) for 1

h at room temperature. Proteins were visualized using SuperSignal West Pico or Femto (Thermo Scientific) and imaged using either an ImageQuant LAS 4000 Chemiluminescent Image Analyzer (General Electric) or Amersham ImageQuant 800 (Cytiva). Primary antibodies used (at a dilution of 1:1000 unless otherwise indicated) for immunoblot include: anti-FLAG (1:2000; Sigma; #F1804), anti-β-actin (1:5000; GeneTex; #GTX629630), anti-acetyl-lysine (acK) (CST; #9814), anti-acetyl-lysine (acK) (Santa Cruz Biotech; # AKL5C1), anti-WNV NS3 (Invitrogen; #PA5-111984), and anti-KAT5 (Santa Cruz Biotech; #sc-166323).

Virus infections and Titer analyses. Infection experiments were performed and processed as described previously (42). Briefly, A549 cells were incubated with WNV at the indicated MOI in serum-free media for 2 h, followed by incubation in complete media for the indicated times.

Plaque assays to determine viral titers were performed as described previously (42). Briefly, supernatants of infected cells were serially diluted in serum-free media and incubated on a confluent monolayer of Vero cells for 2 h, followed by removal of infection media and addition of 1% (w/v) low melting agarose (Lonza; #50101) mixed 1:1 with 2X MEM (described in detail in (42)). Plaques were analyzed after 3-5 days by removing the agar overlay and fixing cells with 2% (w/v) PFA in PBS for 30 min at room temperature, followed by staining with crystal violet in 20% (v/v) methanol. Plaques were counted and reported as PFU/mL, calculated as number of (plaques/well) x (dilution factor)/(infection volume).

Gene silencing using siRNA. Transient gene silencing was achieved by reverse transfecting cells with 60-120 μM of gene-specific siGENOMe SMARTpool siRNAs

(Dharmacon) using RNAiMax transfection reagent (Invitrogen), according to the manufacturer's instructions. The non-targeting siRNA (siGENOME Non-Targeting siRNA Pool #2, D-001206–14-05) was used as a control. The siRNA targeting KAT5 was ordered from Dhamacon (siGENOME M-006301-01-0010). A custom pool of siRNAs, generated by Dharmacon, was used to target the KAT5 exon, with sequences (1) 5′-GCGGGAAGACCTTGCCAAT-3′ (2) 5′- TCCCGGTCCAGATCACACT-3′ (3) 5′-GAGCGGGAGGCCATTCCCG-3′ (4) 5′-GCAGCCCAACCACCGCTCA-3′. A custom siRNA to target the KAT5 intron was generated by Dharmacon with the sequence: 5′-AGGGGAGGTGGGTAGAGCC-3′.

Quantification and Statistical Analysis. All data were presented as means ± SD and analyzed using GraphPad Prism software (version 7). An unpaired two-tailed Student's *t*-test ($P < 0.05$ was considered statistically significant) were used as indicated in the respective legends. Pre-specified effect sizes were not assumed and three biological replicates (n) for each condition. Data were reproduced in independent experiments as indicated in the legends for each figure.

CHAPTER 5

CONCLUSIONS

5.1 Overview of Results

In this dissertation, we have demonstrated that ZIKV NS3 is post-translationally acetylated at residue K389 by the host lysine acetyltransferase KAT5γ, which modulates the RNA binding and unwinding activities of the helicase domain. This regulation by acetylation plays a proviral, regulatory role for the virus to achieve efficient replication. Moreover, we found that KAT5-mediated acetylation of NS3 and control of viral replication is conserved in the related flavivirus WNV.

In Chapter II, we identified ZIKV NS3 as a target for host-mediated post-translational acetylation. Further, we described a mechanism whereby acetylation of ZIKV NS3 at residue K389 within its helicase domain controls its RNA binding and unwinding activities, and thereby allows for successful viral replication.

- ZIKV NS3 is post-translationally acetylated during overexpression at six lysine residues, and during authentic infection at two of these six lysine residues.
- ZIKV NS3 K389, within the RNA binding tunnel of the helicase domain, is robustly acetylated during overexpression and authentic infection.
- Mutation of ZIKV NS3 K389 to a “non-acetylated” arginine residue enhances the RNA binding ability of ZIKV NS3, while mutation to a “hyper-acetylated” glutamine abrogates RNA binding.
- Reduced or too tight RNA binding by mutation of ZIKV NS3 K389 to arginine or glutamine, respectively, correlates with diminished helicase-mediated dsRNA unwinding activity of both NS3 mutants.

- Generation of recombinant ZIKV encoding a NS3 K389R or K389Q mutant protein revealed that mutation of K389 to either residue reduced viral replication, suggesting that K389 acetylation serves a proviral, regulatory role.
- Mutation of K389 does not affect other proviral functions of the ZIKV NS3 protein, such as protease activity, NS5 binding, or antagonism of the RIG-I response.

In Chapter III, we demonstrated that KAT5 is the acetyltransferase responsible for regulating NS3 activity by direct acetylation. Moreover, we determined that only the KAT5γ isoform is responsible for NS3 binding and acetylation as well as for promoting viral replication.

- Several acetyltransferases regulate ZIKV replication, as determined by an unbiased RNAi screen.
- KAT5, and not any of the other proviral candidate acetyltransferases, catalyzes acetylation of ZIKV NS3 at K389.
- KAT5 is required for efficient viral replication across several ZIKV-permissive cell types.
- ZIKV replication is strikingly restricted after treatment of cells with the small molecule KAT inhibitor anacardic acid.
- Only one isoform of KAT5, KAT5γ, binds to NS3 during overexpression and authentic infection.
- Acetylation of ZIKV NS3 and viral replication are reduced only in conditions of KAT5γ silencing, but not during silencing of the KAT5L/KATα isoforms.

- KAT5γ is required for ZIKV replication but not for replication of the RNA viruses EMCV and VSV.
- Ectopic expression of KAT5γ enhances ZIKV NS3 acetylation at K389 and reduces the unwinding capacity of the helicase.
- A construct expressing a dominant-negative form of KAT5γ reduces ZIKV NS3 acetylation at K389 and viral replication, in a dose-dependent fashion.
- KAT5 gene and protein expression is not induced by ZIKV infection.
- KAT5 and KAT5γ are expressed across a wide variety of cell types.
- KAT5γ localizes to ER-membrane derived replication complexes during ZIKV infection.

In Chapter IV, we showed that NS3 acetylation by KAT5 is conserved in the related flavivirus WNV. Moreover, we found that KAT5γ is required for successful WNV replication.

- WNV NS3 is acetylated to a similar degree as ZIKV NS3, while DENV and YFV NS3 proteins are much less acetylated under the conditions tested.
- The major acetyl-lysine site, K389, in NS3 is conserved across many ZIKV and WNV strains.
- Mutation of WNV NS3 K389 results in reduced NS3 acetylation, suggesting conservation of K389 as an acetylated site.
- WNV NS3 is acetylated during authentic infection of A549 cells.
- WNV NS3 binds to only one isoform of KAT5 during overexpression conditions and authentic infection, which corresponds to the size of KAT5γ.

- WNV NS3 acetylation is reduced during KAT5 silencing.
- Silencing of KAT5γ reduces WNV replication.

Taken together, our results demonstrate a previously uncharacterized mechanism promoting successful flavivirus replication. Disruption of the proviral regulatory function of NS3 acetylation by mutation of K389 or through silencing of the responsible acetyltransferase, KAT5γ, strikingly reduced viral replication. This finding identifies a novel host factor for flavivirus replication, providing an exciting target for potential antiviral drug design.

5.2 Concluding remarks and future directions

5.2.1 *Potential mechanisms of KAT5γ targeting for antiviral therapy*

The reliance on KAT5γ for successful viral replication provides a potential novel target for antiviral therapeutics. The first step to determine whether KAT5 inhibition is a potentially effective antiviral target is to conduct preclinical studies, which are typically carried out using mouse models of infection. While the available ZIKV mouse models rely on type I IFN deficient animals, WNV readily infects wildtype mice and induces human-like clinical symptoms. Therefore, a WNV mouse model provides a way to study the effect of KAT5 inhibition on WNV restriction *in vivo*. Of note, the four human KAT5 isoforms are also present in mice, in addition to two unique isoforms (**Fig. 5A, B**). The mouse-specific transcript 4-encoded TIP55 isoform, which is not detected by the pan-KAT5 antibody used throughout this study, has been shown to be important for neuronal development in mouse embryos [131], while the transcript 1-encoded KAT5α isoform has been shown to have a conserved role in DNA damage and transcriptional regulation from mice to humans [201, 202]. As is the case for human KAT5, the other mouse KAT5

isoforms have not been extensively functionally characterized. However, we have shown that the custom KAT5 intron-targeting siRNA used to target human KAT5L/γ also reduces the protein expression of the mouse KAT5L/γ in mouse fibroblast cells (**Fig. 5C**).

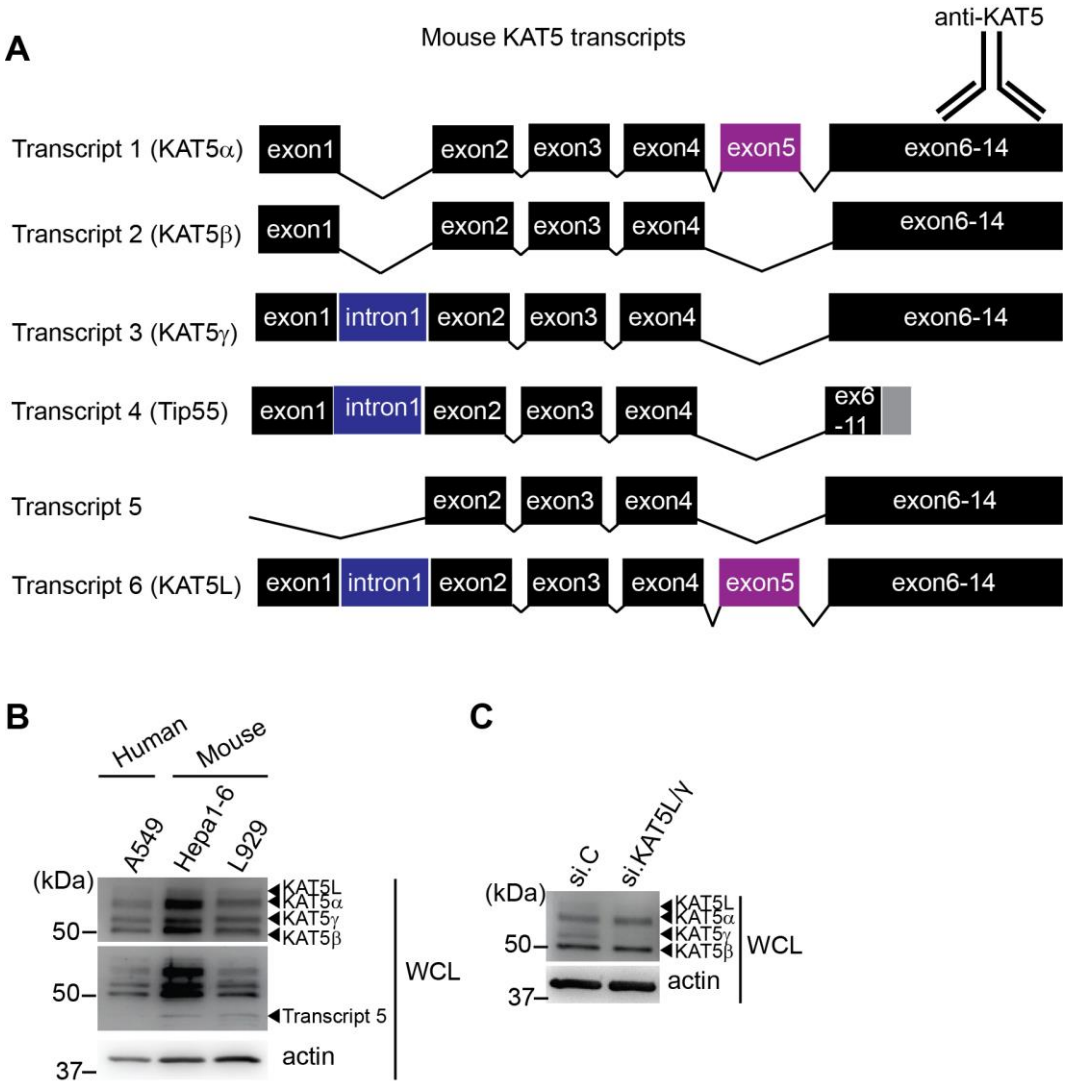

Figure 5.1 KAT5 isoforms in mice and targeting of the mouse KAT5 intron.
(A) Schematic depiction of the six KAT5 isoforms identified in mice.
(B) Comparison of KAT5 protein isoforms in human A549 cells and mouse Hepa1-6 and L929 cells, determined by IB of WCLs using an anti-KAT5 antibody and anti-Actin (loading control).
(C) Silencing of the KAT5L/γ isoforms in mouse L929 cells that were transfected with either si.C or si.KAT5L/γ for 30 h, determined by IB of WCLs using an anti-KAT5 antibody and anti-Actin (loading control).

The ability to silence these isoforms by siRNA provides a mandate for the design of molecules that silence these isoforms *in vivo* by RNA interference, in order to test the effect of KAT5γ silencing on WNV replication in a physiologically relevant model. Most *in vivo* silencing studies utilize lentivirus or adeno-associated virus (AAV) as a vector for delivery of shRNA into the desired tissue of mice [203, 204]. In the case of flavivirus infection, several studies have successfully delivered effective naked shRNA-encoding plasmids [205] and shRNA-packaged lentiviruses and AAVs [206] into the brains of mice by intracranial injection. Once silenced, mice are infected with virus and viral replication and/or pathogenesis are assessed by various measures, such as survival curves and viral titering in mouse organs [205, 206]. In terms of KAT5γ shRNA design, there aren't many options, as this region is only 100 bp long and contains a highly G/C rich sequence. These features may prevent the downstream processing of shRNAs into the siRNAs utilized to silence KAT5L/γ. Outside of shRNA delivery, there have been several studies that directly introduce siRNA into the brains of mice for flavivirus replication studies [207, 208]. These methods would allow for direct intranasal delivery of a naked or neuronal peptide-conjugated KAT5L/γ–targeted siRNA into the brains of mice, allowing for subsequent WNV infection and viral replication assays. However, the feasibility of these silencing approaches are a topic of future research.

In addition to RNA interference, multiple small molecule KAT5 inhibitors have been characterized in the literature. These inhibitors target either the acetyltransferase domain, which is conserved across MYST family KATs (KAT5, KAT6A, KAT6B, and KAT7), the bromodomain, which is conserved across bromodomain-containing KATs (KAT5, KAT2A, KAT2B, KAT3A, and KAT3B), or the acetyl-CoA binding domain, which is weakly

conserved across a variety of KATs [209]. We show herein that anacardic acid, which targets the KAT5 acetyl-CoA binding domain, reveals striking restriction of ZIKV replication. However, since this inhibitor also weakly targets KAT3A, KAT3B, and KAT2A, a more specific inhibitor is required for further development against flaviviruses. Moreover, given the nuclear epigenetic role of KAT5 within cells and organisms, the potential for ER-targeting of small molecule KAT5 inhibitors would greatly enhance the specificity for KAT5γ inhibition, potentially avoiding interference with the gene regulatory roles of nuclear KAT5α. While many strategies for organelle-specific targeting of drugs have been described [210], these have not yet been applied to KAT inhibitors, including those that target KAT5.

In addition to organelle-specific targeting, organ-specific targeting of morpholino-based inhibitors has been achieved. These peptide-conjugated phosphorodiamidate morpholino oligomers (PPMOs) function by linking a small peptide onto a morpholino. Most of these small molecules allow for delivering morpholinos to specific organs, such as the spleen, liver, and lungs. Morpholinos function at the mRNA level, by binding to transcripts and preventing their translation [211]. Whether KAT5 can be specifically targeted by morpholinos has not yet been tested, and represents a future direction for potential *in vivo* KAT5γ-targeting studies.

5.2.2 Pan-viral helicase regulation by acetylation

Herein, we report the first viral helicase whose RNA binding and unwinding activities have been shown to be regulated by acetylation. Since nearly all RNA viruses, and some DNA viruses, encode their own viral helicase enzymes, it will be interesting to test whether other viral families utilize acetylation to regulate their helicase function [212].

Besides the conceptual novelty, this study developed the first optimized assays for quantifying flaviviral RNA binding and unwinding by mammalian-purified viral helicases, in which the acetylation state is maintained, thereby providing a protocol for testing these functions in other viral helicases. Moreover, other RNA binding proteins/enzymes, such as nucleoproteins and viral polymerases, may also be regulated by acetylation, in a manner akin to that of the flavivirus NS3 helicase. In general, post-translational acetylation is a highly understudied mechanism for controlling viral replication, despite the abundance of knowledge regarding the host enzymes responsible for adding and removing this modification in the context of cellular protein acetylation. Our work shows that many human KATs can control ZIKV replication through as-of-yet unknown mechanisms. This family of enzymes, in addition to deacetylase enzymes, thereby represents a panel of potential host factors that support or restrict viral replication.

5.2.3 Emerging flaviviruses and pandemic potential

The emergence of ZIKV in South America in 2015 in which a naïve human population was exposed to a previously-considered largely asymptomatic virus, exemplifies flaviviruses as an epidemic – and potential pandemic – threat. With increasing global travel, urbanization, and encroachment into sylvatic habitats, the chance for exposure to novel pathogens is rising. For example, Spondweni virus (SPOV), closely-related to ZIKV, has been shown to cause serious disease including vascular leakage and shock in some clinical patients. However, its epidemic potential was considered relatively low given its transmission cycle involving mosquito vectors that rarely feed on humans. However, in 2016, SPOV was isolated from a human-feeding mosquito vector in Haiti, confirming the potential risk of this virus to spread to the human population. Usutu

virus, closely-related to WNV, and Ilheus and Rocio viruses, closely-related to JeV, represent additional epidemic flavivirus threats, as they cause human disease similar to their related flavivirus cousins, but may not be restricted by developing and marketed vaccines against WNV and JeV [1].

In addition to newly emerging flaviviruses, re-emergence of known flaviviruses that can cause severe diseases also threatens the global population. For example, despite an effective YFV vaccine, only populations where this virus is endemic are vaccinated against this virus. Additionally, the presence of a non-human primate reservoir prevents the option of eradication through vaccination, as is the case for many flaviviruses [1]. If YFV infection were to reach naïve populations, the prevention of an epidemic would rely on rapid upscale of vaccine production and distribution to prevent its transmission.

The epidemic risk of flavivirus transmission doesn't only rely on reaching naïve populations, but also on genetic changes that may enhance pathogenicity of the virus, as exemplified by the ZIKV epidemic. Genetic changes in the Asian lineage of ZIKV, responsible for the 2013 epidemic in Micronesia and 2015 epidemic in South America, have contributed to enhanced pathogenicity compared to viruses of the African lineage. For example, a single serine-to-asparagine mutation (S139N) in the prM protein has been attributed to enhanced ZIKV infectivity of neuroprogenitor cells, and thus microcephaly, in neonatal mice [213]. Additionally, a single A188V mutation in the NS1 protein was shown to prevent TBK1 and IFN-β mediated restriction of ZIKV, promoting ZIKV replication and transmission [214]. Therefore, mutations that change virus tropism or its ability to evade immune responses may drive re-emergence of novel pathogenic variants of ZIKV and other flaviviruses.

The potential for emergence and re-emergence of flaviviruses mandates the development of anti-pan-flaviviral therapeutics. Herein, we identify the host factor KAT5γ as a potential antiviral target required for both ZIKV and WNV replication. It will be an exciting avenue of future research to test the role of KAT5γ-mediated NS3 acetylation in the replication of various emerging flaviviruses, which may extend the therapeutic repertoire of KAT5γ-targeting antiviral drugs.

REFERENCES

1. Pierson, T.C. and M.S. Diamond, *The continued threat of emerging flaviviruses.* Nat Microbiol, 2020. **5**(6): p. 796-812.
2. Bollati, M., et al., *Structure and functionality in flavivirus NS-proteins: perspectives for drug design.* Antiviral Res, 2010. **87**(2): p. 125-48.
3. Serman, T.M. and M.U. Gack, *Evasion of Innate and Intrinsic Antiviral Pathways by the Zika Virus.* Viruses, 2019. **11**(10).
4. Hamel, R., et al., *Biology of Zika Virus Infection in Human Skin Cells.* J Virol, 2015. **89**(17): p. 8880-96.
5. Mukhopadhyay, S., R.J. Kuhn, and M.G. Rossmann, *A structural perspective of the flavivirus life cycle.* Nat Rev Microbiol, 2005. **3**(1): p. 13-22.
6. Meertens, L., et al., *Axl Mediates ZIKA Virus Entry in Human Glial Cells and Modulates Innate Immune Responses.* Cell Rep, 2017. **18**(2): p. 324-333.
7. Richard, A.S., et al., *AXL-dependent infection of human fetal endothelial cells distinguishes Zika virus from other pathogenic flaviviruses.* Proc Natl Acad Sci U S A, 2017. **114**(8): p. 2024-2029.
8. Carro, S.D. and S. Cherry, *Beyond the Surface: Endocytosis of Mosquito-Borne Flaviviruses.* Viruses, 2020. **13**(1).
9. Ci, Y. and L. Shi, *Compartmentalized replication organelle of flavivirus at the ER and the factors involved.* Cell Mol Life Sci, 2021. **78**(11): p. 4939-4954.
10. Neufeldt, C.J., et al., *Rewiring cellular networks by members of the Flaviviridae family.* Nat Rev Microbiol, 2018. **16**(3): p. 125-142.
11. Lescar, J., et al., *The Dengue Virus Replication Complex: From RNA Replication to Protein-Protein Interactions to Evasion of Innate Immunity.* Adv Exp Med Biol, 2018. **1062**: p. 115-129.
12. Rastogi, M., N. Sharma, and S.K. Singh, *Flavivirus NS1: a multifaceted enigmatic viral protein.* Virol J, 2016. **13**: p. 131.
13. Puerta-Guardo, H., et al., *Flavivirus NS1 Triggers Tissue-Specific Vascular Endothelial Dysfunction Reflecting Disease Tropism.* Cell Rep, 2019. **26**(6): p. 1598-1613 e8.
14. Heaton, N.S., et al., *Dengue virus nonstructural protein 3 redistributes fatty acid synthase to sites of viral replication and increases cellular fatty acid synthesis.* Proc Natl Acad Sci U S A, 2010. **107**(40): p. 17345-50.
15. Zhang, J., et al., *Flaviviruses Exploit the Lipid Droplet Protein AUP1 to Trigger Lipophagy and Drive Virus Production.* Cell Host Microbe, 2018. **23**(6): p. 819-831 e5.
16. Mazeaud, C., W. Freppel, and L. Chatel-Chaix, *The Multiples Fates of the Flavivirus RNA Genome During Pathogenesis.* Front Genet, 2018. **9**: p. 595.

17. Pijlman, G.P., et al., *A highly structured, nuclease-resistant, noncoding RNA produced by flaviviruses is required for pathogenicity.* Cell Host Microbe, 2008. **4**(6): p. 579-91.

18. Goertz, G.P., et al., *Noncoding Subgenomic Flavivirus RNA Is Processed by the Mosquito RNA Interference Machinery and Determines West Nile Virus Transmission by Culex pipiens Mosquitoes.* J Virol, 2016. **90**(22): p. 10145-10159.

19. Manokaran, G., et al., *Dengue subgenomic RNA binds TRIM25 to inhibit interferon expression for epidemiological fitness.* Science, 2015. **350**(6257): p. 217-21.

20. Barnard, T.R., et al., *Molecular Determinants of Flavivirus Virion Assembly.* Trends Biochem Sci, 2021. **46**(5): p. 378-390.

21. Zhao, R., et al., *Flavivirus: From Structure to Therapeutics Development.* Life (Basel), 2021. **11**(7).

22. Luo, D., et al., *Insights into RNA unwinding and ATP hydrolysis by the flavivirus NS3 protein.* EMBO J, 2008. **27**(23): p. 3209-19.

23. Xu, S., et al., *Zika virus NS3 is a canonical RNA helicase stimulated by NS5 RNA polymerase.* Nucleic Acids Res, 2019. **47**(16): p. 8693-8707.

24. Arunajadai, S.G., *RNA unwinding by NS3 helicase: a statistical approach.* PLoS One, 2009. **4**(9): p. e6937.

25. Davidson, R.B., et al., *Allostery in the dengue virus NS3 helicase: Insights into the NTPase cycle from molecular simulations.* PLoS Comput Biol, 2018. **14**(4): p. e1006103.

26. van den Elsen, K., J.P. Quek, and D. Luo, *Molecular Insights into the Flavivirus Replication Complex.* Viruses, 2021. **13**(6).

27. Du Pont, K.E., M. McCullagh, and B.J. Geiss, *Conserved motifs in the flavivirus NS3 RNA helicase enzyme.* Wiley Interdiscip Rev RNA, 2022. **13**(2): p. e1688.

28. Du Pont, K.E., et al., *Motif V regulates energy transduction between the flavivirus NS3 ATPase and RNA-binding cleft.* J Biol Chem, 2020. **295**(6): p. 1551-1564.

29. Tian, H., et al., *The crystal structure of Zika virus helicase: basis for antiviral drug design.* Protein Cell, 2016. **7**(6): p. 450-4.

30. Lam, A.M., D. Keeney, and D.N. Frick, *Two novel conserved motifs in the hepatitis C virus NS3 protein critical for helicase action.* J Biol Chem, 2003. **278**(45): p. 44514-24.

31. Paolini, C., et al., *Mutational analysis of hepatitis C virus NS3-associated helicase.* J Gen Virol, 2000. **81**(Pt 7): p. 1649-58.

32. Kapoor, M., et al., *Association between NS3 and NS5 proteins of dengue virus type 2 in the putative RNA replicase is linked to differential phosphorylation of NS5.* J Biol Chem, 1995. **270**(32): p. 19100-6.

33. Chen, C.J., et al., *RNA-protein interactions: involvement of NS3, NS5, and 3' noncoding regions of Japanese encephalitis virus genomic RNA.* J Virol, 1997. **71**(5): p. 3466-73.

34. Zou, G., et al., *Functional analysis of two cavities in flavivirus NS5 polymerase.* J Biol Chem, 2011. **286**(16): p. 14362-72.

35. Johansson, M., et al., *A small region of the dengue virus-encoded RNA-dependent RNA polymerase, NS5, confers interaction with both the nuclear transport receptor importin-beta and the viral helicase, NS3.* J Gen Virol, 2001. **82**(Pt 4): p. 735-745.

36. Tay, M.Y., et al., *The C-terminal 50 amino acid residues of dengue NS3 protein are important for NS3-NS5 interaction and viral replication.* J Biol Chem, 2015. **290**(4): p. 2379-94.

37. Amberg, S.M. and C.M. Rice, *Mutagenesis of the NS2B-NS3-mediated cleavage site in the flavivirus capsid protein demonstrates a requirement for coordinated processing.* J Virol, 1999. **73**(10): p. 8083-94.

38. Patkar, C.G. and R.J. Kuhn, *Yellow Fever virus NS3 plays an essential role in virus assembly independent of its known enzymatic functions.* J Virol, 2008. **82**(7): p. 3342-52.

39. Gebhard, L.G., et al., *A Proline-Rich N-Terminal Region of the Dengue Virus NS3 Is Crucial for Infectious Particle Production.* J Virol, 2016. **90**(11): p. 5451-61.

40. Kummerer, B.M. and C.M. Rice, *Mutations in the yellow fever virus nonstructural protein NS2A selectively block production of infectious particles.* J Virol, 2002. **76**(10): p. 4773-84.

41. Suthar, M.S., S. Aguirre, and A. Fernandez-Sesma, *Innate immune sensing of flaviviruses.* PLoS Pathog, 2013. **9**(9): p. e1003541.

42. Rehwinkel, J. and M.U. Gack, *RIG-I-like receptors: their regulation and roles in RNA sensing.* Nat Rev Immunol, 2020. **20**(9): p. 537-551.

43. Schneider, W.M., M.D. Chevillotte, and C.M. Rice, *Interferon-stimulated genes: a complex web of host defenses.* Annu Rev Immunol, 2014. **32**: p. 513-45.

44. Liu, H.M., et al., *The mitochondrial targeting chaperone 14-3-3epsilon regulates a RIG-I translocon that mediates membrane association and innate antiviral immunity.* Cell Host Microbe, 2012. **11**(5): p. 528-37.

45. Lin, J.P., Y.K. Fan, and H.M. Liu, *The 14-3-3eta chaperone protein promotes antiviral innate immunity via facilitating MDA5 oligomerization and intracellular redistribution.* PLoS Pathog, 2019. **15**(2): p. e1007582.

46. Riedl, W., et al., *Zika Virus NS3 Mimics a Cellular 14-3-3-Binding Motif to Antagonize RIG-I- and MDA5-Mediated Innate Immunity.* Cell Host Microbe, 2019. **26**(4): p. 493-503 e6.

47. Chan, Y.K. and M.U. Gack, *A phosphomimetic-based mechanism of dengue virus to antagonize innate immunity.* Nat Immunol, 2016. **17**(5): p. 523-30.

48. Weaver, S.C., et al., *Zika virus: History, emergence, biology, and prospects for control.* Antiviral Res, 2016. **130**: p. 69-80.

49. Brasil, P., et al., *Guillain-Barre syndrome associated with Zika virus infection.* Lancet, 2016. **387**(10026): p. 1482.

50. Ventura, C.V., et al., *Zika: neurological and ocular findings in infant without microcephaly.* Lancet, 2016. **387**(10037): p. 2502.

51. Driggers, R.W., et al., *Zika Virus Infection with Prolonged Maternal Viremia and Fetal Brain Abnormalities.* N Engl J Med, 2016. **374**(22): p. 2142-51.

52. Mlakar, J., et al., *Zika Virus Associated with Microcephaly.* N Engl J Med, 2016. **374**(10): p. 951-8.

53. Miner, J.J. and M.S. Diamond, *Zika Virus Pathogenesis and Tissue Tropism.* Cell Host Microbe, 2017. **21**(2): p. 134-142.

54. Olagnier, D., et al., *Mechanisms of Zika Virus Infection and Neuropathogenesis.* DNA Cell Biol, 2016. **35**(8): p. 367-72.

55. Colpitts, T.M., et al., *West Nile Virus: biology, transmission, and human infection.* Clin Microbiol Rev, 2012. **25**(4): p. 635-48.

56. Samuel, M.A. and M.S. Diamond, *Pathogenesis of West Nile Virus infection: a balance between virulence, innate and adaptive immunity, and viral evasion.* J Virol, 2006. **80**(19): p. 9349-60.

57. Brown, A.N., et al., *Tissue tropism and neuroinvasion of West Nile virus do not differ for two mouse strains with different survival rates.* Virology, 2007. **368**(2): p. 422-30.

58. Fernandes, P.O., et al., *Non-structural protein 5 (NS5) as a target for antiviral development against established and emergent flaviviruses.* Curr Opin Virol, 2021. **50**: p. 30-39.

59. Samrat, S.K., et al., *Antiviral Agents against Flavivirus Protease: Prospect and Future Direction.* Pathogens, 2022. **11**(3).

60. Sampath, A. and R. Padmanabhan, *Molecular targets for flavivirus drug discovery.* Antiviral Res, 2009. **81**(1): p. 6-15.

61. Gerber, L., T.M. Welzel, and S. Zeuzem, *New therapeutic strategies in HCV: polymerase inhibitors.* Liver Int, 2013. **33 Suppl 1**: p. 85-92.

62. Pattnaik, A., et al., *Discovery of a non-nucleoside RNA polymerase inhibitor for blocking Zika virus replication through in silico screening.* Antiviral Res, 2018. **151**: p. 78-86.

63. Santos, F.R.S., et al., *Identification of a Potential Zika Virus Inhibitor Targeting NS5 Methyltransferase Using Virtual Screening and Molecular Dynamics Simulations.* J Chem Inf Model, 2020. **60**(2): p. 562-568.

64. Lim, S.P., et al., *Potent Allosteric Dengue Virus NS5 Polymerase Inhibitors: Mechanism of Action and Resistance Profiling.* PLoS Pathog, 2016. **12**(8): p. e1005737.

65. Appaiahgari, M.B. and S. Vrati, *IMOJEV((R)): a Yellow fever virus-based novel Japanese encephalitis vaccine.* Expert Rev Vaccines, 2010. **9**(12): p. 1371-84.

66. Tu, H.A., et al., *Stimulation of B Cell Immunity in Flavivirus-Naive Individuals by the Tetravalent Live Attenuated Dengue Vaccine TV003.* Cell Rep Med, 2020. **1**(9): p. 100155.

67. Kirkpatrick, B.D., et al., *The live attenuated dengue vaccine TV003 elicits complete protection against dengue in a human challenge model.* Sci Transl Med, 2016. **8**(330): p. 330ra36.

68. Hou, J., W. Ye, and J. Chen, *Current Development and Challenges of Tetravalent Live-Attenuated Dengue Vaccines.* Front Immunol, 2022. **13**: p. 840104.

69. Scherwitzl, I., J. Mongkolsapaja, and G. Screaton, *Recent advances in human flavivirus vaccines.* Curr Opin Virol, 2017. **23**: p. 95-101.

70. Muller, M.M., *Post-Translational Modifications of Protein Backbones: Unique Functions, Mechanisms, and Challenges.* Biochemistry, 2018. **57**(2): p. 177-185.

71. Tolsma, T.O. and J.C. Hansen, *Post-translational modifications and chromatin dynamics.* Essays Biochem, 2019. **63**(1): p. 89-96.

72. Shirakura, M., et al., *E6AP ubiquitin ligase mediates ubiquitylation and degradation of hepatitis C virus core protein.* J Virol, 2007. **81**(3): p. 1174-85.

73. Kumar, S., et al., *MARCH8 Ubiquitinates the Hepatitis C Virus Nonstructural 2 Protein and Mediates Viral Envelopment.* Cell Rep, 2019. **26**(7): p. 1800-1814 e5.

74. Abe, T., et al., *ISGylation of Hepatitis C Virus NS5A Protein Promotes Viral RNA Replication via Recruitment of Cyclophilin A.* J Virol, 2020. **94**(20).

75. Wu, M.J., et al., *Palmitoylation of Hepatitis C Virus NS2 Regulates Its Subcellular Localization and NS2-NS3 Autocleavage.* J Virol, 2019. **94**(1).

76. Giraldo, M.I., et al., *K48-linked polyubiquitination of dengue virus NS1 protein inhibits its interaction with the viral partner NS4B.* Virus Res, 2018. **246**: p. 1-11.

77. Hishiki, T., et al., *Interferon-mediated ISG15 conjugation restricts dengue virus 2 replication.* Biochem Biophys Res Commun, 2014. **448**(1): p. 95-100.

78. Thiemmeca, S., et al., *Secreted NS1 Protects Dengue Virus from Mannose-Binding Lectin-Mediated Neutralization.* J Immunol, 2016. **197**(10): p. 4053-4065.

79. Li, J., et al., *The glycosylation site in the envelope protein of West Nile virus (Sarafend) plays an important role in replication and maturation processes.* J Gen Virol, 2006. **87**(Pt 3): p. 613-622.

80. Carbaugh, D.L., R.S. Baric, and H.M. Lazear, *Envelope Protein Glycosylation Mediates Zika Virus Pathogenesis.* J Virol, 2019. **93**(12).

81. Giraldo, M.I., et al., *Envelope protein ubiquitination drives entry and pathogenesis of Zika virus.* Nature, 2020. **585**(7825): p. 414-419.

82. Li, L., et al., *PARP12 suppresses Zika virus infection through PARP-dependent degradation of NS1 and NS3 viral proteins.* Sci Signal, 2018. **11**(535).

83. Choudhary, C., et al., *The growing landscape of lysine acetylation links metabolism and cell signalling.* Nat Rev Mol Cell Biol, 2014. **15**(8): p. 536-50.

84. El-Aneed, A. and J. Banoub, *Elucidation of the molecular structure of lipid A isolated from both a rough mutant and a wild strain of Aeromonas salmonicida lipopolysaccharides using electrospray ionization quadrupole time-of-flight tandem mass spectrometry.* Rapid Commun Mass Spectrom, 2005. **19**(12): p. 1683-95.

85. Dormeyer, W., M. Ott, and M. Schnolzer, *Probing lysine acetylation in proteins: strategies, limitations, and pitfalls of in vitro acetyltransferase assays.* Mol Cell Proteomics, 2005. **4**(9): p. 1226-39.

86. Fujimoto, H., et al., *A possible overestimation of the effect of acetylation on lysine residues in KQ mutant analysis.* J Comput Chem, 2012. **33**(3): p. 239-46.

87. Drazic, A., et al., *The world of protein acetylation.* Biochim Biophys Acta, 2016. **1864**(10): p. 1372-401.

88. Choudhary, C., et al., *Lysine acetylation targets protein complexes and co-regulates major cellular functions.* Science, 2009. **325**(5942): p. 834-40.

89. Kori, Y., et al., *Proteome-wide acetylation dynamics in human cells.* Sci Rep, 2017. **7**(1): p. 10296.

90. Hyndman, K.A. and M.A. Knepper, *Dynamic regulation of lysine acetylation: the balance between acetyltransferase and deacetylase activities.* Am J Physiol Renal Physiol, 2017. **313**(4): p. F842-F846.

91. Narita, T., B.T. Weinert, and C. Choudhary, *Functions and mechanisms of non-histone protein acetylation.* Nat Rev Mol Cell Biol, 2019. **20**(3): p. 156-174.

92. Allfrey, V.G., R. Faulkner, and A.E. Mirsky, *Acetylation and Methylation of Histones and Their Possible Role in the Regulation of Rna Synthesis.* Proc Natl Acad Sci U S A, 1964. **51**: p. 786-94.

93. Zhang, Y., et al., *Overview of Histone Modification.* Adv Exp Med Biol, 2021. **1283**: p. 1-16.

94. Balakrishnan, L., et al., *Acetylation of Dna2 endonuclease/helicase and flap endonuclease 1 by p300 promotes DNA stability by creating long flap intermediates.* J Biol Chem, 2010. **285**(7): p. 4398-404.

95. Li, K., et al., *Regulation of WRN protein cellular localization and enzymatic activities by SIRT1-mediated deacetylation.* J Biol Chem, 2008. **283**(12): p. 7590-8.

96. Muftuoglu, M., et al., *Acetylation regulates WRN catalytic activities and affects base excision DNA repair.* PLoS One, 2008. **3**(4): p. e1918.

97. Li, K., et al., *Acetylation of WRN protein regulates its stability by inhibiting ubiquitination.* PLoS One, 2010. **5**(4): p. e10341.

98. Mooney, S.M., et al., *Pleiotropic effects of p300-mediated acetylation on p68 and p72 RNA helicase.* J Biol Chem, 2010. **285**(40): p. 30443-52.

99. Saito, M., et al., *Monitoring Acetylation of the RNA Helicase DDX3X, a Protein Critical for Formation of Stress Granules.* Methods Mol Biol, 2021. **2209**: p. 217-234.

100. Choi, S.J., et al., *HDAC6 regulates cellular viral RNA sensing by deacetylation of RIG-I.* EMBO J, 2016. **35**(4): p. 429-42.

101. Liu, H.M., et al., *Regulation of Retinoic Acid Inducible Gene-I (RIG-I) Activation by the Histone Deacetylase 6.* EBioMedicine, 2016. **9**: p. 195-206.

102. Gal, J., et al., *The Acetylation of Lysine-376 of G3BP1 Regulates RNA Binding and Stress Granule Dynamics.* Mol Cell Biol, 2019. **39**(22).

103. Arenas, A., et al., *Lysine acetylation regulates the RNA binding, subcellular localization and inclusion formation of FUS.* Hum Mol Genet, 2020. **29**(16): p. 2684-2697.

104. Giese, S., et al., *Role of influenza A virus NP acetylation on viral growth and replication.* Nat Commun, 2017. **8**(1): p. 1259.

105. Hatakeyama, D., et al., *Influenza A virus nucleoprotein is acetylated by histone acetyltransferases PCAF and GCN5.* J Biol Chem, 2018. **293**(19): p. 7126-7138.

106. Chen, H., et al., *HDAC6 Restricts Influenza A Virus by Deacetylation of the RNA Polymerase PA Subunit.* J Virol, 2019. **93**(4).

107. Ma, J., et al., *Acetylation at K108 of the NS1 protein is important for the replication and virulence of influenza virus.* Vet Res, 2020. **51**(1): p. 20.

108. Ott, M., et al., *Tat acetylation: a regulatory switch between early and late phases in HIV transcription elongation.* Novartis Found Symp, 2004. **259**: p. 182-93; discussion 193-6, 223-5.

109. Liefhebber, J.M., et al., *Characterization of hepatitis C virus NS3 modifications in the context of replication.* J Gen Virol, 2010. **91**(Pt 4): p. 1013-8.

110. Lu, C.Y., et al., *Tubacin, an HDAC6 Selective Inhibitor, Reduces the Replication of the Japanese Encephalitis Virus via the Decrease of Viral RNA Synthesis.* Int J Mol Sci, 2017. **18**(5).

111. Zhu, L., et al., *Identification of Lysine Acetylation Sites on MERS-CoV Replicase pp1ab.* Mol Cell Proteomics, 2020. **19**(8): p. 1303-1309.

112. Thomas, Y. and E.J. Androphy, *Human Papillomavirus Replication Regulation by Acetylation of a Conserved Lysine in the E2 Protein.* J Virol, 2018. **92**(3).

113. Kamine, J., et al., *Identification of a cellular protein that specifically interacts with the essential cysteine region of the HIV-1 Tat transactivator.* Virology, 1996. **216**(2): p. 357-66.

114. Yi, J., et al., *Regulation of histone acetyltransferase TIP60 function by histone deacetylase 3.* J Biol Chem, 2014. **289**(49): p. 33878-86.

115. Ikura, T., et al., *Involvement of the TIP60 histone acetylase complex in DNA repair and apoptosis.* Cell, 2000. **102**(4): p. 463-73.

116. Hu, Y., et al., *Homozygous disruption of the Tip60 gene causes early embryonic lethality.* Dev Dyn, 2009. **238**(11): p. 2912-21.

117. Ghobashi, A.H. and M.A. Kamel, *Tip60: updates.* J Appl Genet, 2018. **59**(2): p. 161-168.

118. Cheng, X., V. Cote, and J. Cote, *NuA4 and SAGA acetyltransferase complexes cooperate for repair of DNA breaks by homologous recombination.* PLoS Genet, 2021. **17**(7): p. e1009459.

119. Schleicher, E.M., et al., *The TIP60-ATM axis regulates replication fork stability in BRCA-deficient cells.* Oncogenesis, 2022. **11**(1): p. 33.

120. Niida, H., et al., *Essential role of Tip60-dependent recruitment of ribonucleotide reductase at DNA damage sites in DNA repair during G1 phase.* Genes Dev, 2010. **24**(4): p. 333-8.

121. Mo, F., et al., *Acetylation of Aurora B by TIP60 ensures accurate chromosomal segregation.* Nat Chem Biol, 2016. **12**(4): p. 226-32.

122. Gorrini, C., et al., *Tip60 is a haplo-insufficient tumour suppressor required for an oncogene-induced DNA damage response.* Nature, 2007. **448**(7157): p. 1063-7.

123. Chen, G., et al., *Role of Tip60 in human melanoma cell migration, metastasis, and patient survival.* J Invest Dermatol, 2012. **132**(11): p. 2632-41.

124. Takino, T., et al., *Tip60 regulates MT1-MMP transcription and invasion of glioblastoma cells through NF-kappaB pathway.* Clin Exp Metastasis, 2016. **33**(1): p. 45-52.

125. Halkidou, K., et al., *Expression of Tip60, an androgen receptor coactivator, and its role in prostate cancer development.* Oncogene, 2003. **22**(16): p. 2466-77.

126. Shiota, M., et al., *Tip60 promotes prostate cancer cell proliferation by translocation of androgen receptor into the nucleus.* Prostate, 2010. **70**(5): p. 540-54.

127. Cao, X. and T.C. Sudhof, *A transcriptionally [correction of transcriptively] active complex of APP with Fe65 and histone acetyltransferase Tip60.* Science, 2001. **293**(5527): p. 115-20.

128. Li, Z. and L.J. Rasmussen, *TIP60 in aging and neurodegeneration.* Ageing Res Rev, 2020. **64**: p. 101195.

129. Sheridan, A.M., et al., *PLIP, a novel splice variant of Tip60, interacts with group IV cytosolic phospholipase A(2), induces apoptosis, and potentiates prostaglandin production.* Mol Cell Biol, 2001. **21**(14): p. 4470-81.

130. Legube, G. and D. Trouche, *Identification of a larger form of the histone acetyl transferase Tip60.* Gene, 2003. **310**: p. 161-8.

131. Acharya, D., et al., *TIP55, a splice isoform of the KAT5 acetyltransferase, is essential for developmental gene regulation and organogenesis.* Sci Rep, 2018. **8**(1): p. 14908.

132. Doyon, Y., et al., *Structural and functional conservation of the NuA4 histone acetyltransferase complex from yeast to humans.* Mol Cell Biol, 2004. **24**(5): p. 1884-96.

133. Ran, Q. and O.M. Pereira-Smith, *Identification of an alternatively spliced form of the Tat interactive protein (Tip60), Tip60(beta).* Gene, 2000. **258**(1-2): p. 141-6.

134. Hass, M.R. and B.A. Yankner, *A {gamma}-secretase-independent mechanism of signal transduction by the amyloid precursor protein.* J Biol Chem, 2005. **280**(44): p. 36895-904.

135. Ravichandran, P., et al., *Nuclear Localization Is Not Required for Tip60 Tumor Suppressor Activity in Breast and Lung Cancer Cells.* DNA Cell Biol, 2020. **39**(11): p. 2077-2084.

136. Shin, S.H. and S.S. Kang, *Phosphorylation of Tip60 Tyrosine 327 by Abl Kinase Inhibits HAT Activity through Association with FE65.* Open Biochem J, 2013. **7**: p. 66-72.

137. Sliva, D., et al., *Tip60 interacts with human interleukin-9 receptor alpha-chain.* Biochem Biophys Res Commun, 1999. **263**(1): p. 149-55.

138. Lee, E.J., et al., *Endoplasmic Reticulum (ER) Stress Enhances Tip60 (A Histone Acetyltransferase) Binding to the Concanavalin A.* Open Biochem J, 2012. **6**: p. 1-10.

139. Gao, S.S., et al., *TIP60 K430 SUMOylation attenuates its interaction with DNA-PKcs in S-phase cells: Facilitating homologous recombination and emerging target for cancer therapy.* Sci Adv, 2020. **6**(28): p. eaba7822.

140. Charvet, C., et al., *Phosphorylation of Tip60 by GSK-3 determines the induction of PUMA and apoptosis by p53.* Mol Cell, 2011. **42**(5): p. 584-96.

141. Zheng, H., et al., *A posttranslational modification cascade involving p38, Tip60, and PRAK mediates oncogene-induced senescence.* Mol Cell, 2013. **50**(5): p. 699-710.

142. Brauns-Schubert, P., et al., *CDK9-mediated phosphorylation controls the interaction of TIP60 with the transcriptional machinery.* EMBO Rep, 2018. **19**(2): p. 244-256.

143. Fang, X., et al., *Acetylation of TIP60 at K104 is essential for metabolic stress-induced apoptosis in cells of hepatocellular cancer.* Exp Cell Res, 2018. **362**(2): p. 279-286.

144. Xiao, Y., et al., *Dynamic interactions between TIP60 and p300 regulate FOXP3 function through a structural switch defined by a single lysine on TIP60.* Cell Rep, 2014. **7**(5): p. 1471-1480.

145. Col, E., et al., *HIV-1 Tat targets Tip60 to impair the apoptotic cell response to genotoxic stresses.* EMBO J, 2005. **24**(14): p. 2634-45.

146. Peng, L., et al., *SIRT1 negatively regulates the activities, functions, and protein levels of hMOF and TIP60.* Mol Cell Biol, 2012. **32**(14): p. 2823-36.

147. Creaven, M., et al., *Control of the histone-acetyltransferase activity of Tip60 by the HIV-1 transactivator protein, Tat.* Biochemistry, 1999. **38**(27): p. 8826-30.

148. Awasthi, S., et al., *A human T-cell lymphotropic virus type 1 enhancer of Myc transforming potential stabilizes Myc-TIP60 transcriptional interactions.* Mol Cell Biol, 2005. **25**(14): p. 6178-98.

149. Reitsma, J.M., et al., *Antiviral inhibition targeting the HCMV kinase pUL97 requires pUL27-dependent degradation of Tip60 acetyltransferase and cell-cycle arrest.* Cell Host Microbe, 2011. **9**(2): p. 103-14.

150. Li, Z., et al., *The KAT5-Acetyl-Histone4-Brd4 axis silences HIV-1 transcription and promotes viral latency.* PLoS Pathog, 2018. **14**(4): p. e1007012.

151. Jha, S., et al., *Destabilization of TIP60 by human papillomavirus E6 results in attenuation of TIP60-dependent transcriptional regulation and apoptotic pathway.* Mol Cell, 2010. **38**(5): p. 700-11.

152. Ma, G., et al., *Histone acetyl transferase TIP60 inhibits the replication of influenza a virus by activation the TBK1-IRF3 pathway.* Virol J, 2018. **15**(1): p. 172.

153. Song, Z.M., et al., *KAT5 acetylates cGAS to promote innate immune response to DNA virus.* Proc Natl Acad Sci U S A, 2020. **117**(35): p. 21568-21575.

154. Dai, J., et al., *Acetylation Blocks cGAS Activity and Inhibits Self-DNA-Induced Autoimmunity.* Cell, 2019. **176**(6): p. 1447-1460 e14.

155. Li, K., W.W. Phoo, and D. Luo, *Functional interplay among the flavivirus NS3 protease, helicase, and cofactors.* Virol Sin, 2014. **29**(2): p. 74-85.

156. Ding, Q., et al., *Species-specific disruption of STING-dependent antiviral cellular defenses by the Zika virus NS2B3 protease.* Proc Natl Acad Sci U S A, 2018. **115**(27): p. E6310-E6318.

157. Chambers, T.J., et al., *Mutagenesis of the yellow fever virus NS2B protein: effects on proteolytic processing, NS2B-NS3 complex formation, and viral replication.* J Virol, 1993. **67**(11): p. 6797-807.

158. Selisko, B., et al., *Regulation of Flavivirus RNA synthesis and replication.* Curr Opin Virol, 2014. **9**: p. 74-83.

159. Matusan, A.E., et al., *Mutagenesis of the dengue virus type 2 NS3 proteinase and the production of growth-restricted virus.* J Gen Virol, 2001. **82**(Pt 7): p. 1647-1656.

160. Brecher, M., J. Zhang, and H. Li, *The flavivirus protease as a target for drug discovery.* Virol Sin, 2013. **28**(6): p. 326-36.

161. Gack, M.U., et al., *TRIM25 RING-finger E3 ubiquitin ligase is essential for RIG-I-mediated antiviral activity.* Nature, 2007. **446**(7138): p. 916-920.

162. Tsetsarkin, K.A., et al., *A Full-Length Infectious cDNA Clone of Zika Virus from the 2015 Epidemic in Brazil as a Genetic Platform for Studies of Virus-Host Interactions and Vaccine Development.* mBio, 2016. **7**(4).

163. Major, E.O., et al., *Establishment of a line of human fetal glial cells that supports JC virus multiplication.* Proc Natl Acad Sci U S A, 1985. **82**(4): p. 1257-61.

164. Sapparapu, G., et al., *Neutralizing human antibodies prevent Zika virus replication and fetal disease in mice.* Nature, 2016. **540**(7633): p. 443-447.

165. Kumar, A., et al., *Zika virus inhibits type-I interferon production and downstream signaling.* EMBO Rep, 2016. **17**(12): p. 1766-1775.

166. Brien, J.D., H.M. Lazear, and M.S. Diamond, *Propagation, quantification, detection, and storage of West Nile virus.* Curr Protoc Microbiol, 2013. **31**: p. 15D 3 1-15D 3 18.

167. Coleman, O., et al., *Filter-Aided Sample Preparation (FASP) for Improved Proteome Analysis of Recombinant Chinese Hamster Ovary Cells.* Methods Mol Biol, 2017. **1603**: p. 187-194.

168. Ali, I., et al., *Lysine Acetylation Goes Global: From Epigenetics to Metabolism and Therapeutics.* Chem Rev, 2018. **118**(3): p. 1216-1252.

169. Squatrito, M., C. Gorrini, and B. Amati, *Tip60 in DNA damage response and growth control: many tricks in one HAT.* Trends Cell Biol, 2006. **16**(9): p. 433-42.

170. Jaiswal, B. and A. Gupta, *Modulation of Nuclear Receptor Function by Chromatin Modifying Factor TIP60.* Endocrinology, 2018. **159**(5): p. 2199-2215.

171. Yasunaga, A., et al., *Genome-wide RNAi screen identifies broadly-acting host factors that inhibit arbovirus infection.* PLoS Pathog, 2014. **10**(2): p. e1003914.

172. Krishnan, M.N., et al., *RNA interference screen for human genes associated with West Nile virus infection.* Nature, 2008. **455**(7210): p. 242-5.

173. Wapenaar, H., et al., *Enzyme kinetics and inhibition of histone acetyltransferase KAT8.* Eur J Med Chem, 2015. **105**: p. 289-96.

174. Hoffmann, H.H., et al., *TMEM41B Is a Pan-flavivirus Host Factor.* Cell, 2021. **184**(1): p. 133-148 e20.

175. Brown, J.A., et al., *Targeting cancer using KAT inhibitors to mimic lethal knockouts.* Biochem Soc Trans, 2016. **44**(4): p. 979-86.

176. Sun, Y., et al., *Inhibition of histone acetyltransferase activity by anacardic acid sensitizes tumor cells to ionizing radiation.* FEBS Lett, 2006. **580**(18): p. 4353-6.

177. McGuire, A., et al., *Quantifying Tip60 (Kat5) stratifies breast cancer.* Sci Rep, 2019. **9**(1): p. 3819.

178. Savidis, G., et al., *Identification of Zika Virus and Dengue Virus Dependency Factors using Functional Genomics.* Cell Rep, 2016. **16**(1): p. 232-246.

179. Sun, Y., et al., *A role for the Tip60 histone acetyltransferase in the acetylation and activation of ATM.* Proc Natl Acad Sci U S A, 2005. **102**(37): p. 13182-7.

180. Sharma, A., et al., *CRISPR/Cas9-Mediated Fluorescent Tagging of Endogenous Proteins in Human Pluripotent Stem Cells.* Curr Protoc Hum Genet, 2018. **96**: p. 21 11 1-21 11 20.

181. Yu, J., A. Boyapati, and K. Rundell, *Critical role for SV40 small-t antigen in human cell transformation.* Virology, 2001. **290**(2): p. 192-8.

182. Wies, E., et al., *Dephosphorylation of the RNA sensors RIG-I and MDA5 by the phosphatase PP1 is essential for innate immune signaling.* Immunity, 2013. **38**(3): p. 437-49.

183. Chan, J.F., et al., *Improved detection of Zika virus RNA in human and animal specimens by a novel, highly sensitive and specific real-time RT-PCR assay targeting the 5'-untranslated region of Zika virus.* Trop Med Int Health, 2017. **22**(5): p. 594-603.

184. Daep, C.A., J.L. Munoz-Jordan, and E.A. Eugenin, *Flaviviruses, an expanding threat in public health: focus on dengue, West Nile, and Japanese encephalitis virus.* J Neurovirol, 2014. **20**(6): p. 539-60.

185. Wiley, C.A. and L. Chimelli, *Human Zika and West Nile virus neurological infections: What is the difference?* Neuropathology, 2017. **37**(5): p. 393-397.

186. Saiz, J.C., et al., *Pathogenicity and virulence of West Nile virus revisited eight decades after its first isolation.* Virulence, 2021. **12**(1): p. 1145-1173.

187. Platt, D.J., et al., *Zika virus-related neurotropic flaviviruses infect human placental explants and cause fetal demise in mice.* Sci Transl Med, 2018. **10**(426).

188. Centers for Disease, C. and Prevention, *Intrauterine West Nile virus infection--New York, 2002.* MMWR Morb Mortal Wkly Rep, 2002. **51**(50): p. 1135-6.

189. Grant, A., et al., *Zika Virus Targets Human STAT2 to Inhibit Type I Interferon Signaling.* Cell Host Microbe, 2016. **19**(6): p. 882-90.

190. Aliota, M.T., et al., *Characterization of Lethal Zika Virus Infection in AG129 Mice.* PLoS Negl Trop Dis, 2016. **10**(4): p. e0004682.

191. Tripathi, S., et al., *A novel Zika virus mouse model reveals strain specific differences in virus pathogenesis and host inflammatory immune responses.* PLoS Pathog, 2017. **13**(3): p. e1006258.

192. Yockey, L.J., et al., *Type I interferons instigate fetal demise after Zika virus infection.* Sci Immunol, 2018. **3**(19).

193. Yockey, L.J., et al., *Vaginal Exposure to Zika Virus during Pregnancy Leads to Fetal Brain Infection.* Cell, 2016. **166**(5): p. 1247-1256 e4.

194. Lazear, H.M., et al., *A Mouse Model of Zika Virus Pathogenesis.* Cell Host Microbe, 2016. **19**(5): p. 720-30.

195. Graham, J.B., J.L. Swarts, and J.M. Lund, *A Mouse Model of West Nile Virus Infection.* Curr Protoc Mouse Biol, 2017. **7**(4): p. 221-235.

196. Shrestha, B., et al., *CD8+ T cells use TRAIL to restrict West Nile virus pathogenesis by controlling infection in neurons.* J Virol, 2012. **86**(17): p. 8937-48.

197. Wolf, R.F., et al., *Baboon model for West Nile virus infection and vaccine evaluation.* Virology, 2006. **355**(1): p. 44-51.

198. da Fonseca, N.J., Jr., et al., *Sequence, structure and function relationships in flaviviruses as assessed by evolutive aspects of its conserved non-structural protein domains.* Biochem Biophys Res Commun, 2017. **492**(4): p. 565-571.

199. Mastrangelo, E., et al., *Crystal structure and activity of Kunjin virus NS3 helicase; protease and helicase domain assembly in the full length NS3 protein.* J Mol Biol, 2007. **372**(2): p. 444-55.

200. Urban, I., et al., *TIP60/KAT5 is required for neuronal viability in hippocampal CA1.* Sci Rep, 2019. **9**(1): p. 16173.

201. Bassi, C., et al., *The acetyltransferase Tip60 contributes to mammary tumorigenesis by modulating DNA repair.* Cell Death Differ, 2016. **23**(7): p. 1198-208.

202. Ravens, S., et al., *Tip60 complex binds to active Pol II promoters and a subset of enhancers and co-regulates the c-Myc network in mouse embryonic stem cells.* Epigenetics Chromatin, 2015. **8**: p. 45.

203. Manjunath, N., et al., *Lentiviral delivery of short hairpin RNAs.* Adv Drug Deliv Rev, 2009. **61**(9): p. 732-45.

204. Xie, R., et al., *AAV Delivery of shRNA Against TRPC6 in Mouse Hippocampus Impairs Cognitive Function.* Front Cell Dev Biol, 2021. **9**: p. 688655.

205. Pacca, C.C., et al., *RNA interference inhibits yellow fever virus replication in vitro and in vivo.* Virus Genes, 2009. **38**(2): p. 224-31.

206. Anantpadma, M. and S. Vrati, *siRNA-mediated suppression of Japanese encephalitis virus replication in cultured cells and mice.* J Antimicrob Chemother, 2012. **67**(2): p. 444-51.

207. Kumar, P., et al., *A single siRNA suppresses fatal encephalitis induced by two different flaviviruses.* PLoS Med, 2006. **3**(4): p. e96.

208. Beloor, J., et al., *Small Interfering RNA-Mediated Control of Virus Replication in the CNS Is Therapeutic and Enables Natural Immunity to West Nile Virus.* Cell Host Microbe, 2018. **23**(4): p. 549-556 e3.

209. Wu, J., et al., *Small molecule inhibitors of histone acetyltransferase Tip60.* Bioorg Chem, 2011. **39**(1): p. 53-8.

210. Zheng, N., et al., *The subcellular distribution of small molecules: a meta-analysis.* Mol Pharm, 2011. **8**(5): p. 1611-8.

211. Hawner, M. and C. Ducho, *Cellular Targeting of Oligonucleotides by Conjugation with Small Molecules.* Molecules, 2020. **25**(24).

212. Kwong, A.D., B.G. Rao, and K.T. Jeang, *Viral and cellular RNA helicases as antiviral targets.* Nat Rev Drug Discov, 2005. **4**(10): p. 845-53.

213. Yuan, L., et al., *A single mutation in the prM protein of Zika virus contributes to fetal microcephaly.* Science, 2017. **358**(6365): p. 933-936.

214. Xia, H., et al., *An evolutionary NS1 mutation enhances Zika virus evasion of host interferon induction.* Nat Commun, 2018. **9**(1): p. 414.